Università di Pisa

Facoltà di Ingegneria

Dipartmento di Ingegneria Chimica, Chimica Industriale e Scienza dei Materiali

Fluid Mixing Online and In Microdevices

A dissertation submitted for the degree of Doctor of Philosophy

By

Mina Roudgar

Supervisors:
Prof. Roberto Mauri
Prof. Elisabetta Brunazzi

February, 2012

Fluid Mixing Online and In Microdevices

A dissertation submitted for the degree of Doctor of Philosophy

Supervisors:

Prof. Roberto Mauri ____________________

Prof. Elisabetta Brunazzi ____________________

Committee members:

Prof. Alberto Brucato ____________________

Prof. Pietro Poesio ____________________

Prof. Gian Paolo Beretta ____________________

Candidate:

Mina Roudgar ____________________

Date: ____________________

ABSTRACT

Microfluidics and polymer MEMS are the most promising technologies to realize biochemical analysis systems on a chip with low cost, tiny fluid sample, fast chemical/biochemical reaction, and high detection accuracy capabilities. Sample processing, chemical/biochemical reaction, and sample detection are considered as the three major tasks required for lab-on-a-chips.

Micropumps, microvalves and micromixers are also considered as key components in handling microfluidics in the lab- on-a-chips. There have been numerous efforts to develop on-chip active micropumps and microvalves. However, the realization of active microfluidic components in an on-chip disposable platform has been considered as one of the most difficult tasks in terms of fabrication, system integration, reliability, and cost. Consequently, the development of passive microfluidic components is a good alternative to the active components if they can provide the same level of functionality.

In this research, passive mixing using geometric and initial conditions variations in microchannels were studied due to its advantages over active mixing in terms of simplicity and ease of fabrication. Because of the nature of laminar flow in a microchannel, the geometric variations were designed to improve lateral convection to increase cross-stream diffusion. Previous research using this approach was limited, and a detailed research program using computational fluid dynamic (CFD) solvers, various shapes, sizes and layouts of geometric structures was undertaken for the first time. Mixing efficiency was evaluated by using mass fraction distributions.

Different types of geometric and initial conditions variations were researched. First, Structures were used to investigate the effect channel geometry on fluid mixing and flow patterns. Secondly, we applied different initial velocity in each inlet to see the effect of Reynolds number applied on mixing behavior. Third, we applied different kind of fluid in each inlet to visualize the effect of viscosity and finally we create new split and stair geometries to enhance the mixing efficiency.

Contents

List of Figures

List of Tables

Nomenclature

List of Variables

Symbol	Description	SI unit
A	Surface of control volume	m^2
D_h	Hydraulic diameter	m
D	Diffusion coefficient	$m^2\ s^{-1}$
F	Force	N
f	Body force	N
G	Gravitational acceleration	$m\ s^{-2}$
H	Depth of channel	m
Kn	Knudsen number	
L	Length of the channel	m
L_{in}	Length of the inlet channel	m
m	Mass	kg
N	number of molecules in a fluid point	
p	Pressure	Pa
Pe	Péclet number	
$\dot{V}$	Volumetric flow rate	m^3s^{-1}
Re	Reynolds number	
t	Time	*s*
t_c	Convection time	*s*
t_D	Diffusion time	*s*
t_R	Rayleigh time	s
T	Temperature	K
$\bar{u}$	Mean velocity in the channel	$m\ s^{-1}$

u	Velocity field	m s^{-1}
u_x	velocity along x-axis	m s^{-1}
u_y	velocity along y-axis	m s^{-1}
u_z	velocity along z-axis	m s^{-1}
W	width of channel	m
x	x-coordinate	m
y	y-coordinate	m
z	z-coordinate	m
λ	Mean free path of a molecule	m
μ	Dynamic viscosity	Pa s
v	kinematic viscosity	m^2 s^{-1}
ρ	Density	kg m^{-3}
α	Angle degree	
δ_m	Degree of mixing	
σ	mixing efficiency	

Chapter 1

Introduction

1.1 Background and Significance of the Research

Microfluidics is a multidisciplinary field at the intersection comprising physics, chemistry, biological and engineering and biotechnology that studies the behavior of fluids at the microscale. It involves the development of miniaturized systems that are related to handling small volumes of fluids. The concept of microfluidics originated in the 1970's with the development of the microscale gas chromatographic air analyzer at Stanford[1] and the ink jet printing nozzle array at IBM[2] . During the initial years, the growth in this area was slow with primary focus on flow sensors, micropumps and microvalves. However, the conceptual paper by Manz et al.[3] in 1990 triggered an avalanche of developments and discoveries leading to the exponential growth of the microfluidics field in both the commercial and academic areas[4]-[5]-[6] . This burgeoning is due to the emergence of the concept of lab-on-a-chip (LOC) that has revolutionized the microelectromechanical systems (MEMS) community, especially microfluidics.

LOC is a microscale laboratory consisting of a network of microchannels, valves, reaction chambers, electrodes and sensors. It is generally a few square centimeters in size and capable of handling small volumes of fluids to perform a combination of analysis for biological, clinical, or pharmaceutical applications. Miniaturization of these analytical systems offers many advantages, such as increasing throughput, reducing analysis time, reducing quantity of expensive reagents, improving accuracy, integrating reference standards, increased function due to integration, reduced contamination due to low-cost disposable devices, and increased portability[7]-[8]-[9] . To date, these integrated analytical systems have been applied to many biological applications such as enzyme assays[10] , DNA restriction fragment analysis[11] , DNA sequencing[12] , PCR amplification[13]-[14]-[15] and electrophoretic analysis[16]-[17]-[18]. Significant work with cells has also been done using these LOC devices such as cell lysing[18], cell manipulation[19], cell separation[20] and cell patterning[21] .

For many of these miniaturized biological assays mixing is needed in microchannels for blending, emulsification and suspensions of two or more fluids, or mixing of reactants for process initiation. The mixing unit has to provide sufficient mixed solution in a confined length of a micro-device, and before the point where detection is taking place. Mixing in microfluidic devices can be achieved by active mixing methods and passive mixing methods. Active micromixers employ external forces, beyond the energy associated with the flow, in order to perform mixing. However, the active micromixers, which have excellent mixing capabilities, they cost high and they are not well suited for use in applications involving sensitive species (e.g., biological samples).Compared with active micromixers, passive mixers have the advantages of low cost, ease of fabrication and integration with microfluidic systems, no complex control units, and no additional power input. Therefore, as a contribution to building this critical unitfor µTAS, the author presents his research on passive microfluidic mixing with geometric variations.

1.2 Statement of the Problem

To achieve a homogenous mixed solution of samples and reagents in a microfluidic device, the dimensions such a device are too small to put reliable mechanical agitation to stir the fluids. Naturally, the Reynolds numbers of microfluidic devices are low due to their small dimensions. Hence, viscosity predominates the flows, especially for aqueous solutions of most bio-materials. In such viscous flows, even though one can put mechanical agitation into a microfluidic device, it is not likely to efficiently improve mixing performance[22] . Hence, mixing relies on the virtue of molecular diffusion.

On the one hand, microchannels are elegant and efficient for mixing fluids in narrow channels with dimensions up to a few tens of microns. Mixing can be completed by diffusion without any other stirring assistance. This makes microfluidics a very controllable and predictable technique for rapid mixing. On the other hand, it is difficult to drive flow through such small channels due to viscosity. Although fluid can be driven electrokinetically, electrokinetically driven flows introduce some other problems, such as surface chemistry, gas bubbles created by electrolysis and Joule heating. Pressure driven mechanisms have commonly been used in microfluidic devices, however, a relatively wider channel is necessary to reduce the pressure drop. In addition, sometimes a sufficient volume of fluid is needed for a detection stage, and this also requires a relatively large channel. For microchannels with dimensions over 100 μm, diffusion is not generally effective within the confined space of micro-devices, especially for bio-materials with very low diffusion coefficients. These require a long channel for adequate residual time for diffusion to take place.

However, the pressure drop is proportional to the length, and it is difficult to drive the flow through a long microchannel. For the above reasons, methods have to be found to reduce the diffusion distance between fluid streams without restricting the flow. In brief, microfluidic mixing is challenging and attracts the attention of many researchers.

1.3 Objectives and Scope of the Research

The principal objective of this research was to improve the passive mixing efficiency using geometric configurations and initial variation in microchannels. Although many researchers have been attempting to apply active mechanisms to improve mixing performance in a microfluidic device, the complexity of active mechanisms makes it difficult to fabricate and expensive to make. Passive mechanisms have been studied extensively, however, previous research on passive mixing has concentrated on typically one of geometric factors, and an overall view of geometric configurations and their effect on mixing is not clear. Therefore, it is the intention of this research to provide a comprehensive research on passive mixing with various geometric configurations. To achieve this goal, this research systematically investigated the relation between various geometric configurations towards microfluidic mixing by using computational fluid dynamic (CFD) simulations and experimental validations.

As microfluidics is so diverse that a particular design for mixing may be efficient for some applications, it may not be efficient for other applications. Therefore, an overall systematic investigation of geometric configurations is necessary to provide useful guidelines for the design of microfluidic mixing components.

- At the early stage of this research, the theories on microfluidics and microfluidic mixing needed to be identified and clarified. From a certain point of view, microfluidics is just another terminology for flow in a micro-domain with slow motion and not necessarily a new technology. Therefore, existing theories for incompressible slow motion flow may help the research on micro-flow and microfluidic mixing.
- The major tool for the research is computational fluid dynamics (CFD) package. In order to provide accurate simulation results, necessary customized coding needed to be developed to improve the quality of CFD simulations. These include using external mesh generator to provide uniform mesh and import to the CFD package for simulation.

The research focused on mixing of two fluids in a microchannel with dimensions larger than 100μm, and with the Reynolds numbers were typically less than 700, but sufficient enough to produce a detectable volume of solution.

1.4 Outline of This Thesis

To achieve the objectives of this research, the very first step was to understand what had been researched and why there were still problems. This was addressed in chapter 2 by a review of literature and related theories to microfluidic mixing. Chapter 2 also demonstrates the complexity and diversity of microfluidic mixing.

In chapter 3, the methodology to conduct CFD simulations and construct a simple experimental rig is described. There are various geometric which may be incorporated in a microchannel, however, it is impractical to micro- machine each of the designs and experimentally test them. Consequently, CFD was applied to extract useful information for designing passive microfluidic mixers. To validate CFD simulations, selected designs were micro-fabricated and tested, and compared to the simulation results.

From chapter 4-6 we have discussed about result .The thesis was concluded with conclusions and recommendations for future research in chapter 7. This chapter highlighted a number of important outcomes emerging from the present study. The investigation of geometric structures to achieve better disruption flows to create useful convection for mixing provided useful design guidelines for microfluidic mixing.

Chapter 2

Literature Review

2.1 Overview

In this chapter, the fundamentals of microfluidics and theories related to mixing are first reviewed in sections 2.2 and 2.3 to understand the specialty of mixing in micro-scaled devices. Then, in section 2.4 fluid drive mechanisms are briefly described. The existing microfluidic mixing techniques were categorized into active and passive micro-mixers, which were covered in sections 2.5. Section 2.6 summarizes the findings of the literature review and identifies the areas of research which form the basis of the present research.

2.2 Background

In fluid dynamics, in order to study the flow pattern transition from laminar to fully developed turbulent flow, the Reynolds number must exceed the first critical transitional number (Re_{cr1} » 2300) and even the second critical number ($\mathrm{Re}_{cr2} > 10^5$). When the Reynolds number is larger than the first transitional Reynolds number, the flow turns to turbulent under the disturbance, however, as soon as the disturbance is removed, the flow turns back to laminar flow. When the Reynolds number is beyond the second critical transitional number, any disturbance to the flow causes turbulent flow, and remains turbulent even after the disturbance was removed[23]. For the majority of microfluidic devices, the dimensions were well below 1*mm*, which made the Reynolds numbers well below the critical transitional thresholds. Therefore, it was generally accepted that flow in microfluidic devices was laminar, especially when the working fluid was liquid.

Laminar flow was better understood and easier to manipulate than turbulent flow, therefore, the laminar nature of microfluidics was an advantage. On the other hand, microfluidic mixing could not obtain any assistance from turbulence. This meant that any mixing was to be performed by virtue of diffusion, and diffusion was driven by the concentration gradient between two or more fluids, in accordance with Fick's law[24]. In fact, all the mixing processes for miscible fluids are completed by diffusion eventually. The engineering challenge is to make the diffusion path small enough that the process can take place rapidly.

In a macroscopic mixing process, mechanical agitations are normally applied to create turbulent or chaotic advection. Turbulence stretch and break down large fluid streams into smaller fluid filaments, so that the diffusion path can be reduced to a microscopic scale. Eventually, the mixing process is completed by diffusion to create a homogenous solution. However, it is impractical to bring mechanical agitation into a microchannel for two reasons: first, it is difficult to fabricate; and secondly, it is not an effective approach due to the low Reynolds number in a microchannel[22]. Diffusion in a microchannel up to a few tens of micron width was found to be efficient for most applications. However, when the size of a microchannel was more than a hundred microns, pure molecular diffusion could be very slow to achieve complete mixing.

The length of channel to achieve a complete mixing by virtue of diffusion would be very long. As the resistance to the flow was proportional to the length of the channel, this also meant increasing pressure drop and the micropump might fail to drive the fluids through the channels. This makes it difficult to design microfluidic chips with such long channels, therefore, it was necessary in the present research to investigate the techniques to improve mixing within the confined space of microfluidic devices. In the following sections, the fundamentals of microfluidics and mixing are discussed, and the existing active and passive microfluidic mixing methods are reviewed.

2.3 Fundamental Theories for Microfluidics

When a fluidic channel is scaled down to micro-scale, the scaling effects make some physical parameters, such as gravity and inertia, less important than parameters like surface tension and viscosity. Conventional fluid mechanics still applies to study microfluidics, however, some assumptions need to be clarified.

2.3.1 Flow Phenomena in Microchannel Reactors

The flow phenomena in microchannel have been studied extensively during past decades. Currently, the flow phenomena are analyzed using the Navier-Stokes equations but a number of publications have shown that the small hydraulic diameter makes the flows in microscale different from the one in macroscale and the Navier-Stokes equations are incapable for describing the occurring phenomena[25]. Some neglected parameters in macroscale flows may be significant in the microscale. The observation by Ma and Gerner[26] shows that the molecular effect on the momentum transfer in directions other than the streamwise direction can increase significantly when the length of the flow channels are reduced and the continuum assumption becomes invalid. The variation in fluid properties (e.g., fluid viscosity) can occur by the variation of temperature in the transport fluid flowing in microscale which causes invalidation of constant properties assumption[27].

Flows in microchannel are predominantly laminar,[28] because the small hydraulic diameter makes the Reynolds numbers very small. Molecular effects also become more significant in microchannels when the characteristic length decreases to the point that the continuum assumption becomes invalid[29]. In macroscale flows with large diameter channels, the flow pattern is mainly dominated by volumetric forces, such as gravity, while at the microscale flow patterns are strongly influenced by surface forces, such as interfacial tension and wall friction, and diffusive fluxes, which in turn are described through viscosity and mass and thermal diffusivities[30].

The traditional non-dimensional parameters used to characterize fluid flow phenomena is the Reynolds number, Re,

$$\mathrm{Re} = \frac{\rho \mathrm{u_m D_h}}{\mu} \tag{2.1}$$

Where	Re	Reynolds number [-]
	ρ	fluid density [kg m^{-3}]
	u_m	mean fluid velocity [ms^{-1}]
	D_h	hydraulic diameter [m]
	μ	fluid viscosity [Pa s]

The hydraulic diameter is defined as the ratio between four times the area of a cross section and its perimeter,and for a rectangular channel it is given by [31]

$$\mathrm{D_h} = \frac{2\mathrm{WH}}{\mathrm{W + H}} \tag{2.2}$$

Where	W	width of the channel [m]
	H	height of the channel [m]

The adimensional number that characterizes mass transport is the Péclet number (Pe), which is defined as the ratio between the material flux due to convection and that of transverse diffusion, i.e.,

$$\mathrm{Pe} = \frac{\mathrm{u_m D_h}}{\mathrm{D}} \tag{2.3}$$

where D is the molecular diffusivity. In microchannels, the Pechet number is rather large, i.e. Pe > 100, due to the fact that the Schmidt number,

$$\mathrm{Sc} = \frac{\nu}{\mathrm{D}} \tag{2.4}$$

is quite large, i.e. typically Sc = 10^3-$10^{4.}$ This relatively large discrepancy between convective and diffusive timescales implies that the downstream distances (Δy_m) over which fluids must travel to become completely intermixed can be of the order of several centimeters:

$$\Delta \mathrm{y_m} \sim \mathrm{u_m} \times \left(\frac{\mathrm{D_h^2}}{\mathrm{D}}\right) = \mathrm{Pe} \times \mathrm{D_h} \tag{2.5}$$

2.3.2 Continuum

In fluid mechanics, a fluid is a substance that deforms continuously under shear stress. Fluids are composed of molecules in motion. A truly detailed picture of flow will presumably track each individual molecule. However, this was still impractical for current computational or experimental resources. Instead of tracking individual molecules, the fluid could typically be treated as a continuum, which could be infinitely divisible and had a thermophysical property value at each point in space.

In practice, there is a smallest elementary volume that the fluid could be divided into. This volume constitutes what is generally referred as the material point, and should contain a sufficient number of molecules, N, so that the fluctuations of all thermophysical properties can be neglected. According to the theory of non equilibrium thermodynamics, assuming that N = 10^6 is large enough to achieve a statistically meaningful measure of, say, the fluid density ρ (Fig. 2.1), we see that the continuum assumption holds true for an average length scale d » 1μm for gases and d » 100nm for liquids. To quantify how good the continuum assumption is,

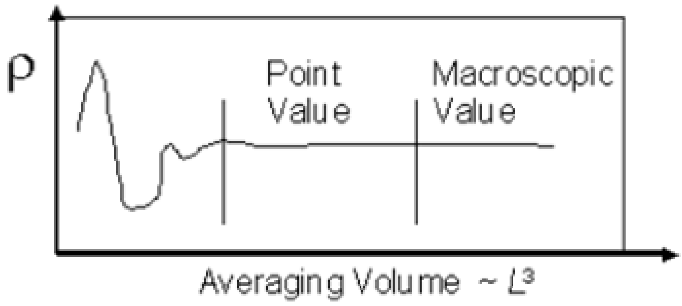

Fig. 2.1. Statical fluid thermophysical point value

The Knudsen number (Kn) can be used, which is defined as the ratio of the mean-free-path of the molecules (λ) to the characteristic dimension L of the device, i.e.,

$$\mathrm{Kn} = \frac{\lambda}{\mathrm{L}} \tag{2.6}$$

The flow regions could be divided into four zones in accordance with the Knudsen number. They were continuum, slip, transition and free-molecular flow. For liquids with low molecular weight, For such liquid flows, the continuum assumption is valid when the channel is over the micron scale[32]. Therefore, the continuity equation could be written in Equation 2.7,

$$\nabla . \mathrm{u} = 0 \tag{2.7}$$

where u is velocity field.

2.3.3 Conservation of Momentum

The conservation of linear momentum is actually Newton's Second Law, i.e.,

$$\sum \mathbf{F} = \frac{d(mu)}{dt} \tag{2.8}$$

while **F** represents all the forces that are applied on the system, m is the mass, u is the velocity and t is the time. Applying the conservation principle to a differential element volume of a fluid, a general conservation equation for momentum can be derived:

$$\rho \frac{Du}{Dt} = \rho\left(\frac{\partial u}{\partial t} + u.\nabla u\right) = f - \nabla p + \mu \nabla^2 u \tag{2.9}$$

where ρ is the density of the fluid. The applied forces to the system, i.e. the RHS of the equation above, include both body forces and surface forces. The formers consist of gravity, electromagnetic force (Lorentz force) etc., while the latters are included within pressure.

2.3.4 Hydrodynamic Characteristic Times

Characteristic times will be used in the following sections to establish some dimensionless groups:

1. The convective (or viscous) time scales the time for a perturbation to propagate in the liquid,

$$t_c = \frac{d}{u} \tag{2.10}$$

where d is a dimension and u is the velocity of the liquid.

2. The diffusional time is the time taken by a perturbation to diffuse in the liquid,

$$t_D = \frac{d^2}{\nu} \tag{2.11}$$

where $\nu = \mu/\rho$ is the kinematic viscosity (m^2/s), d is the diffusion distance, and t_D is the time required to diffuse across distance l. This equation had been widely used in interpreting microfluidic mixing. In fact, reducing the diffusion length by a factor n, the diffusion time decreases n^2 times, showing that mixing can be greatly improved by reducing the diffusion distance between fluid streams.

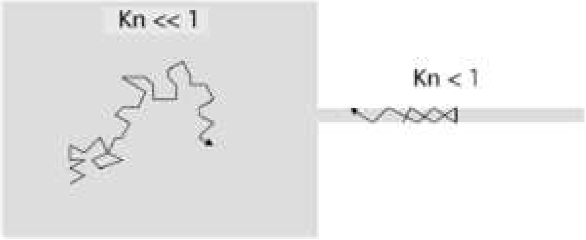

Fig. 2.2. Schematic of microscale (Kn<<1) and nanoscale (Kn>1) chambers.

3. The Rayleigh time is a time scale of the perturbation of an interface under the action of inertia and surface tension[33]-[34]-[35]

$$t_R = \sqrt{\rho d^2/\gamma} \tag{2.12}$$

2.4 Pumping The Fluids in Microfluidics

Micropump is one of the key components in Bio MEMS/NEMS and microfluidic systems where the transportation of fluid is indispensable. The key features of micropumps include dimension, range of pumping rate, pumping pressure, operation voltage, power consumption, process compatibility with other parts of the system, etc. The importance and specific range for each feature is different from system to system and application to application for which the micropumps are applied.

There are many application fields of micropumps. For lab-on-a-chip or micro total analysis systems (μ-TAS) applications, micropumps should be able to transport sample reagents to perform many functions including delivery, mixing, reaction, analysis, or discharging of reagents. In this case, accurate control of flow rate is important to increase the accuracy and reliability of analytical results. On the other hand, power consumption and operation voltage are not a big issue because the chips are typically installed in a macro control/interface system. On the contrary, in application of the microfluidic chips for a portable or hand-held analytical system, micropumps should provide low voltage operation and low power consumption in addition to accurate flow control. In order to develop the various types of micropumps that meet specific system requirements, many researchers have designed and implemented many different types of micropumps.

In general, micropumps can be classified as either mechanical or non-mechanical micropumps[36]. The micropumps that have moving mechanical parts such as pumping diaphragm and check valves are referred to as mechanical micropumps where as those involving no mechanical moving parts are referred to as non-mechanical micropumps. Mechanical type micropump needs a physical actuator or mechanism to perform pumping function. The most popular mechanical micropumps discussed here include electrostatic, piezoelectric, thermopneumatic, shape memory alloy (SMA), bimetallic, ionic conductive polymer film (ICPF), electromagnetic and phase change type. Non-mechanical type of micropump has to transform certain available non-mechanical energy into kinetic momentum so that the fluid in microchannels can be driven. Non-mechanical micropumps include magnetohydrodynamic (MHD), electrohydrodynamic (EHD), electroosmotic, electrowetting, bubble type, flexural planar wave (FPW), electrochemical and evaporation based micropump. The classification of micropumps is shown in figure 2.3.

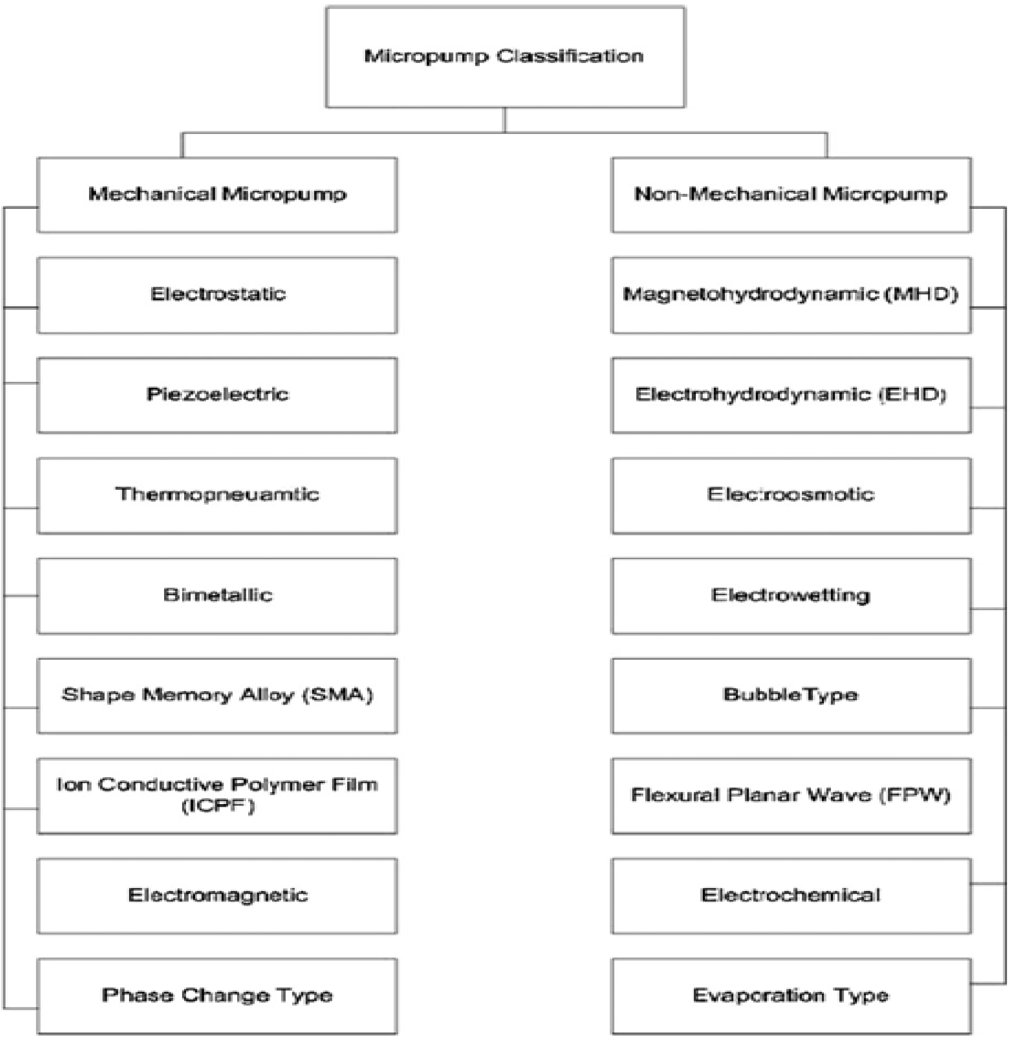

Fig. 2.3. Classification of micropump with different actuation methods.

2.4.1 Mechanical Micropumps

The most common types of mechanical micropumps are displacement pumps involving a pump chamber which is closed with a flexible diaphragm. A schematic illustration of diaphragm type mechanical micropump is shown in figure 2.4.

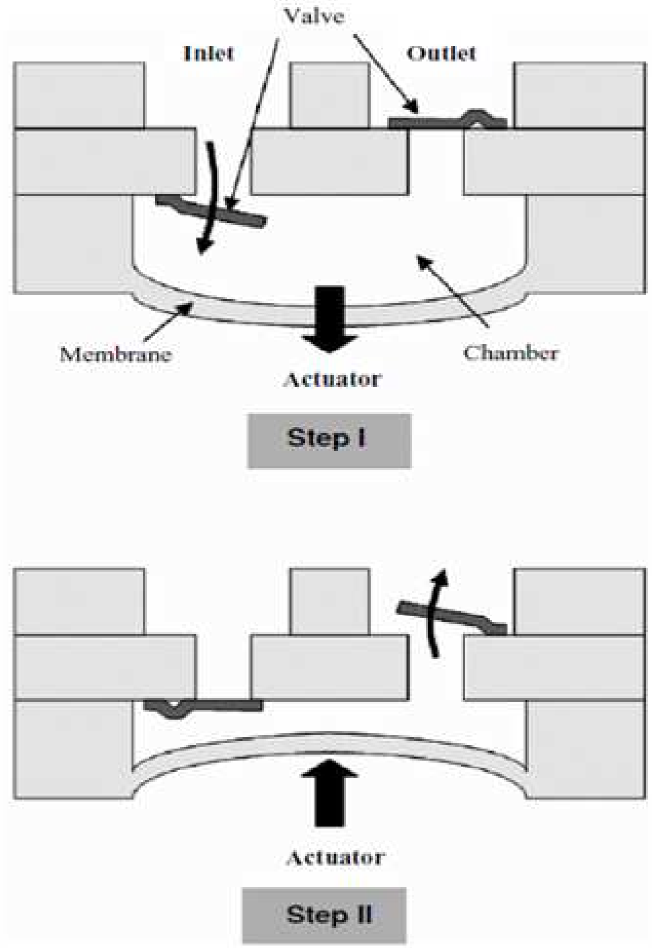

Fig. 2.4. Schematic view and working principle of reciprocating membrance micropums.

Fluid flow is achieved by the oscillatory movement of the actuator diaphragm which creates under and over pressure (p) in the pump chamber. Under pressure in the pump chamber results in the flow of fluid inside the pump chamber through the inlet valve. Over pressure in the pump chamber transfers the fluid out of the pump chamber through the outlet valve. Mechanical micropump designs may contain single pump chamber or sequentially arranged multiple pump chambers in series or in parallel. Such types of micropumps are called peristaltic micropumps. Peristaltic movement of diaphragms in the sequentially arranged pump chambers, transfers the fluid from the inlet to the outlet. Peristaltic micropumps can be operated by various actuation mechanism including piezoelectric[37], thermopneumatic[38] , pneumatic[39]-[40]-[41] and electrostatic actuators[42] . Syringe Micropumps are another important group of micropumps. Unlike other micropumps, most syringe micropumps are composed of three parts[43]-[44]-[45]-[46]-[47]-[48]-[49] a reservoir in which pumping fluids are contained; a nozzle through which pumping liquid flows; and an actuator that, in most cases, is located in the reservoir to push the fluid. Syringe micropumps are useful in all application fields where accurate, steady and nonfluctuant flow control is required. Thereby, most syringe micropumps have adopted actuators that show reliable controllability from the induced signals, although they are slow in response.

Microvalves are another important element of mechanical micropumps. Microvalves are classified as passive or active. Passive valves do not include any actuation and their effect is obtained from a difference in pressure between the inlet and the outlet of the valve. Active valves, on the contrary, are operated through an actuating force and offer improved performance, but with increase complexity and fabrication costs.

2.4.2 Non-mechanical Micropumps

Non-mechanical micropumps require the conversion of non-mechanical energy to kinetic energy to supply the fluid with momentum. These phenomena are practical only in the microscale. In contrast to mechanical micropumps, nonmechanical pumps generally have neither moving parts nor valves so that geometry design and fabrication techniques of this type of pumps are relatively simpler. However they have limitations such as the use of only low conductivity fluids in electrohydrodynamic micropumps. Moreover the actuation mechanisms are such that they interfere with the pumping liquids. Since the early 1990s, many non-mechanical micropumps have been reported. Non-mechanical micropumps with different actuation methods are summarized in figure 2.3.

2.5 Micromixing Strategies

In the past decade, a sizeable amount of research has been directed towards developing new micromixing strategies. Recent review papers give a holistic view of these micromixing techniques and applications[50]-[51]-[52]-[53]-[54]. In general, mixing strategies can be classified as either active or passive (Fig. 2.5.), depending on the operational mechanism.

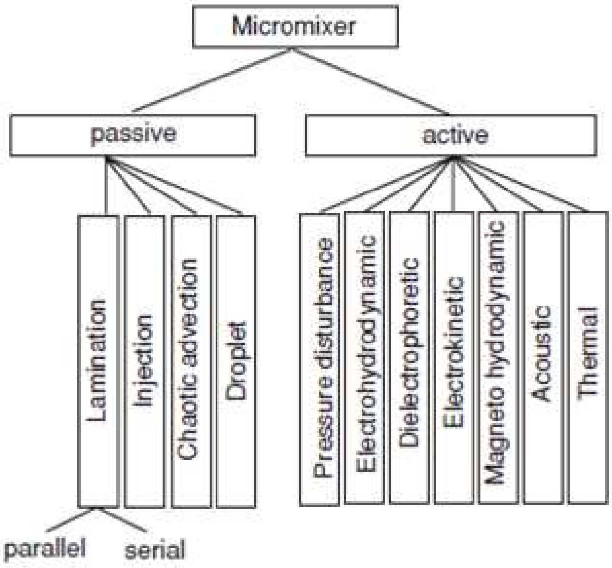

Fig. 2.5. Classification scheme for micromixer.

2.5.1 Active Micromixers

Active micromixers employ external forces, beyond the energy associated with the flow, in order to perform mixing. Some examples of techniques developed to accomplish this include electro-osmosis[55] , magnetic stirring[56], bubble- induced acoustic actuation[57] and ultrasonic effects[58] . A distinct advantage over passive type micromixers is that these systems can be activated on-demand. While generally effective in generating turbulence for rapid fluid mixing in short length-scales, these designs are often not easy to integrate with other microfluidic components and typically add substantial complexity to the fabrication process. Moreover, since high electric fields, mechanical shearing, or generation of nontrivial amounts of heat are involved, they are not well suited for use in applications involving sensitive species (e.g., biological samples).

Pressure field disturbance

Pressure field disturbance was used in one of the earliest active micromixers. Deshmukh *et al*[59] reported a T-mixer with pressure disturbance (Fig. 2.6a). The mixer is integrated in a microfluidic system. An integrated planar micropump drives and stops the flow in the mixing channel to divide the mixed liquids into serial segments and make the mixing process independent of convection. The performance of this micromixer was later discussed by Deshmukh *et al* in their other paper[60]. The pressure disturbance can also be generated by an external micropump[61]. Another alternative method to pressure disturbance is the generation of pulsing velocity[62]-[63] (Fig. 2.6b). Glasgow and Aubry[61] demonstrated a simple T-mixer and its simulation with a pulsed side flow at a small Reynolds number of 0.3. The paper did not elaborate further on the generation of the pulsed flow. In the work of Niu and Lee[62], the pressure disturbance was achieved by introducing a computer-controlled source–sink system. This design is partly similar to that of Evans *et al*[64] . The performance of the mixing process is related to the pulse frequency and the number of mixing units. A further modeling work on pressure disturbance was reported by Okkels and Tabeling[65]. However, the analysis focused only on the mixing pattern in the chamber.

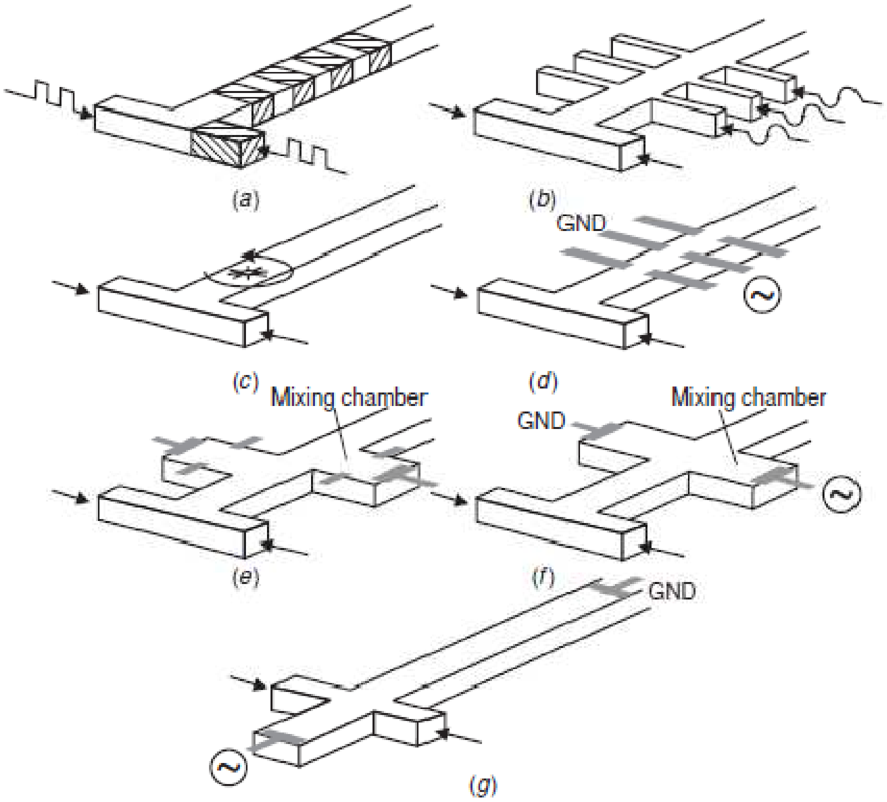

Fig. 2.6. Active micromixers: (*a*) serial segmentation, (*b*) pressure disturbance along the mixing channel, (*c*) integrated microstirrer in the mixing channel, (*d*) electrohydrodynamic disturbance, (*e*) dielectrophoretic disturbance, (*f*) electrokinetic disturbance in the mixing chamber and (*g*) electrokinetic disturbance in the mixing channel.

Suzuki and Ho[66] reported a micromixer with integrated conductors. The electrical conductors generate a magnetic field, which in turn moves magnetic beads of 1–10 μm in diameter. The disturbance caused by the magnetic beads improves mixing significantly. Disturbance can also be generated by an integrated magnetic microstirrer as reported by Lu *et al*[67]. The micromachined stirrer is placed at the interface between two liquids in a T-mixer. An external magnetic field drives the stirrer at a speed between 100 rpm and 600 rpm.

Electrohydrodynamic disturbance

The structure of the micromixer with eletrohydrodynamic disturbance[68] is similar to the concept reported by Niu and Lee[62]. Instead of pressure sources, electrodes are placed along the mixing channel (Fig. 2.6d). A series of titanium wires is placed in the direction perpendicular to the mixing channel. By changing the voltage and frequency on the electrodes good mixing was achieved after less than 0.1 s at a low Reynolds number of 0.02.

Dielectrophoretic disturbance

Dielectrophoresis (DEP) is the polarization of a particle relatively to its surrounding medium in a non-uniform electrical field. This effect causes the particle to move to and from an electrode. Deval *et al*[69] and Lee *et al*[70] reported a dielectrophoretic micromixer (Fig. 2.6e). Chaotic advection was generated by embedded particles with a combination of electrical actuation and local geometry channel variation.

Electrokinetic disturbance

Electrokinetic flow can be used to transport liquid in micromixers as an alternative to pressure driven flow. Jacobson *et al*[71] reported electrokinetically driven mixing in a conventional T-mixer. Lettieri *et al* proposed the use of the electrokinetic effect to disturb the pressure-driven flow in a micromixer[72] . In another case[73], oscillating electro-osmotic flow in a mixing chamber is caused by an ac voltage. The 13 pressure-driven flow becomes unstable in a mixing chamber (Fig. 2.6f) or in a mixing channel (Fig. 2.6g). Tang *et al* also utilized an electrokinetic flow to improve mixing[74] . Similar to the previous pressure-driven approach[58] , switching on or off the voltage supplied to the flow generates fluid segments in the mixing channel. This flow modulation scheme was capable of injecting reproducible and stable fluid segments into microchannels at a frequency between 0.01 Hz and 1 Hz.

Magneto hydrodynamic disturbance

The magneto hydrodynamic effect[75] has been used in micromixers. In the presence of an external magnetic field applied dc voltages on the electrodes generate Lorentz forces, which in turn can induce roll and fold of the liquids in a mixing chamber. This concept only works with an electrolyte solution.

Acoustic disturbance

Acoustic actuators were used to stir fluids in micromixers. The proof of concept for acoustic mixing was reported by Moroney *et al*[76] with a flexible-plate-wave (FPW) device. Zhu and Kim[77] gave an analysis of the focused acoustic wave model in a mixing chamber. The vibration can be controlled by changing the frequency and the voltage of the input signal. The concept of acoustically induced flow, or acoustic streaming, was also used as an active mixing scheme[78] . Focused acoustic streaming with different electrode patterns was used for mixing[79] . Besides the integrated design, stirring at high frequency can also be realized by an external pump[80] . Ultrasonic mixing may have problems in applications for biological and chemical analysis because of the temperature rise caused by acoustic energy. Many biological fluids are highly sensitive to temperature. Furthermore, ultrasonic waves around 50 kHz are harmful to 14 biological samples because of the possible cavitations. The acoustic micromixer reported by Yasuda[81] used loosely focused acoustic waves to generate stirring movements. The mixer operated without any significant temperature increase and could be used for temperature-sensitive fluids. Further acoustic devices for mixing water and ethanol as well as water and uranine were reported by Yang *et al*[82]-[83] . Liu *et al*[84]-[85] used acoustic streaming induced around an air bubble for mixing. Yaralioglu *et al*[86] also utilized acoustic streaming to disturb the flow in a conventional Y-mixer.

Thermal disturbance

Since the diffusion coefficient depends highly on temperature, thermal energy can also be used to enhance mixing[87]-[88]. Mao *et al*[86] generated a linear temperature gradient across a number of parallel channels in order to investigate the temperature dependence of fluorescent dyes. This approach can possibly be used for micromixing. The other design[87] utilized a thermal bubble to generate disturbance in a mixing channel.

2.5.2 Passive Micromixers

Passive mixers, avoid active mixers problems by exploiting characteristics of specific flow fields to mix species without application of external electrical or mechanical forces. These gentle designs are also often more straightforward to build and interface with other microfluidic components. Passive micromixers can be broadly sub-classified into designs based on lamination, rotation, injection and droplet techniques.

Parallel lamination micromixers

Fast mixing can be achieved by decreasing the mixing path and increasing the contact surface between the two phases. Parallel lamination splits the inlet streams into a number of substreams, then join them into one stream as laminae. The basic design is a long microchannel with two inlets to its geometry; these designs are often called the Tmixer or the Y-mixer[89]-[90]-[91] (Fig. 2.7*a* and *b*). Since the basic T-mixer entirely depends on molecular diffusion, a long mixing channel is needed. Besides the abovementioned concept of lamination of multiple streams, mixing at extremely high Reynolds numbers could also result in a short mixing length[92]-[93] .A chaotic flow is expected at these high Reynolds numbers. The induced vortices significantly enhance the mixing efficiency.

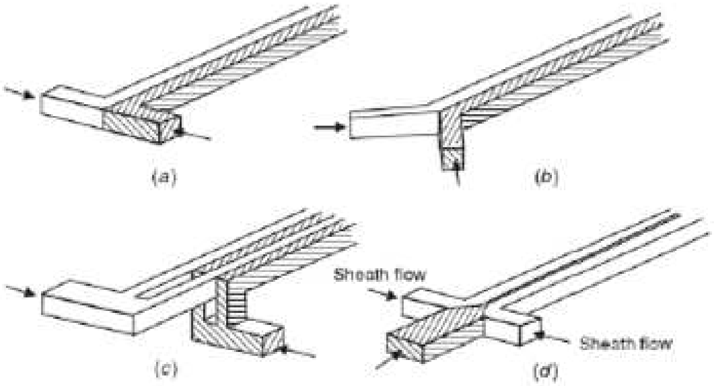

Fig. 2.7. Parallel lamination micromixer: (a) the basic T-mixer and (b) Y-mixer, (c) the concept of parallel lamination and (d) the concept of hydraulic focusing.

Serial lamination micromixer

Similar to parallel lamination micromixers, serial lamination micromixers alsoenhance mixing through splitting and later joining the streams as shown in Fig. 2.8[94]-[95]-[96]-[97] . The inlet streams are first joined horizontally and then in the next stage vertically. After a number of splitting and joining stages, all the liquid layers created, can be laminated. The concept of the serial lamination micromixer can also be applied to electrokinetic flows as reported by He *et al*[98] (Fig. 2.8d). Using electro-osmosis flows between the multiple intersecting microchannels, mixing is clearly enhanced. A similar design for a pressure-driven flow was reported by Melin *et al*[99]. However, this design only works for a plug of the two mixed liquids.

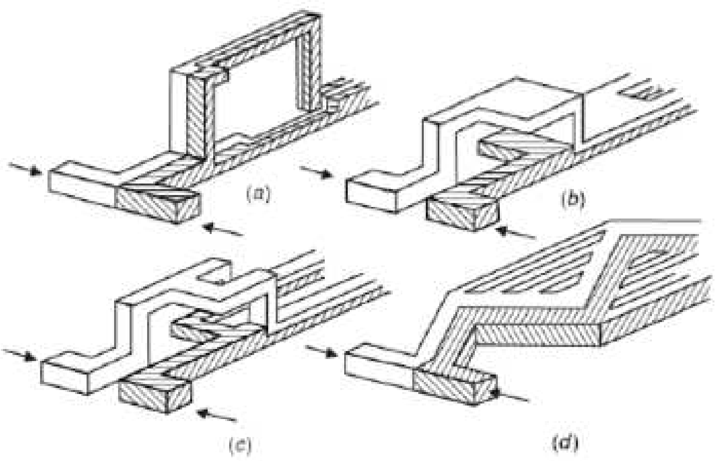

Fig. 2.8. Serial lamination mixer: (a) join-split-join, (b) split-join, (c) split-split-join and (d) multiple intersecting microchannels.

Injection

Injection-type micromixers are similar to parallel lamination mixers, except that only one of the inlet streams is split into multiple streams and then injected into the other flowing stream. Typically, arrays of micro-nozzles are used to inject microplumes of one fluid on top of the other in order to increase the overall contact surface area and consequently increase diffusive mixing. Miyake et al. were amongst the first to utilize this concept in a mixer design that had 400 nozzles arranged in a square array (Fig. 2.9)[100]. Capillary flows have also been used to generate microplumes[101] although these mixers are capable of rapidly increasing the contact area between different species, fabrication of the complex setup involved requires a multi-level procedure that can be quite tedious. Moreover, it can be challenging to reproducibly fabricate arrays involving hundreds of micro-nozzles with precision.

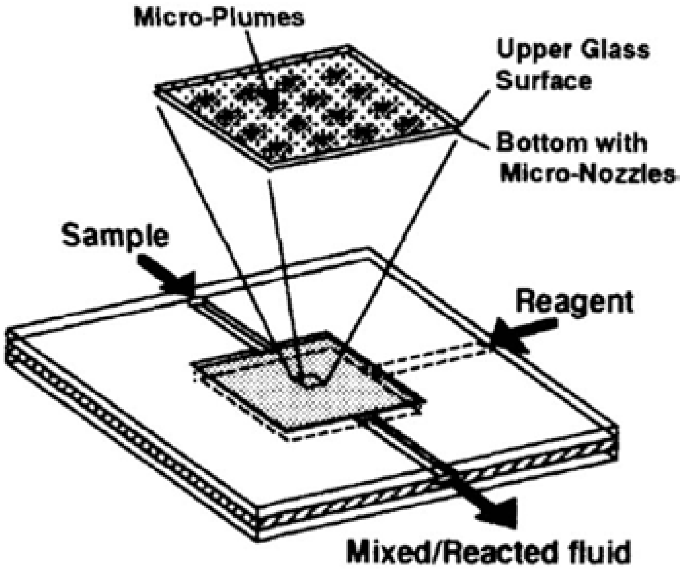

Fig. 2.9. Example of an injection-type micromixer. The mixing is first filled with one fluid and the second fluid is injected directly into the first fluid via micro-nozzles positioned below. Micro-plumes are generated thereby increasing the overall contact area between the two fluids for rapid diffusive mixing to occur. The micro-nozzles are separated from each other by 100 μm and a mixing area of area 2 mm × 2 mm accommodates up to 400 nozzles.

Chaotic advection at high Reynolds number.

The simplest method to get chaotic advection is to insert obstacles structures in the mixing channel. Wang *et al* reported a numerical investigation of obstacles at high Reynolds numbers[102] . This work found that obstacles in a microchannel at low Reynolds numbers cannot generate eddies or recirculations (Fig. 2.10b). However, the results demonstrated that obstacles could improve mixing performance at high Reynolds numbers. Under this condition, the asymmetric arrangement of obstacles could alter the flow directions and force fluids to merge and create transversal mass transport. Lin *et al*[103] used cylinders placed in a narrow channel to enhance mixing. The next method to generate chaotic advection is using zig-zag microchannels to produce recirculation around the turns at high Reynolds numbers (Fig. 2.10c).

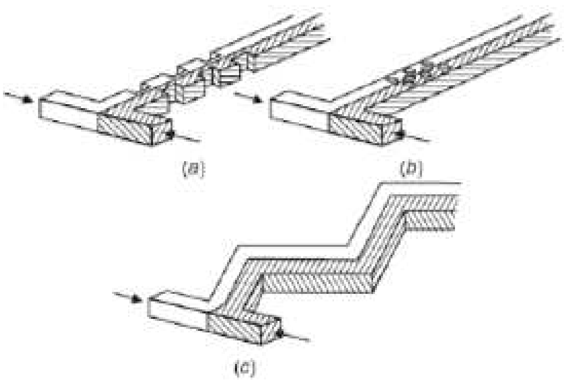

Fig. 2.10. Planar designs for mixing with chaotic advection at high Reynolds number: (a) obstacles on wall, (b) obstacles in the channel and (c) a zig-zag shaped channel.

Chaotic advection at intermediate Reynolds numbers.

Hong *et al*[104] demonstrated an in-plane micromixer with two-dimensional modified Tesla structures. The Coanda effect in this structure causes chaotic advection and improves mixing significantly. Liu *et al*[105] reported a three-dimensional serpentine mixing channel constructed as a series of C-shaped segments positioned in perpendicular planes (Fig. 2.11b). The micromixer consists of two inlet channels joined in a T-junction, a straight channel and a sequence of six mixing segments. An interesting observation of the micromixer is that chaotic advection only occurs at relatively high Reynolds numbers (Re = 25–70) when the mixing process becomes faster. Figure 2.11shows various other channel geometries that are designed to generating chaotic mixing at high Reynolds umber.

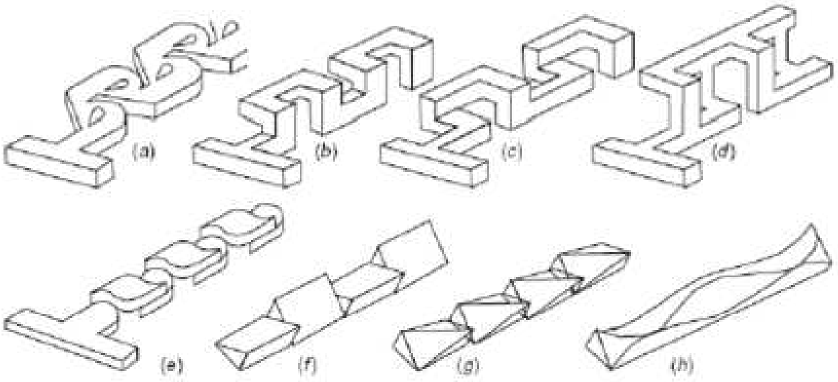

Fig. 2.11. Micromixer designs for mixing with chaotic advection at intermediate Reynolds numbers: (*a*) modified Tesla structure, (*b*) C-shape, (*c*) L-shape, (*d*) connected out-of-plane L-shapes, (*e*) twisted microchannel and ((*f*), (*g*), (*h*)) other designs of twisted channel .

Chaotic advection at low Reynolds numbers.

Similar to macroscale mixers, rips or grooves on the channel wall can produce chaotic advection. Johnson *et al*[106] were the first to investigate this phenomenon. Almost at the same time, Stroock *et al* investigated this effect and published their results in *Science*[107] Two different groove patterns were considered. The so-called staggered herringbone mixer (Fig. 2.12c) can work well at a Reynolds number range from 1 to 10. This concept can be applied to electrokinetic flow by modifying the surface charge[108] . The effect of chaotic advection with the ripped channel was numerically investigated by Wang *et al*[109]. Kim *et al* [110] improved the design of Stroock *et al* [107].with embedded barriers parallel to the flow direction.

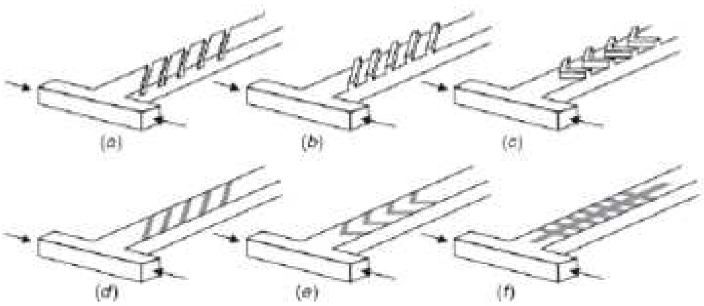

Fig. 2.12. Modification of mixing channel for chaotic advection at low Reynolds numbers: (*a*) slanted ribs, (*b*) slanted grooves, (*c*) staggered-herringbone grooves and (*d*)–(*f*) patterns for surface modification in a micromixer with electrokinetic flows.

Droplet

Another solution for reducing the mixing path is to form droplets of the mixed liquids (Fig. 2.13). The movement of a droplet causes an internal flow field and makes mixing inside the droplet possible. In general, droplets can be generated and transported individually using pressure[111] or capillary effects such as thermocapillary[112] and electrowetting[113] . Furthermore, droplets can be generated due to the large difference of surface forces in a small channel with multiple immiscible phases such as oil/water or water/gas[114]. Hosokawa et al[111] reported the earliest droplet micromixer. Handique and Burns reported an analytical model for droplet mixing actuated by thermocapillary[112]. Paik et al[113] reported different mixing schemes with the electrowetting concept. Droplets can be merged and split repeatedly to generate the mixing pattern. The merged droplet can then be transported around using electrowetting. The other droplet micromixer design used flow instability between two immiscible liquids[114]-[115]. Using a carrier liquid such as oil, droplets of the aqueous samples are formed. While moving through the microchannel, the shear force between the carrier liquid and the sample accelerated the mixing process in the droplet.

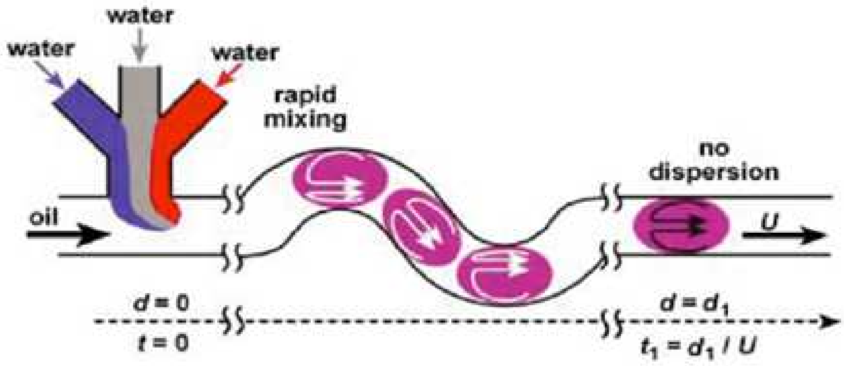

Fig. 2.13. Example of droplet-ased micromixer. The streams to be flow in a laminar manner before encountering a flowing immiscible liquid to give rise to tiny droplet or plugs. As the droplets flow through varying channel geometries, internal recirculation causes the engulfed streams to get rapidly intermixed. The maximum cross-sectional feature in the mixer was 50 µm.

2.6 Summary

In a typical microfluidic device, the Reynolds number is low and the flow is laminar. Therefore, the mixing of two or more fluid streams in microfluidic devices is due to diffusion, which is a slow process and therefore requires large mixing lengths. On the other hand, for microfluidic applications towards biomedical or chemical diagnostics, such as lab-on-a chip, it is very important to mix two or more reagents and test samples thoroughly within short distances, before detection can take place. In fact, a) mixing needs to be done in a confined area; b) the volume of fluids for detection should be adequate and sufficiently mixed. Therefore, microfluidic mixing is challenging and, as a consequence, many mixing methods have been developed. Based on the mixing mechanism, micro-mixers have pure molecular diffusion at one end and chaotic mixing on the other. Based on structures, micro-mixers can be categorized in active and passive. Most of the active micro-mixers enhance mixing by stirring the flow. Stirring can be done mechanically or by the means of magneto-hydrodynamic (MHD), electrohydrodynamic (EHD) or by acoustic streaming to create secondary flows. The secondary flows can stretch and fold material lines to reduce the diffusion path between fluid streams, and hence, enhance mixing. Most active micro-mixers are complex to fabricate and require an external power source. On the other hand, passive micromixers are simpler, as they reduce the mixing length by splitting and recombining the fluid streams. Recently, passive chaotic micro-mixers were investigated by using 3D serpentine type channels. Most of the research to date focused on one or a few passive structures, and a full understanding of geometric structures, with their influence on mixing and flow patterns, had not yet been achieved.

Chapter 3

Numerical Modeling and Experimental Methodology

3.1 Introduction

In chapter 2, the literature review found that it was important and necessary to study passive micromixers with in-situ geometric variations to enhance mixing. These geometric variations included channel shape, structures inside channel and geometric topology of channel walls. For the large number of parameters involved, it was difficult to conduct the research by experiments. Though some researchers delicately utilized micro particle imaging velocimetry (μPIV) to measure the whole flow field, these techniques are limited to particular applications, and typically, to slow shallow flow field due to the depth of field of optical lens[116]. Moreover, Computational Fluid Dynamics (CFD) can neglect un-important factors in the real environment, and focuses on the fundamental principles of the problem, therefore, CFD can be a versatile tool for studying laminar incompressible flows.

The existing CFD softwares can be divided into three categories. One is the general CFD packages for macroscopic scale analysis, such as Fluent, CFX, which are based on the Navier-Stokes equations. One way to apply this kind of CFD softwares to microfluidics is to understand the principles and the structures of the packages, and then modify some parameters to model a microfluidic device by utilizing the user program interface embedded in the software. This category of CFD package, in general, is well tested and usually implemented with a versatile CAD system for pre-processing and visualization tools for post-processing. Therefore, the users can treat the packages as black boxes and concentrate on the analysis. However, if the structure of the package needs to be changed for simulating the special flow behavior in a microscopic scale, they may face problems. Because the users normally cannot access the source code of the packages for modification, and even if they can, it is a time consuming and a difficult task for the individual researcher.

The second group of CFD package is specially designed for microfluidics, such as MemCFD from Coventor Inc. and CFDACE+ from CFDRC Inc. These softwares enable users to do some quick simulations and designs, and hence, save time. However, compared to the general CFD package, they have a much smaller user group, and a shorter history. Furthermore, the theory of microfluidics was still under development. Therefore, the users should be aware of the restrictions of these softwares. In addition, because the surface/volume ratio is high in microfluidics devices, a CFD package should be able to simulate the interfacial effects, such as capillary flow and electrokinetic flow.

The third group, eg. DiffPack and Matlab, contains some general tools, for example, partial differential equation (PDE) solvers, which can complement CFD packages for developing microfluidic models. This group has the greatest flexibility. Nevertheless, the development and validation of numerical coding were expensive, time consuming, and the performance of the simulation depends very much on the experience of individual researchers. For the above reasons, a microfluidic CFD package, MemCFDTM, was chosen as the primary tool to study the microfluidic mixing. MemCFD embeds Fluent and Fidap solvers to solve Navier-Stokes equations and has functions to simulate multi-species mixing, pressure-driven flows as well as electro-osmotic flows. Fluent and Fidap are the stateof- art CFD solvers to date, and MemCFD also has integrated advanced modelling and visualization tools, therefore, MemCFD can provide reliable and high quality simulations.

In this chapter, section 3.2 introduces the CFD fundamentals. Section 3.3 describes the special requirements of microfluidic modelling.

3.2 Fundamentals of Computational Fluid Dynamics (CFD)

3.2.1 Overview

The technological value of computational fluid dynamics has become undisputed. In microfluidics, it might be very difficult to experimentally diagnose the flow behavior at micron or sub-micron scales. However, it is still feasible for CFD to be used to simulate micro-flow as long as the validation of continuity is maintained (in Section 2.3.2). For the understanding of the significance and limitation of CFD in microfluidics, a basic knowledge is introduced in this section. CFD simulation can be divided into three stages, pre-processing (modelling), analysis (solve Navier-Stokes equations) and post-processing (results output). Among these CFD modules, the solvers are the core of the problem.

3.2.2 CFD Solvers

The boundary conditions associated with flows of practical interest are usually so complicated that an exact solution of the Navier-Stokes equations is unavailable, and it is necessary to seek a numerical solution. Computational techniques replace the governing partial differential equations with systems of algebraic equations that can be solved numerically. Since the governing equations are nonlinear, the computational solver usually proceeds iteratively. Therefore, if the numerical algorithm that performs the iteration is stable, and the discrete equations are faithful representations of the governing (i.e. partial differerntial) equations, then the computational solution can be made arbitrarily close to the true solution of governing equations by refining the grid. However, the refinement is restricted by computer resources and accumulation of errors during the iteration. Therefore, optimized grid size should be applied to obtain sufficient accuracy.

In general, there are many methods for discretizing the physical domain, including finite difference method (FDM), finite volume method (FVM), finite element method (FEM) and spectral method. FDM is very well developed and very straightforward to understand the discretization of PDEs. However, FDM requires regular shape of mesh elements and cannot be used to solve problems with complex geometric shape. In general, FDM is rarely used in most of the contemporary CFD codes. FVM and FEM are found commonly used, and are based on the theory of weighted residual methods (WRM). A weighted residual method assumes that the solution can be represented analytically. The starting point for a weight residual point is to assume an approximate solution, and then the partial differential equations can be replaced by a system of algebraic equations or a system of ordinary differential equations for time-dependent problems. By substituting the exact solution, an equation residual is generated. The integral of the weighted residual over the computational domain should be zero to determine the necessary coefficients of the system of algebraic equations or the system of ordinary differential equations in general. Different choices for the weight (trial) function give rise to different methods in the class of methods of weight residuals. This forms the theoretical foundation of the finite element and finite volume methods.

Finite Element Analysis

In the Finite Element Method, the solution domain can be discretized into a number of uniform or non-uniform finite elements that are connected via nodes. The change of the dependent variable with regard to location is approximated within each element by an interpolation function. The interpolation function is defined relative to the values of the variable at the nodes associated with each element. The original boundary value problem is then replaced with an equivalent integral formulation. The interpolation functions are then substituted into the integral equation, integrated, and combined with the results from all other elements in the solution domain. The results of this procedure can be reformulated into a matrix equation of the form, which is subsequently solved for the unknown variable. The finite element method was developed initially as an ad hoc engineering procedure for constructing matrix solutions for stress and displacement calculations in structural analysis. The method was placed on a sound mathematical foundation by considering the potential energy of the system and giving the finite element method a variational interpretation.

However, very few fluid dynamic (or heat transfer) problems can be expressed in a variational form. For many situations, the Galerkin method is used to define the trial function or shape functions in the engineering literature for solving variational problems[117] .Consequently, most of the finite element applications in fluid dynamics have used the Galerkin finite element formulation. The Galerkin finite element method has two different features from traditional weighted residual methods. Firstly, the approximate solution is written directly in terms of the nodal unknowns. The second important feature is that the approximating functions are chosen exclusively from low-order piecewise polynomials restricted to contiguous elements. The finite element method discretizes flow domain in two stages. First a piecewise interpolation is introduced over discrete or finite elements to connect the local solution to the nodal values. The second stage uses a weighted residual method to obtain algebraic equations connecting the solution nodal values. Both stages introduce errors. Small element size can achieve more accurate interpolation, however, this induces more interpolation steps and the error of each interpolation is accumulated, therefore, a restriction on the smallest element size should be placed in the computation.

Finite Volume Analysis

Finite volume analysis divides the computational domain into many sub-domains, and the weighted function is assigned unity if inside a sub-domain or zero if outside. The finite volume method calculates the values of the conserved variables averaged across the sub-domain and provides an appropriate framework for enforcing conservation at the discretized equation level. In this way the conservation properties inherent in the governing equations are preserved. This is a particular advantage in obtaining accurate solutions for internal flows.

Finite volume method, which has been used for both incompressible and compressible flow, has two major advantages. First it has good conservation properties, as mentioned above. Second it allows complicated computational domains to be discretized in a structured and/or unstructured manner.

In summary, the finite volume method is preferable to other methods as a result of the fact that boundary conditions can be applied non-invasively. This is true because the values of the conserved variables are located within the volume element, and not at nodes or surfaces. Finite volume methods are especially powerful on coarse non-uniform grids and in calculations where the mesh moves to track interfaces. For the above reasons, the finite volume method was used extensively in this research.

3.3 CFD Modeling in Microfluidics

For the dimensions of the microfluidic devices and the fluids investigated in this research, the Knudsen number (Section 2.3.2) is approximately zero and continuum holds true. Therefore, the computational fluid dynamic tools can be applied in the investigation of passive microfluidic mixing. However, viscosity is critical and cannot be ignored for a successful simulation. For solving Navier-Stokes equations coupled with convection-diffusion equations, finite volume method was used extensively for its advantage of mass conservation.

Although the governing equations (i.e. the Navier-Stokes vector equation together with the convective-diffusive scalar equation) are well known and do not need to be dealt with, when CFD solvers are applied to micro-flows, there are several practical issues that need to be considered. In particular, in this Chapter we define the appropriate system of units that will be used, and the boundary conditions to be applied.

3.3.1 System of Units in Microfluidics

As the characteristic lengths of microfluidic devices are of the order a few microns to a few millimeters, it is practical to use micron as the unit of length. The units of length (L), time interval (T), temperature (θ) and electrical current (A) are regarded as the reference (M-L-T-θ-A) system, and other units are derived from them. Therefore, the dimensional system for microfluidic are mass (kg), length (μm), time interval (second), temperature (Kelvin) and current (pico Ampere). When applying the reference magnitudes to derive other ones, the dimensional homogeneity principles must be followed. Then, we can derive the following units used in microfluidics (Table 3.1). Other units, which are not listed in this table, can be derived by the same rules.

3.3.2 Boundary Conditions

Boundary conditions are necessary for the CFD solvers to initialize the simulation and achieve rational results. In microfluidic applications with liquids inside the channel, the Reynolds number is low and the flow is generally laminar as stated in section 2.3. As viscosity dominates the flow domain, the velocity close to the wall is zero. For most of the simulations run in this research, the boundary conditions were set as steady, laminar, Newtonian, with one fluid (or two fluids to solve diffusion-convection problems). The inlets were assigned volumetric flow rate/velocity, or pressure boundary conditions.

Table 3.1 Systems of units in microfluidics

Parameter	Symbol	Microfluidic units
Mass	m	Kg
Length	l	µm
Time interval	t	s
Temperature	T	K
Pressure	P	M Pa
Density	ρ	Kg μm^{-3}
Diffusivity	D	$\mu m^2\ s^{-1}$
Force	F	µN
Stress	σ_{ij}	M Pa
Velocity	u	$\mu m\ s^{-1}$
Viscosity	µ	M Pa s

Slip flow

According to the laminar flow fluid theory, friction factor is independent of wall surface roughness for the flow in macroscale but in microscale, molecular interaction with the walls increases relatively to intermolecular interaction when compared to macroscale flows. Two boundary conditions are usually applied to characterize the flow phenomena in smooth channel in macroscale. No-slip boundary condition is the most common type of wall boundary condition implementation which can be applied for the assumption that the fluid next to the wall has the velocity as the wall which is normally zero. Another boundary condition is slip boundary condition where the shear stress at the wall is zero and the velocity of the fluid near the wall is not retarded by wall friction effects.

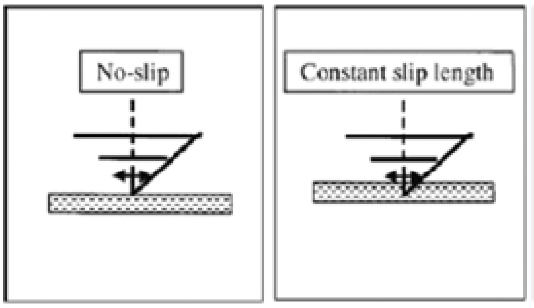

Fig. 3.1. No-slip and slip boundary flow[118] (Shui et al., 2007)

Slip flow is an important consideration because it may allow a significant reduction in the friction pressure drop and thus the pumping power required for microchannel reactors is less. While the underlying physical cause of slip is still not fully understood, what is clearly known is that an apparent slip occurs more readily on the surface which has opposite wet ability to the fluid, on rough surfaces, and at high shear rates. Slip may therefore become important in microchannel, as surface modification can be designed and assembled into microchannel reactors, surface roughness becomes significant relative to the channel size and due to their small dimensions, it is possible to obtain large shear rates[119] .

Recently, many researchers have suggested that the well-accepted no-slip boundary condition may not be suitable to predict the flow in microscale. Fluid slip may develop from soluble and entrained gases which form a gap near the wall. The effect of wall slip was studied by[120] Tretheway *et al.* (2002). It has been proved that no-slip boundary condition cannot be applied for all cases of flow in microchannels. By the experiment which was done to measure the velocity of water flowing in rectangular microchannel with dimension 30 μm height and 300 μm width at different positions from the wall with no-slip (water and hydrophilic wall) and slip (water and hydrophobic wall) boundary condition. The comparison of water velocity profiles from the experiment with no-slip and slip boundary condition show in figure 3.2.

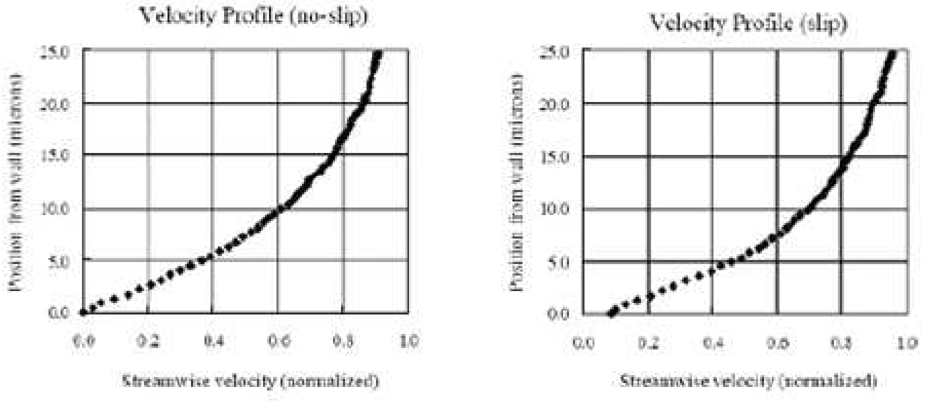

(a) (b)

Fig. 3.2. Velocity profiles of water flowing in microchannel with no-slip (a) and slip (b) boundary condition[121].

Figure 3.2a shows that no slip boundary condition can be used with the water flows in hydrophilic wall condition can as can be seen from the velocity profile at the wall position which approaches to zero while the velocity profile in figure 3.2b at the wall is larger than zero so the slip boundary condition can be applied. It can be concluded that no-slip boundary condition is not always valid and may not be accurate for fluid flow in microchannel but it depends on the interactions between the fluid and the properties of the wall surface.

3.3.3 Building Numerical Models for Micro-Flows

A high quality CFD simulation depended very much on the pre-processing stage, which includes meshing and boundary condition settings. Therefore, mesh quality is very critical to the accurate simulations. More uniform mesh and aspect ratio of mesh elements can improve the accuracy of numerical simulations. To calibrate the CFD models, mesh sensitivity and uniformity studies were performed.

Mesh Sensitivity Study

For a general CFD solution of the governing equations over a range of significantly different grid resolutions should be presented to demonstrate grid-independent or grid convergent result. Denser mesh elements can give better accuracy, however, the solving and post-processes would be slowed down and sometimes halt the system's operation. To give a sample of benchmarking process, a viscous flow in a rectangular microchannel was used to calibrate the CFD model.

3.4 Soft Lithography and Replica Molding

Soft lithography and replica molding is the process in which a polymeric microfluidic device is fabricated. This chapter will discuss the fabrication process in detail, discussing the required equipment and parameters which must be optimized to provide consistent and uniform PDMS surface properties. Since some of the chemicals used for the process can be dangerous, a brief summary on important safety issues and handling information will be reported. As well, for each fabrication step, this report will evaluate other alternative technologies available and how closely it can achieve the desired outcome. Common defect problems and design constraints for working with PDMS will also be discussed. By properly understanding all the factors affecting the fabrication process, a better insight can be gained and thereby improve the chances of producing high quality microfluidic chips.

The process of soft lithography and replica molding can be split into two portions: the creation of a master mold, and the creation of the subsequent individual polymeric microfluidic device. An overview of the fabrication process is shown in figure 3.3.

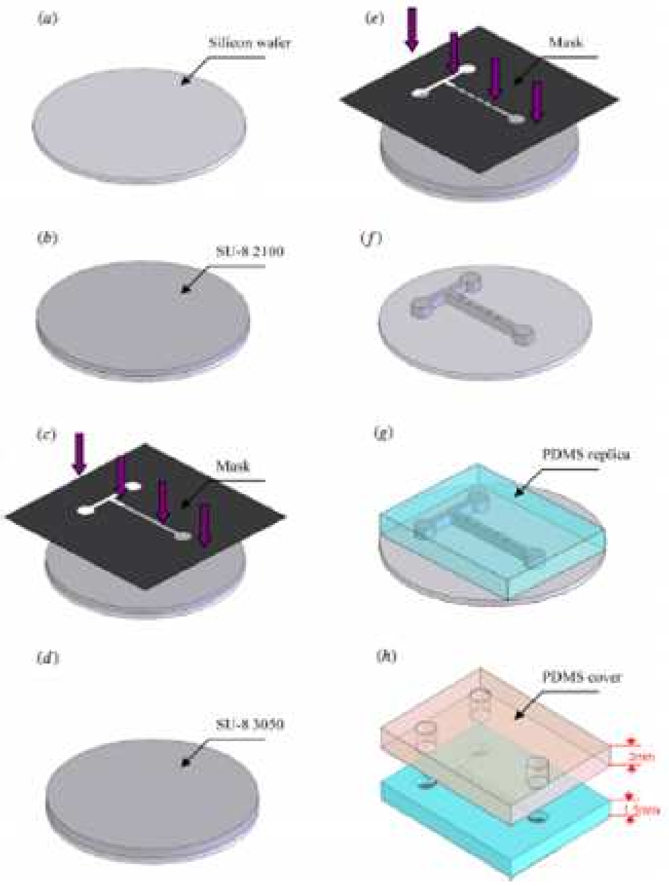

Fig. 3.3. Fabrication steps of the microchannel: (a) clean wafer, (b) first spin coating, (C) second spin coating, (e) second exposure, (f) development, (g) PDMS mold making and (h) UV/ozone and bonding.

3.4.1 Mask Fabrication

Soft lithography begins with a design that is printed onto a mask. A mask contains transparent and opaque regions corresponding to the patterns which are transferred onto the photoresist for the master fabrication. The photoresist used is SU-8, a negative photoresist that, when exposed by UV light, undergoes crosslinking thereby hardening the material and reducing the etching rate compared to noncrosslinked material. Therefore, the transparent regions on the mask must correspond to the raised channel regions on the master.

3.4.2 Designing the Layout

By using Corel Draw programs, it is possible to create the prints for any microfluidic device layout with very minimal costs. Once the design is complete, it is printed onto a mask, either directly using a laser printer with a transparency medium, or using an electron or laser beam source directed onto a chrome mask. There are two main types of masks commonly used for soft lithography applications. Chrome masks are used when high resolutions and small feature sizes in the range of 10 μm to 500 nm are required for the microfluidic channel layouts. Laser printed transparency masks are used when the channel widths are larger than 10 μm. It is interesting to note that the channel size in the fabrication of the master is dependent on the resolution of the printed mask; the widths and lengths of channel structures depend on the printed mask alone, however, the depths obtainable in the channel structures are dependent on the spincoated thickness of the photoresist, which will be discussed further in this chapter.

3.4.3 Chrome Mask

The utilization of a chrome mask can bring benefits in specific applications, such as the manufacturing of small rectangular posts for enhancing turbulent mixing in high Reynolds number flow[121] . as points of adhesion for seeding and growing cells[122] ,or as structural support of microchannels consisting of small heights but large widths which are prone to collapse. Due to its high costs and difficult fabrication process, all applications discussed in this report do not involve the use of chrome masks.

3.4.4 Laser Printed Transparency Mask

A more common method for producing masks in soft lithography applications is the use of commercial or “off the shelf” laser printers. Mask designs are printed using monochrome laser printer onto a normal transparency film. For laser printers, the constraining variable is the dots per inch (dpi) achievable by the printer. Commercial laser plotters can achieve a resolution of 20,000 dpi providing minimum feature sizes of approximately 12.5 μm. Due to the high initial and maintenance costs of such a printer, usually the design is outsourced. Lower resolution printers may be utilized depending on the application but should be used with caution. For example, transparency masks can be printed with a laser printer with 2400 dpi resolution, which can be utilized to fabricate structures larger than a width of approximately 500 μm. However, as the required feature sizes (such as channel width) decreases, the powder particles of the laser printer becomes relatively large compared to the channel width. In the extreme case, where the structures are at a scale that is just resolvable by the printer, certain sections of the channel will be blocked.

3.4.5 Substrate Types and Preparation

After the mask is obtained, the actual fabrication process begins with the selection of the substrate. The photoresist is then applied to the chosen substrate to form the master mold. The most common substrates used are glass and silicon. Glass substrates used in the fabrication of microfluidic devices are of the 1” by 3” microscope slides or 3” x 4” rectangular slides. These slides are inexpensive to use, with the average price of $0.50 for a microscope slide and $7.00 for a large slide. However, these have to be cleaned either using RCA or piranha-etch cleaning processes. In addition, due to its amorphous molecular structure, typically glass has a high degree of surface roughness, providing poor adhesion. Subsequently, these substrates require a more complicated fabrication process to compensate for their poor physical features, and also detrimentally affecting the reusability of the finished aster. Only simple (one level) fabrication involving relatively large dimension structures (greater than 500 μm in both length and width) should be made on glass substrates. Large surface area structures provide more points of contact between the photoresist and the substrate, providing better adhesion properties and subsequently improving reusability. On the other hand, silicon substrates are regularly used in the electronics fabrication industry, in which tight constraints such as surface uniformity and flatness is tightly controlled. Thus, the surface roughness is small and the substrate is uniform. This helps promote adhesion between the wafers and that of the SU-8 photoresist. In addition, no cleaning is necessary, as silicon wafers are fabricated directly for clean-room facility use. However, the disadvantage includes its relatively high costs of approximately $25.00 per wafer. In addition, due to the larger surface areas, more photoresist is required for spincoating. To increase the cost effectiveness, several designs are usually combined into each silicon wafer. It is possible, but rare for PDMS to be used for substrates. Due to the softness of the PDMS material, the substrate may deform, such that it is harder to control the accuracy of the relief structures. Any errors would be correspondingly transferred onto the final PDMS product. Even though the soft lithography fabrication process does not require a clean-room environment, it is important that the air is dust-free. In addition, all substrates should be cleaned prior to use. Any dust particles contaminating the substrate during photoresist deposition or during subsequent soft baking will distort the surface. For example, if the substrate contained dust particles during SU-8 deposition and spincoating, the contaminants acts as barriers to the flow of the photoresist, creating streaking patterns throughout. In addition, if dust particles fall onto the substrate during soft baking, these will result in halo patterns and pits surrounding the particles, as shown in figure 3.4.

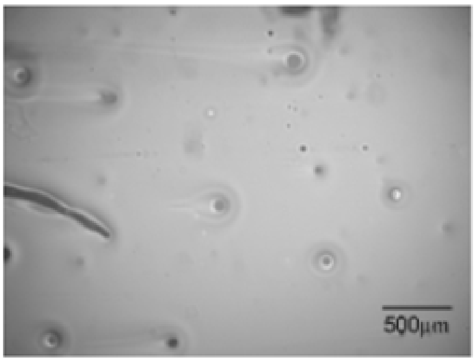

Fig. 3.4. Halos and pits surround locations of bubbles formed during spincoating.

SU-8 is a high contrast, epoxy based photoresist designed for micromachining and other microelectronic applications, where a thick chemically and thermally stable image is desired.

The exposed and subsequently cross-linked portions of the film are rendered insoluble to liquid developers. SU- 8 has very high optical transparency above 360nm, which makes it ideally suited for imaging near vertical sidewalls in very thick films. SU-8 is best suited for permanent applications where it is imaged, cured and left in place.

3.4.6 Process Guidelines

SU-8 is most commonly processed with conventional near UV (350-400nm) radiation, although it may be imaged with e-beam or x-ray. i-line (365nm) is recommended. Upon exposure, cross-linking proceeds in-two-steps (1) formation of a strong acid during the exposure process, followed by (2) acid-initiated, thermally driven epoxy cross-linking during the post exposure bake (PEB) step.

A normal process is: spin coat, soft bake, expose, post expose bake (PEB) and develop. A controlled hard bake is recommended to further cross-link the imaged SU-8 structures when they it will remain as part of the device. The entire process should be optimized for the specific application. A baseline process is given here to be used as a starting point.

3.4.7 Substrate Pretreatment

To obtain maximum process reliability, substrates should be clean and dry prior to applying the SU-8 resist. Start with a solvent cleaning, or a rinse with dilute acid, followed by a DI water rinse. Where applicable, substrates should be subjected to a piranha etch / clean (H_2SO_4 & H_2O_2). To dehydrate the surface, bake at 200°C for 5 minutes on a hotplate. For applications that require electroplating and subsequent removal of SU-8 apply MicroChem's OmniCoat prior to processing SU-8.

3.4.8 Coat

SU-8 resists are designed to produce low defect coatings over a very broad range of film thickness. The film thickness versus spin speed data displayed in table 3.2. and figure 3.5. provide the information required to select the appropriate SU-8 resist and spin conditions, to achieve the desired film thickness.

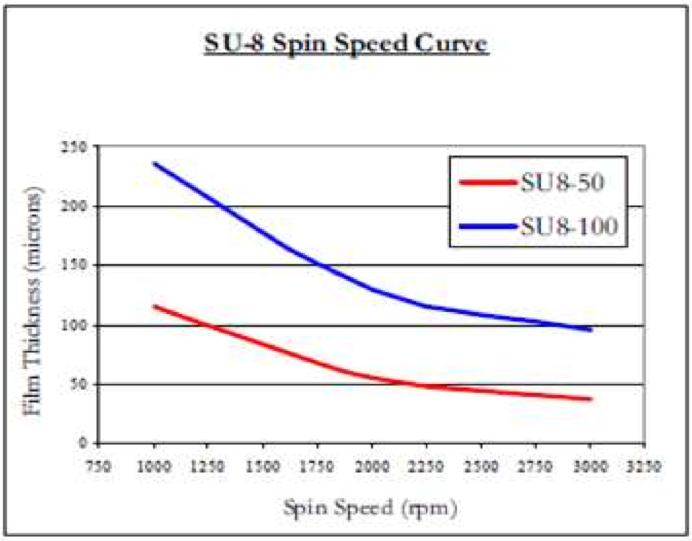

Fig. 3.5. Spinspeed vs. thickness curves for selected SU-8 resists.

The recommended coating conditions are:

(1) STATIC Dispense: Approximately 1ml of SU-8 per inch of substrate diameter. (2) Spread Cycle: Ramp to 500 rpm at 100 rpm/second acceleration. Hold at this speed for 5-10 seconds to allow the resist to cover the entire surface. (3) Spin Cycle: Ramp to final spin speed at an acceleration of 300 rpm/second and hold for a total of 30 seconds.

Table 3.2. Thickness vs. spin speed data for selected SU-8

Product Name	Viscosity (cSt)	Thickness (µms)	Spin Speed (rpm)
		40	3000
SU-8 50	12250	50	200
		100	1000
		100	3000
SU-8 100	51500	150	2000
		250	1000

3.4.9 Soft Bake

After the resist has been applied to the substrate, it must be soft baked to evaporate the solvent and density the film. SU-8 is normally baked on a level hot plate, although convection ovens may be used. The following bake times are based on contact hot plate processes. Bake times should be optimized for proximity and convection oven bake processes since solvent evaporation rate is influenced by the rate of heat transfer and ventilation. For best results, ramping or stepping the soft bake temperature is recommended. Lower initial bake temperatures allow the solvent to evaporate out of the film at a more controlled rate, which results in better coating fidelity, reduced edge bead and better resist -to-substrate adhesion. Refer to table 3.3 for TWO STEP contact hot plate process recommendations.

Table 3.3 Recommended soft bake parameters

Product Name	Thickness (µms)	Pre-bake @65°C	Softbake @95°C
	40	5	15
SU-8 50	50	6	20
	100	10	30
	100	10	30
SU-8 100	150	20	50
	250	30	90

3.4.10 Expose

SU-8 is optimized for near UV (350-400nm) exposure.1.line exposure tools are recommended. SU-8 is virtually transparent and insensitive above 400nm but has high actinic absorption below 350nm. This can be seen in Figure 3.6. Excessive dose below 350nm may, therefore, result in over exposure of the top portion of the resist film, resulting in exaggerated negative sidewall profiles or T-topping. The optimal exposure dose will depend on film thickness (thicker films require higher dosage) and process parameters. The exposure dose recommendations in table 3.4 are based on source intensity measurements taken with an i-line (365nm) radiometer and probe.

Expose tip: When using a broad spectral output source, for best imaging results, i.e. straightest sidewalls, filter out excessive energy below 350nm. Catastrophic adhesion failure, severely negative sidewalls and excessive cracking often indicate an under cross-linking condition. To correct the problem, increase the exposure dose and/or increase the post exposure bake (PEB) time.

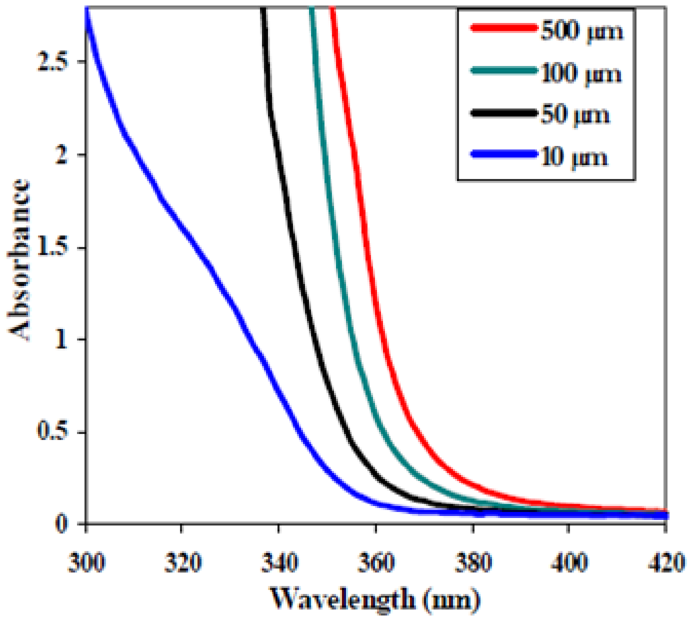

Fig. 3.6. SU-8 absorbance vs.film thickness.

Table 3.3. Recommended exposure dose processe.

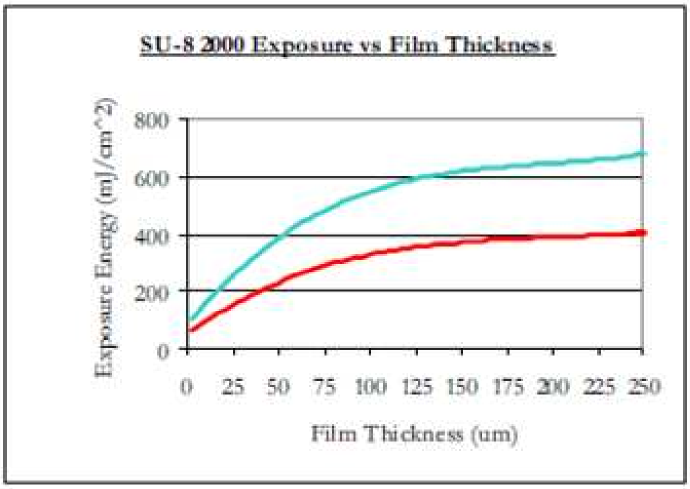

3.4.11 Post Exposure Bake

Following exposure, a post expose bake (PEB) must be performed to selectively cross-link the exposed portions of the film. This bake can be performed either on a hot plate or in a convection oven. Optimum cross-link density is obtained through careful adjustments of the exposure and PEB process conditions. The bake recommendations below are based on results obtained with a contact hot plate.

PEB tip: SU-8 is readily cross-linked and can result in a highly stressed film. To minimize stress, wafer bowing and resist cracking, a slow ramp or TWO STEP contact hot plate process, as shown in table 3.4, is recommended. Rapid cooling after PEB should be avoided.

Table 3.4. Recommended post exposure bake parameters

Product Name	Thickness (µms)	Pre-bake @65°C	Softbake @95°C
	40	1	4
SU-8 50	50	1	5
	100	1	10
	100	1	10
SU-8 100	150	1	12
	250	1	20

3.4.12 Develop

SU-8 resists have been optimized for use with MicroChem’s SU-8 Developer. Immersion, spray or spray- puddle processes can be used. Other solvent based developers such as ethyl lactate and diacetone alcohol may also be used. Strong agitation is recommended for high aspect ratio and/or thick film structures. Recommended develop times are given in table 5 for immersion processes. These proposed develop times are approximate, since actual dissolution rates can vary widely as a function of agitation rate, temperature and resist processing parameters.

Table 3.5. Recommended develop processes

Product Name	Thickness (µms)	Development (minutes)
	40	6
SU-8 50	50	6
	100	10
	100	10
SU-8 100	150	15
	250	20

3.4.13 Rinse and Dry

Following development, the substrate should be rinsed briefly with isopropyl alcohol (IPA), then dried with a gentle stream of air or nitrogen.

Rinse tip: If a white film is produced during rinse, this is an indication that the substrate has been under developed. Simply immerse or spray the substrate with SU-8 developer to remove the film and complete the development process. Repeat the rinse step.

3.4.14 Hard Bake (cure)

SU-8 has good mechanical properties, therefore hard bakes are normally not required. For applications where the imaged resist is to be left as part of the final device, the resist may be ramp/step hard baked between 150-200°C on a hot plate or in a convection oven to further cross link the material. Bake times vary based on type of bake process and film thickness.

3.4.15 Remove

SU-8, after expose and PEB, is a highly cross-linked epoxy, which makes it extremely difficult to remove with conventional solvent based resist strippers.MicroChem’s Remover PG will swell and lift off minimally cross-linked SU-8 2000 However, if OmniCoat has been applied immersion in Remover PG should effect a clean and thorough Lift-Off of the SU-8 2000 Material. It will not remove fully cured or hard baked SU-8 2000 without the use of OmniCoat. Alternate removal processes include immersion in oxidizing acid solutions such as piranha etch / clean, plasma ash, RIE, laser ablation and pyrolosis. To remove minimally cross-linked SU-8 2000, or if using Omnicoat, with Remover PG, heat the bath to 50-80°C and immerse the substrates for 30-90 minutes. Actual strip time will depend on resist thickness and cross-link density For more information on MicroChem Omnicoat and Remover PG please see the relevant product data sheets.

3.4.16 Storage

Store SU-8 resists upright in tightly closed containers in a cool, dry environment away from direct sunlight at a temperature of 40-70°F(4-21°C). Store away from light, acids, heat and sources of ignition. Shelf life is twelve months from date of manufacture.

3.4.17 Disposal

SU-8 resists may be included with other waste containing similar organic solvents to be discarded for destruction or reclaim in accordance with local state and federal regulations. It is the responsibility of the customer to ensure the disposal of SU-8 resists and residues made in observance all federal, state, and local environmental regulations.

3.4.18 Environmental, Health and Safety

Consult product Material Safety Data Sheet before working with SU-8 resists. Handle with care. Wear chemical goggles, chemical gloves and suitable protective clothing when handling SU-8 resists. Do not get into eyes, or onto skin or clothing. Use with adequate ventilation to avoid breathing vapors or mist. In case of contact with skin, wash affected area with soap and water. In case of contact with eyes, rinse immediately with water and flush for 15 minutes lifting eyelids frequently. Get emergency medical assistance. The information is based on our experience and is, we believe to be reliable, but may not be complete. We make no guarantee or warranty, expressed or implied, regarding the information, use, handling, storage, or possession of these products, or the application of any process described herein
or the results desired, since the conditions of use and handling of these products are beyond our control.

3.4.19 Solvent compatibility

Solvent compatibility of SEBS gels was characterized by measuring swelling ratios of elastomer samples after immersion in different solvents at room temperature, similar to procedures previously employed for PDMS.115 Dimensions of rectangular pieces were measured using precision calipers and placed in the solvents for 24 h, after which their lengths were measured again while still in the solvent. Swelling ratios were determined as the ratio of the final to initial lengths. Measurements were made from five separate pieces and then averaged to compute the final swelling ratio. These results (Table 3.6.) indicate that SEBS gels are compatible with a wide range of solvents.

Table 3.6. swelling ratios for SEBS gels ranging from 9-33 wt% copolymer.

Solvent	Swelling ratio
Acetone	1.02-1.15
2-propanol	0.86-0.94
Methanol	1.00
Ethanol	1.00
Water	1.00
Sodium hydroxide solution (aq. 50% w/w)	1.02-1.07
Sulfuric acid	1.00*
Toluene	Incompatible
chloroform	Incompatible

*Only 33 wta5 gel composition was tested.

3.5 Microfluidic Mixing Visualization

Most of the conventional fluid field measurement methods were not suitable for microfluidic environments. Even though the µPIV technique has been researched since 1998[123], its complexity forbids it being widely used in general microfluidic research centers. For studying microfluidic mixing, fluorescent dyes, food colouring dyes, and ultraviolet absorption techniques have been used for measurement and evaluation ofmixing performance. In this research, food colouring dyes are used to visualize the flow and mixing process.

Two colouring aqueous solutions have been applied in the study. One was mixture of water and 2:4% food dye E102 and E122 (Yellow). Another one was mixture of water and 2:1% food dye E133 (blue) (Queen Fine Foods Pty Ltd, Australia). The two aqueous solutions were respectively introduced to the channel from two inlets by capillary effect. The viscosity of the food dye/water solution was estimated as being approximately the same as water, and the diffusion coefficient was calculated according to the chemical groups[124]. Figure 3.7. shows the laboratory testing devices for visualizing mixing performance.

The micro-mixer was filled with two different food colouring dye aqueous solutions, and the broadening of mixed region was observed under an optical microscope. The image was captured by a charge-coupled device (CCD) camera, and then transferred to the image capture card in the computer.

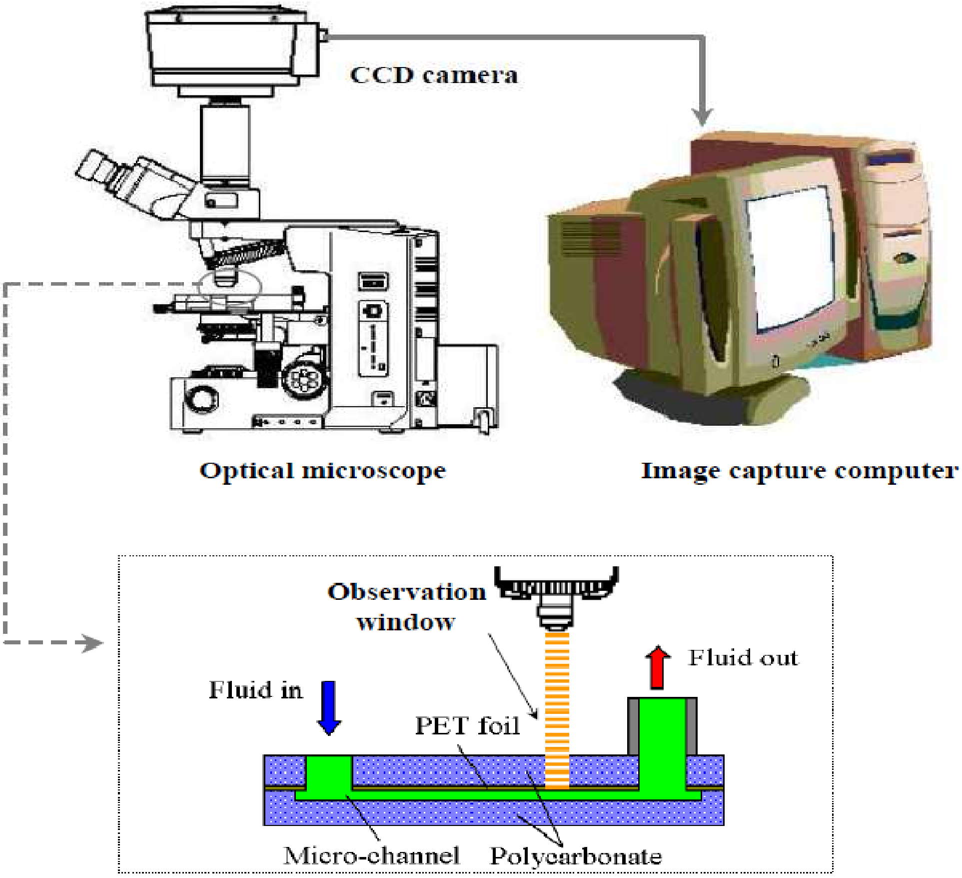

Fig 3.7. Laboratory setup for micro-mixing visualization.

3.6 Summary

Most of micro flows are laminar with non-slip boundary conditions. For laminar incompressible viscous flow, advanced microfluidic CFD techniques can be applied to provide accurate solutions to microfluidic problems. To achieve a reliable CFD prediction of fluid behavior, the model needed to be built carefully with the assistance of a sensitivity study. The simulation of mass transport was very sensitive to the mesh quality. To achieve a reliable CFD simulation, the mesh density should be done.

Typical simulations were selected to be validated by experiments. Simple experimental testing equipment was setup for carrying out tests. The equipment included an optical microscope, a CCD camera and an image capture computer. The simple laboratory configuration could give qualitative comparisons between experiment visualizations and numerical simulations. A fabrication technique to produce simple micromixers in microchannels was also described.

In the fabrication of a microfluidic device, many factors must be considered.

- Dimensions such as length and width of the microchannels are mainly constrained by the minimum resolution obtainable by commercial printers. In addition, once the masks are obtained, the lengths and widths of the microchannel layouts cannot be changed.
- Conversely, the microchannel depth can be changed for different masters depending on the fabrication process based upon the following spincoating parameters:
  - Photoresist viscosity (or grade)
  - Spin speed
  - Spin duration
- UV exposure dose, soft bake, PEB, and development times are dependent on the thickness of the photoresist layer.
- Slow cooling rates and sufficient wait times in between heating processes should be employed to reduce thermal stresses and prolong reusability of the masters.

Chapter 4

Mixing Patterns in T-Micromixers

4.1 Introduction

Effective mixing in small volumes is a crucial step in many chemical and biochemical processes, where microreactors are used to ensure a fast homogenization of the reactants. Physically, liquid flows in microfluidic channels are characterized by low values of the Reynolds number and, in general, large values of the Peclet number. Accordingly, since general strategies of flow control in microfluidic devices should not depend on inertial effects, reduction of the mixing length requires that there must be transverse flow components. In this chapter, three-dimensional numerical simulations were performed to study the flow dynamics and mixing characteristics of liquid flows inside T-type micromixers. The effects of various operating and design parameters on the flow dynamics and the mixing quality were investigated in order to optimize the mixing process. Due to the simple fabrication technology of passive T-shaped micromixers (hereby indicated as T-micromixers;(Fig. 4.1)) and its easy implementation in complex microfluidic systems, flow mixing mechanisms in this type of mixers were the focus of many investigations. The present study focuses on improving the mixing efficiency of T-micromixers by investigating the effects of different flow parameters, such as the inlet flow velocity, the diffusion coefficient and several geometrical parameters such as the width, height and inlet angle of the mixing channel. To do that, a commercial Computational Fluid Dynamic (CFD) code, i.e. FLUENT 6.3 by Ansys Inc., was used to solve the three-dimensional flow and mass transfer equations in the proposed geometrical configurations.

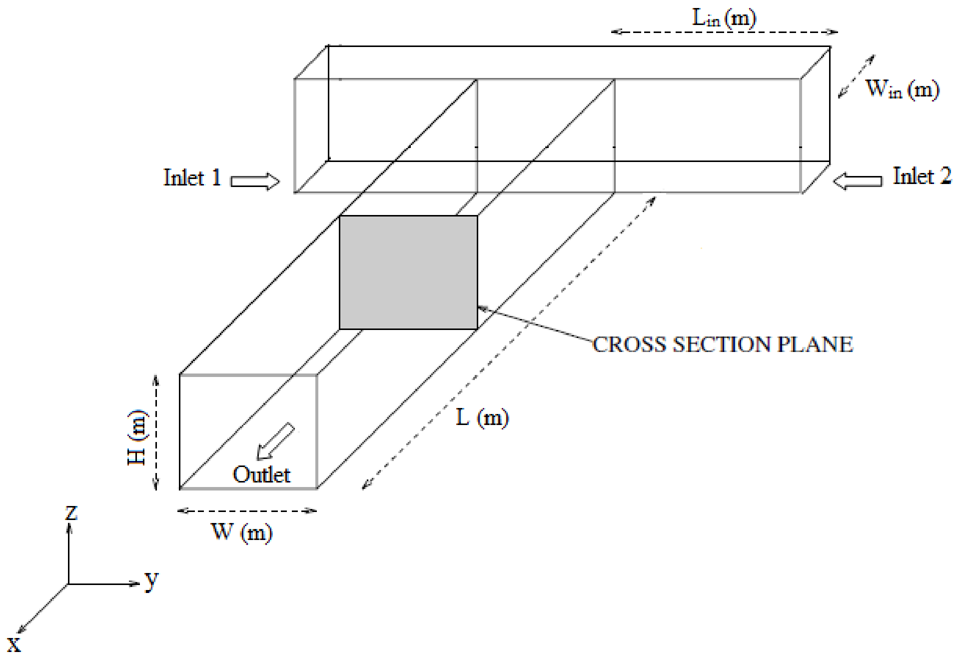

Fig. 4.1. Schematics of the T-mixer.

4.2 Design and Numerical Modeling

In order to obtain high quality structured mesh elements, a CFD reprocessing package, Gambit v2.04, was used to build 3D models and 8-node hexahedral elements.

For all the studies in this chapter, the T-type (Y-type) channels were used, with two inlets and one outlet .The width of the inlets is half of the width of the outlet channel. In order to reduce computing time, we used inlets channel length of only 1 mm while the velocity profile of a fully developed flow is set to both entrances (Sec. 4.3 and Chap 8) and length of the mixing channel has fixed to 3×10 $^{-3}$ m. The length of the inlet, L_{in}, is not critical but should be sufficient for fully developed flow or we should use fully developed velocity profile in each inlet (Sec. 4.3 and Chap8) .The main channel length is should be enough to reach fully developed flow while we use out flow as a boundary conditions for outlet but in pressure outlet boundary condition we need just to have mixing zone (Sec. 4.3).

The simulation was run as 3D, steady, laminar, Newtonian, with no slip wall, velocity inlet and pressure outlet boundary conditions for two fluids to evaluate the dispersion of one fluid into another.

Two fluids entered the two inlets respectively (red dye aqueous solution and blue dye aqueous solution), with a diffusion coefficient, $D = 3\times 10^{-10}$ m^2/s, which was calculated according to their chemical groups [123](Reid et al. 1987). The results in Figure 4.2 show that two fluid streams colored red and blue were pumped into a T-type mixer via two inlets. The mass fraction of fluid 1 was determined as a relative percentage to fluid 2. A mass fraction of 0.0 indicates 100% concentration of fluid 1, and a mass fraction of 0.5 denotes a complete mixture with equal quantities of fluid 1 and 2. A mass fraction of 1.0 denotes a 100% concentration of fluid 2. As the concentration of two streams equaled each other, the mass fraction of homogenous solution would be 50%.

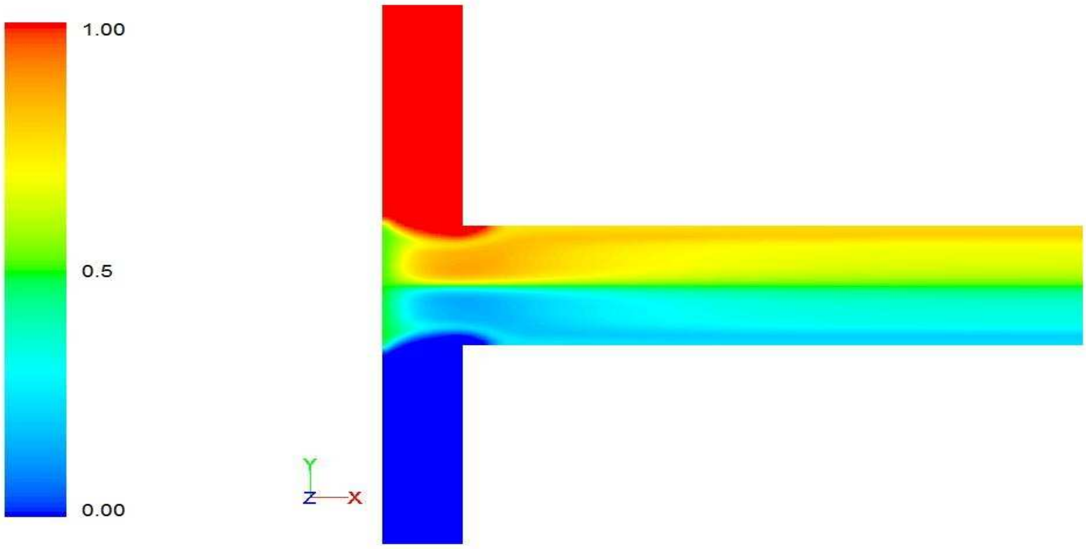

Fig. 4.2. mass fraction in contour plot.

4.3. The Channel Length (inlet and mixing)

The minimum required inlet lenght that ensures a solution independent of the inlet lenght is determined numerically by Hussong[125] and soleymani[126].

Hussong showed that inlet length (L_{in}) should be at least three times the channel height $L_{in} \geq 3H$ in other case flow can be forced back to a reflectional-symmetric flow state, if a fully developed velocity profile is prescribed too close to the mixing channel inlets.

The fully developed velocity profile in a closed rectangular conduit can be easily obtained by solving the Navier-Stokes equations with no-slip boundary conditions at the walls and a constant axial pressure gradient *G*. For our purposes, the most convenient form of this solution is [127]-[128]:

$$u(x,z) = -\frac{G}{2\mu}x(X-x) - \frac{4GX^2}{\mu\pi^3}\sum_{k\ \mathrm{odd}}\frac{1}{k^3}\sin\left(k\pi\frac{x}{Y}\right) \left[\mathrm{Cosh}\left(k\pi\frac{z}{x}\right) - \mathrm{Tanh}\left(\frac{k\pi}{2\eta}\right)\mathrm{Sinh}\left(k\pi\frac{z}{x}\right)\right] \tag{4.1}$$

where u is the fluid velocity along the *y* axis, X and Z are the sizes of the conduit, while η=X/Z is the aspect ratio.

From this expression, we can derive the pressure gradient *G* as a function of mean velocity $\bar{u}$, finding:

$$G = -\frac{12\mu\bar{u}}{Y^2}\left[1 - \frac{192}{\pi^5}\eta\sum_{k\ \mathrm{odd}}\frac{1}{k^5}\mathrm{Tanh}\left(\frac{k\pi}{2\eta}\right)\right]^{-1} \tag{4.2}$$

Soleymani et al. analyzed the set of data obtained from numerical simulations and defined the length of the mixing zone (control volume) at the inlet, L_y, and along the mixing channel L_x as the distance from the confluence of the inlet channels at which the flow is deflected, and the length of the mixing channel in which the streamlines are strongly bent and the laminar flow has not readjusted, respectively (Fig. 4.3).

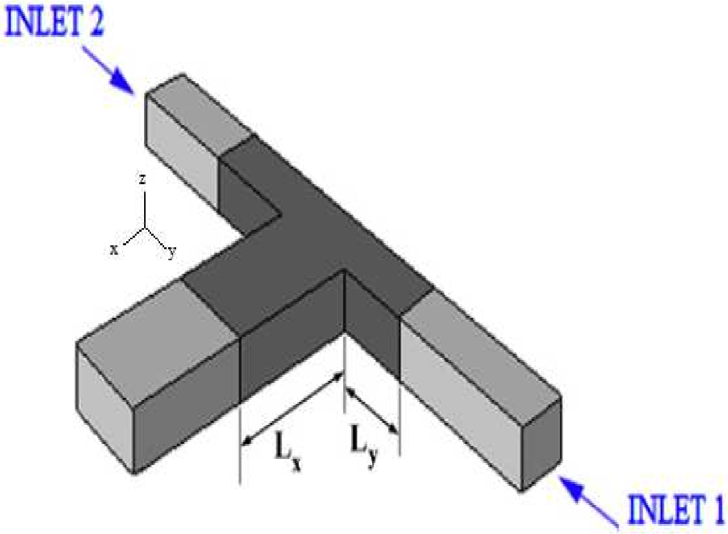

Fig. 4.3. Mixing zone (the dark area) in a T-mixer.

$$\frac{L_x}{D_h} = \begin{cases} (0.0576 + 0.00156\mathrm{Re})(1 - 0.1635\mathrm{Dr} + 4.2433\mathrm{Dr}^2) \text{ if } K < 100 \\ (-2.389 + 0.0348\mathrm{Re})(1 - 1.458\mathrm{Dr} + 1.0856\mathrm{Dr}^2) \text{ if } K \geq 100 \end{cases} \tag{4.3}$$

where Re is the Reynolds number in the mixing channel based on the hydraulic diameter of the mixing channel, D_h, Dr is the ratio between the hydraulic diameter of the mixing channel and the hydraulic diameter of the inlet channels, $D_h/D_{h\text{- in}}$ and K is the identification number describing the flow regime inside a micro T-mixer, defined as,

$$K = \mathrm{Re}^{0.82}\left(\frac{W_{in}}{H}\right)^{-0.79}\left(\frac{D_{h-in}}{d_h}\right)^{-1.5}\left(\frac{W}{H}\right)^{0.15} \tag{4.4}$$

It has been shown that at the critical value of K = 100 a transition from vortex flow to the engulfment flow regime can be observed. Above the critical value of K = 100, the flow is in the engulfment regime.

In the same way, the correlation for the L_y is the following:

$$\frac{\mathrm{L_y}}{\mathrm{D_{h-in}}} = \begin{cases} (0.6342 + 0.0038\mathrm{Re_{in}})(-3531\mathrm{Dr_{in}^{-1}} + 1 + 0.131\mathrm{Dr_{in}}) \\ \text{if } \mathrm{K} < 100 \\ (9.1852 + 0.01334\mathrm{Re_{in}})(-0.5744\mathrm{Dr_{in}^{-1}} + 1 - 0.3521\mathrm{Dr_{in}}) \\ \text{if } \mathrm{K} \geq 100 \end{cases} \tag{4.5}$$

where $\mathrm{Re_{in}}$ is the Reynolds number in the inlet channels based on the hydraulic diameter of the inlet channels, $\mathrm{D_{h\text{-}in}}$. Here $\mathrm{Dr_{in}}$ is defined as,

$$\mathrm{Dr_{in}} = {}^{\mathrm{D_{h-in}}}\!/_{\mathrm{D_{h-w/2}}} \tag{4.5}$$

where $\mathrm{D_{h\text{-}\ w/2}}$ is the hydraulic diameter of a rectangular surface of dimensions W/2 × H (half of the width of the mixing channel × the depth of the channels). The proposed correlations for the calculation of the control volume dimensions ($\mathrm{L_x}$ and $\mathrm{L_y}$). More discussion in this subject is available in chapter 8.

4.4 Results and Discussions

4.4.1 Flow rate

First, we investigated the effects of varying flow rates with a fixed channel geometry, with height H = 2×10^{-4}m and width W = 3×10^{-4}m .In this and the following subsections, we have assumed that the inlet flow rates are equal to each other, while the case of different flow rates is considered in section 4.4.4. In figure 4.4., the degree of mixing is plotted as a function of the Reynolds number

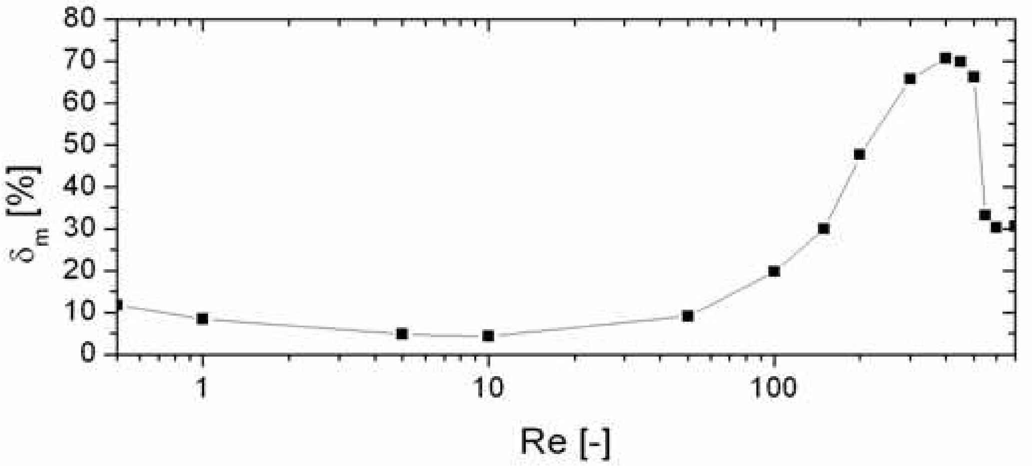

Fig. 4.4. Variation of the degree of mixing δ_m as a function of the Reynolds number, Re, for width W=3×10^{-4}m, and height H=2×10^{-4}m.

at the outlet. to quantitatively evaluate the performance of mixing, The mixing quality can be evaluated through the mean square deviation of the normalized concentration[129]-[130], which is defined at any cross section (in the plane yz) normal to the flow direction, x, as,

$$\sigma^2(\mathrm{x}) = \frac{1}{A}\int_{\mathrm{A}} \left[\frac{\mathrm{c(x,y,z)}}{\bar{\mathrm{c}}(\mathrm{x})} - 1\right]^2 \mathrm{dydz}$$

i.e.,

$$\sigma^2(x) = \frac{1}{N}\sum_{i=1}^{N}\left(\frac{c_i(x)}{\bar{c}(x)} - 1\right)^2 \tag{4.6}$$

where N is the number of sampling points within the cross section A, c_i is the concentration of one of the two species at point i, while $\bar{c}$ is its mean concentration within the cross section, i.e.

$$\bar{c}(x) = \frac{1}{A}\int_A c(x,y,z)\,dydz = \frac{1}{N}\sum_{i=1}^{N} c_i \tag{4.7}$$

Clearly, since the velocity field is not uniform within a cross section, $\bar{c}$ will vary along the channel. At steady state, $\bar{c}$ tends asymptotically (at large x, when the concentration field is uniform) to the contaminant flow to total flow rate ratio,

$$\bar{c}_{cm} = \frac{\dot{V}}{\dot{V}_{tot}} = \frac{\int_A c(x,y,z)\,u(x,y,z)\,dydz}{\int_A u(x,y,z)\,dydz}$$

i.e.,

$$\bar{c}_{cm} = \frac{\sum c_i u_i}{\sum u_i} = \frac{\sum c_i u_i}{N\bar{u}} \tag{4.8}$$

where u_i is the axial velocity at point i, while $\bar{u}$ is the mean velocity. This is the “cup mixing” or “bulk” average concentration,[131] that is the concentration that we would measure if we collected the efflux from the channel in a cup and mix the content to yield a uniform concentration.

To appreciate the difference between the two averages, consider two fluid species, say 1 and 2, that at the inlet occupy the right and left side of a 2D Poiseuille channel flow. Denoting by $\dot{m}_1$, ρ_1, A_1 and $\dot{m}_2$, ρ_2, A_2 the mass flow rate, density and cross sectional area of fluid 1 and of fluid 2, respectively (with $\dot{m} = \dot{m}_1 + \dot{m}_2$ and $A=A_1+A_2$), we easily find the following relation:

$$\frac{\dot{m}_1}{\dot{m}_2} = \left(\frac{\rho_1}{\rho_2}\right)\left(\frac{A_1}{A_2}\right)^2 \tag{4.9}$$

Therefore, we see that, as the minority fluid (with slower velocity or larger density) species has a lower mean velocity, it occupies more space within the channel than its share based on mass flow rates.

Consider, for example, the case when $\rho_1 = \rho_2$ and $\dot{m}_1 = 4\dot{m}_2$, i.e. $\dot{m}_2/\dot{m} = 1/5$, so that $A_1 = 2A_2$., i.e., $A_2/A=1/3$. Then, applying Eq. (4.7) and Eq. (4.8), we see that at the entrance the mean concentration is $\bar{c} = A_2/A = 1/3$, while the bulk mean concentration is$\bar{c}_{cm} = \dot{m}_2/\dot{m} = 1/5$. Now, when we move down the channel, the bulk concentration will remain constant, while the mean concentration will decrease. In fact, as fluid *2* moves towards the central part of the cross section, it would also accelerate so that, effectively, it will occupy a smaller portion of the cross section. At the end, the mixture will have a uniform concentration, so that $\bar{c} = \bar{c}_{cm} = 1/5$.

Based on the above considerations, we will use a definition of mixing efficiency based on material fluxes, instead of concentration, as the former, not the letter, are conserved quantities. Accordingly, we define a cup mixing flow variance as:

$$\sigma_{cm}^2(x) = \frac{1}{A}\int_A \left[\frac{u(x,y,z)c(x,y,z)}{\bar{u}\,\bar{c}_{cm}} - 1\right]^2 dydz$$

i.e.

$$\sigma_{cm}^2 = \frac{1}{N}\sum_{i=1}^{N}\left(\frac{u_i\,c_i}{\bar{u}\,\bar{c}_{cm}} - 1\right)^2 \tag{4.10}$$

where $\bar{u}\bar{c}_{cm}$ is the (constant) contaminant flux. Finally, note that in the important case where $\dot{V}_1 = \dot{V}_2$, Eq. (4.9) shows that $S_1=S_2$ and therefore $\bar{c}$, like $\bar{c}_{cm}$, is constant at each cross section.

For sake of convenience, here we will use the following definition of degree of mixing,

$$\delta_m = 1 - \sigma_{cm} \tag{4.11}$$

We expect that δ_m increases monotonically with x, tending asymptotically to 1 as the two fluids mix completely.

Based on the average velocity and the hydraulic diameter in the mixing channel, the Reynolds number was let vary from 0.5 to 700. As we see, when we increase the Reynolds number, at first (i.e. for $Re < 10$) the mixing efficiency decreases, then (at $Re \cong 10$) it starts to increase, until (at $Re \cong 300$) it reaches a plateau; at this point, at $Re \cong 500$, it starts to decrease sharply, until (at $Re \cong 550$) it reaches a constant value. As we will see in the following, similar behavior was observed also for different values of the channel width and heights.

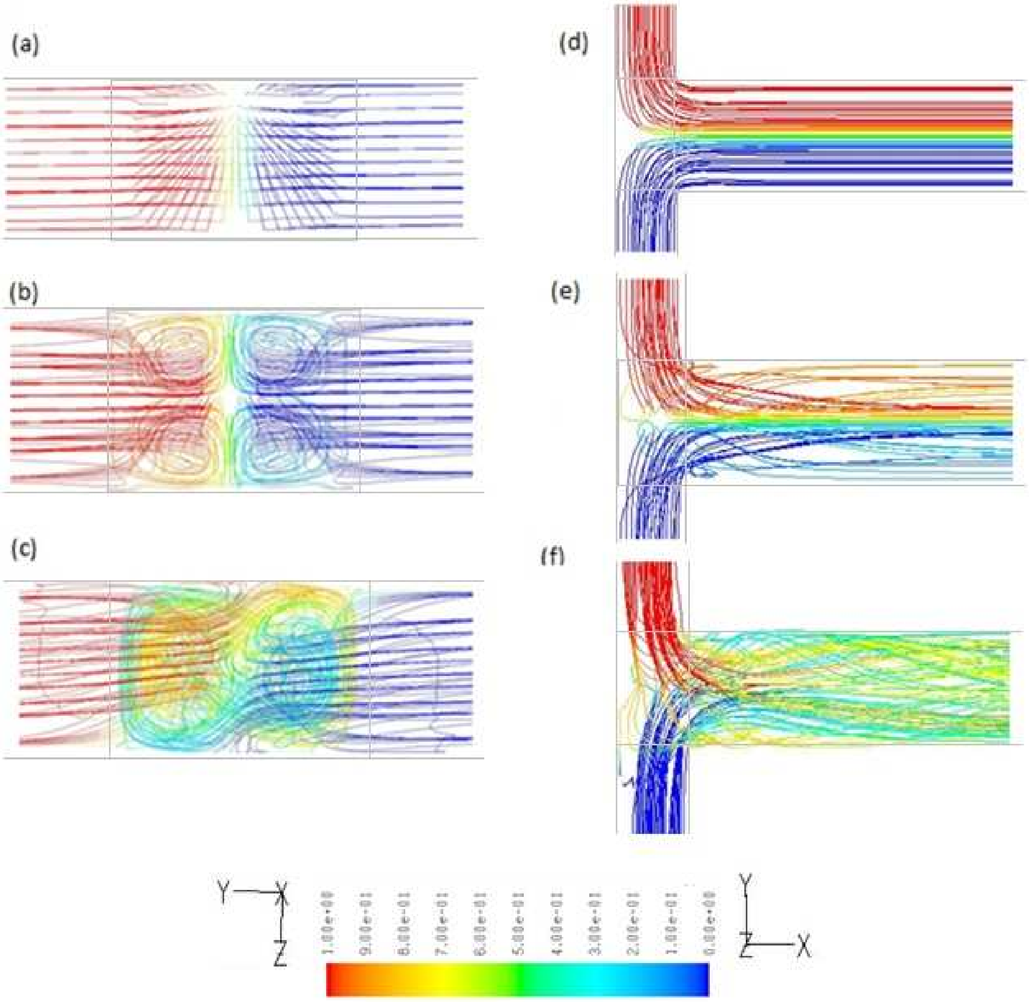

Fig. 4.5. Pathlines at the entrance and along the mixing channel for different flow regimes, namely, stratified, vortex and engulfment flows. (a),(d) Re = 10; (b),(e) Re = 150, and (c),(f) Re = 300. Here W=3×10 $^{-4}$m and H=2×10 $^{-4}$m.

In figure 4.5 the streamlines at different Reynolds numbers are shown. We see that at very low Reynolds numbers (in our case Re < 50) the flow is strictly laminar (stratified flow) and the mixing is entirely due to molecular diffusion (Fig. 4.5a and 4.5d). Accordingly, when the flow rate increases, provided that the flow regime remains stratified, the mixing efficiency will decrease, as the fluid residence time decreases.

For moderate ($50<Re<200$) Reynolds numbers, we observe the formation of vortices at the confluence of the inlet flows, (Fig. 4.5b and e) indicating the predominance of convective transfer, thus explaining the increase in the mixing efficiency seen in figure 2. However, the main mixing principle is still diffusion and the axial mirror symmetry within the mixing channel is preserved.

At higher Reynolds numbers ($200<Re<550$), though, complex convection-dominated mixing mechanisms are observed and the axial mirror symmetry breaks down (Fig. 4.5c and f). The ensuing engulfment increases the contact area, thus reducing the mixing length and further increasing the degree of mixing. The critical Reynolds number, where this transition takes place, depends on the geometry and the flow conditions, as we indicate below.

4.3.2 Effect of Channel Widths

The aspect ratio H/W of the mixing channel is one of the critical parameter of microchannels. In all the simulations in this subsection, the channel height H was kept constant at 2×10^{-4}m, while the width was let vary between 75×10^{-6}m and 7×10^{-4}m . Again, the flow rates in the two inlets were assumed to be equal to each other, with the Reynolds number at the outlet varying from 0.5 to 700. Figures 4.6(a) and (b) show the variation of the mixing efficiency as a function of the outlet Reynolds number with different values of W. We see that, while, when $W > 2\times10^{-4}$m the plots exhibit the same characteristic as those explained in the previous subsection, for smaller values of W, after an initial decrease, the mixing efficiency increases and seems to tend to a constant value, without ever reaching the decreasing region.

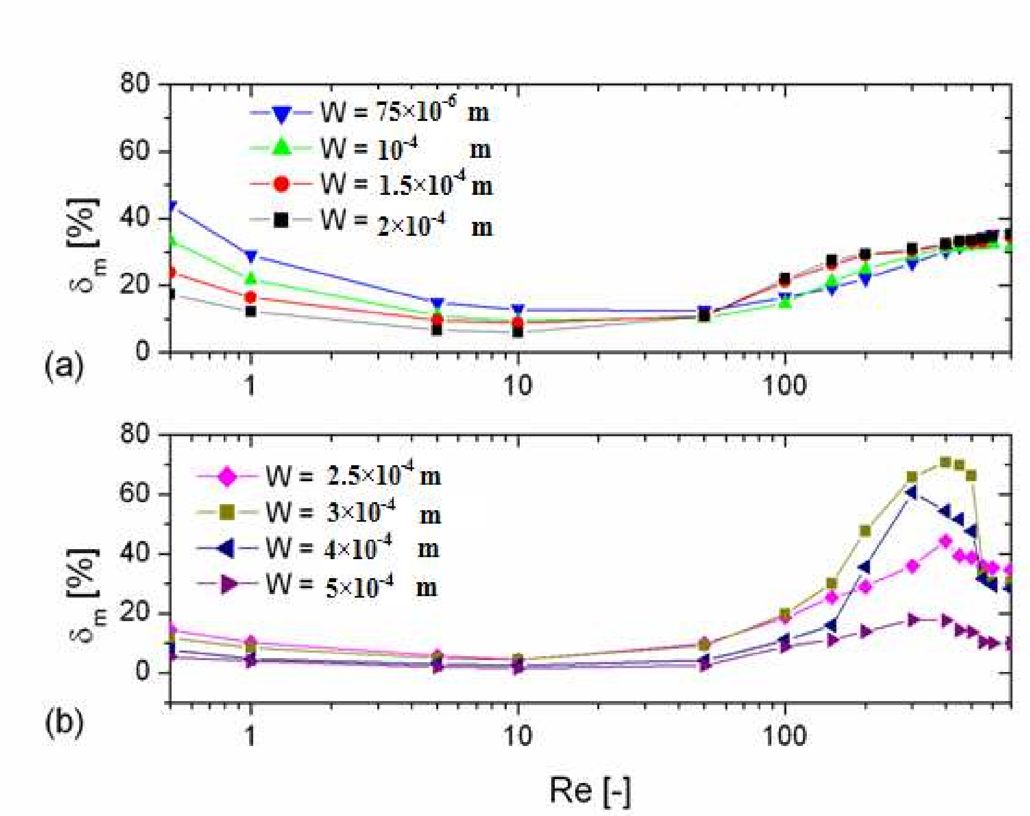

Fig. 4.6. Variation of the degree of mixing, δ_m, as a function of the Reynolds number, Re, for different values of the width, W, and fixed height, $H=2\times10^{-4}$m.

These results can be explained considering the changes in the flow patterns and the appearance of vortices occurring at different aspect ratios and flow rates. In fact, for high aspect ratios, i.e. small W (Fig.4.7a and e), the engulfment regime is never observed, as there is not enough “room” to form structured vortices, unless we have turbulent flow. On the other hand, for small aspect ratios, i.e. large W, transitions from stratified to vortex flow (Fig.4.7b and f) and then to engulfment flow (Fig.4.7c and g) are observed. Accordingly, decreasing the aspect ratio (i.e. increasing *W*) leads to damping the vortices, thus decreasing the mixing efficiency (Fig.4.7 d and h).

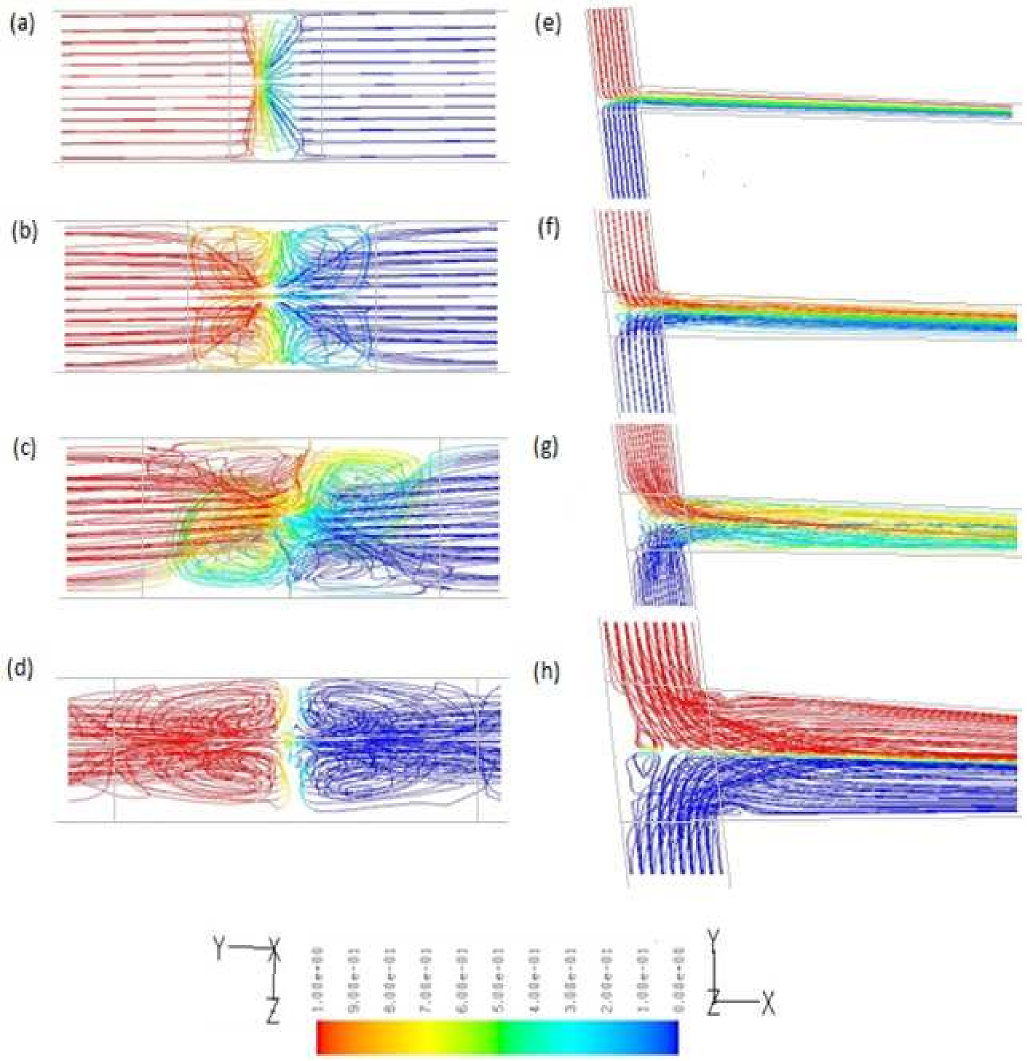

Fig. 4.7. Pathlines at the entrance and along the mixing channel for $H=2\times10^{-4}m$, $Re = 300$ and at different widths; (a),(e) $W=75\times10^{-6}$m ; (b),(f) $W=2\times10^{-4}$m ; (c),(g) $W=3\times10^{-4}$m; and (d),(h) $W=5\times10^{-4}$m

4.3.3 Effect of Channel Heights

In all the simulations of this subsection, the channel width W was kept constant at 2×10^{-4}m , while the height was let vary between 75×10^{-6}m and 3×10^{-4}m . At low height (Fig.4.8a and e), the flow inside the mixing channel tends to be in the stratified regime, due to high friction at the wall. Therefore, at small Reynolds numbers, the degree of mixing decreases at increasing H, while it increases at large Reynolds numbers, as the limited height within the channel tends to damp all vortices. Similar to what we observed in the previous subsection (i.e. when we varied W), when H is increased, changes in the flow patterns are observed, namely, a transition from stratified flow to vortex flow (Fig. 4.8b and f) and then to engulfment flow (Fig. 4.8c and g). In particular, we determined a value of H, where the degree of mixing reaches a maximum, corresponding to an optimal vortex formation. Then, increasing the aspect ratio even further leads to a vortex damping (Fig. 4.8d and h) and therefore to a decrease of the degree of mixing. The degree of mixing as a function of Reynolds number for different geometry is shown in figure 4.9.

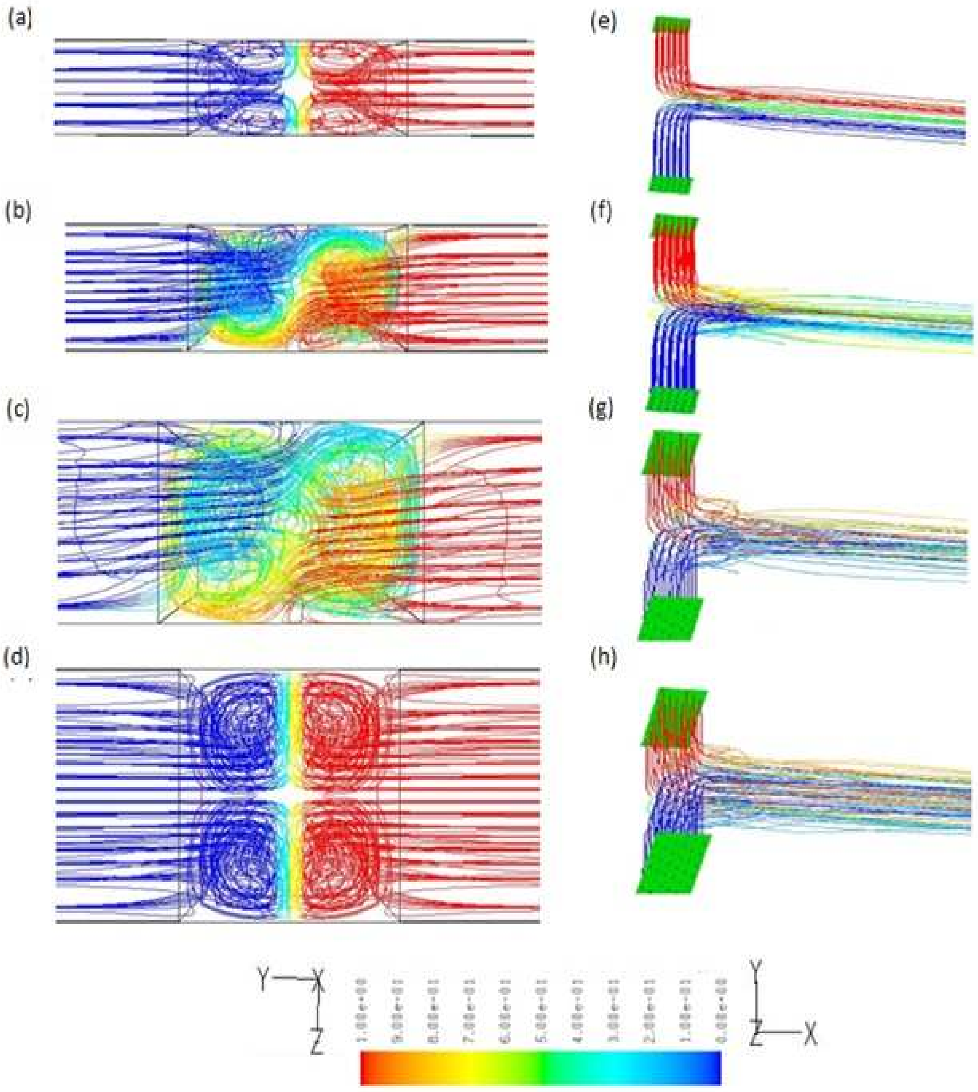

Fig. 4.8. Pathlines at the entrance and along the mixing channel for a fixed width, $W=2\times10^{-4}$m , Re = 200 and different heights, H (a),(e) $H = 75\times10^{-6}$m, (b),(f) $H = \times10^{-4}$m ; (c),(g) $H = 2\times10^{-4}$m, and (d),(h) $H=3\times10^{-4}$m.

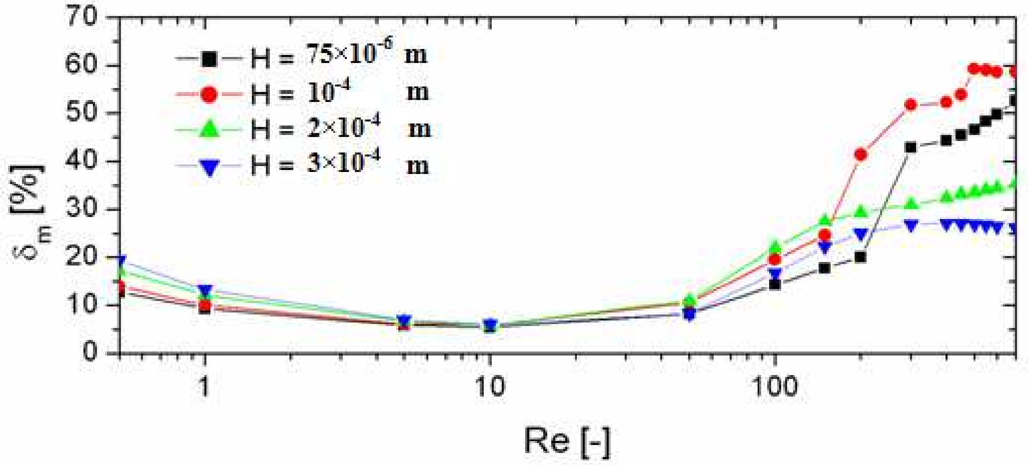

Fig. 4.9. Degree of mixing δ_m as a function of the Reynolds number, Re, for different channel heights, H, and width $W=2\times10^{-4}$m .

The results described in this and in the last subsections can also be formulated in terms of the dependence of the degree of mixing on either the aspect ratio (Fig.4.10) or the hydraulic diameter (Fig. 4.11). Again, we observe the general trend that a) at low Re smaller widths cause better mixing; b) at large Re lower heights cause vortex damping and therefore worsen mixing; c) for moderate aspect ratios, at large Re we observe the appearance of large vortices, even engulfment, which increase the degree of mixing.

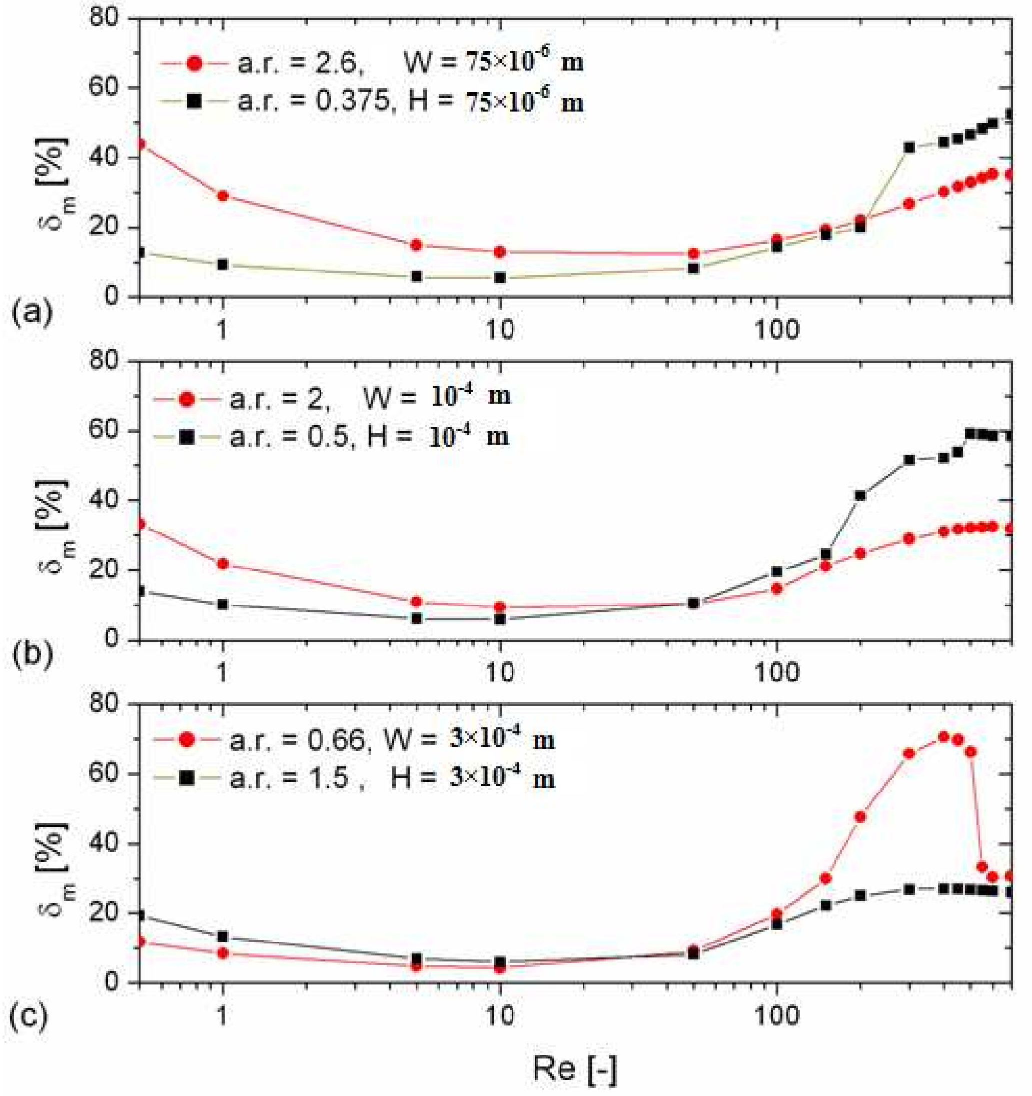

Fig. 4.10 Degree of mixing δ_m as a function of the Reynolds number, Re, for different aspect ratios, a.r., and fixed hydraulic diameter; D_h; (a) $D_h = 1.09\times10^{-4}$m ; (b) $D_h = 1.33\times10^{-4}$m and (c) $D_h = 2.40\times10^{-4}$m.

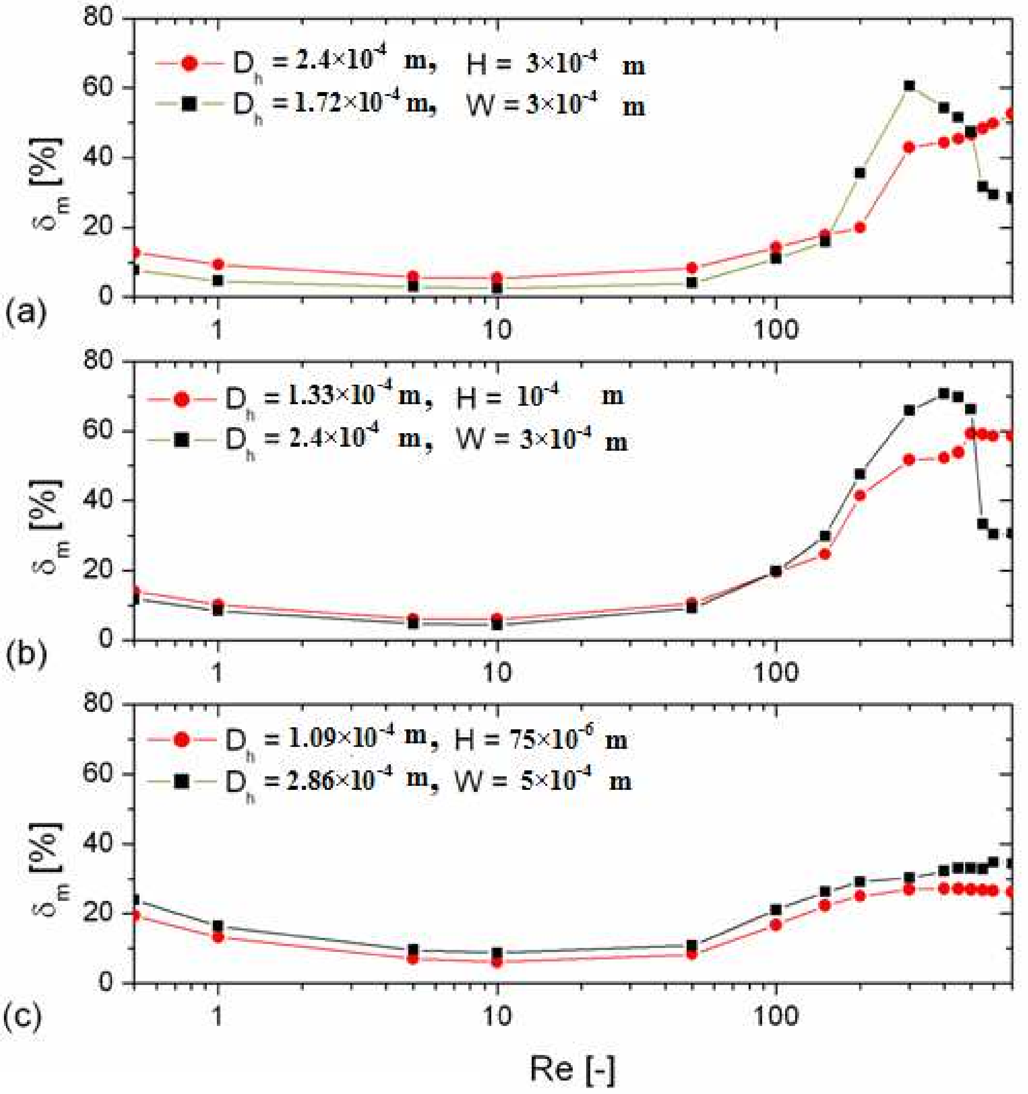

Fig. 4.11 Degree of mixing δ_m as a function of the Reynolds number, Re, for different hydraulic diameter D_h and fixed aspect ratio, a.r.; (a) a.r = 1.5; (b) a.r = 0.55 and (c) a.r = 0.4.

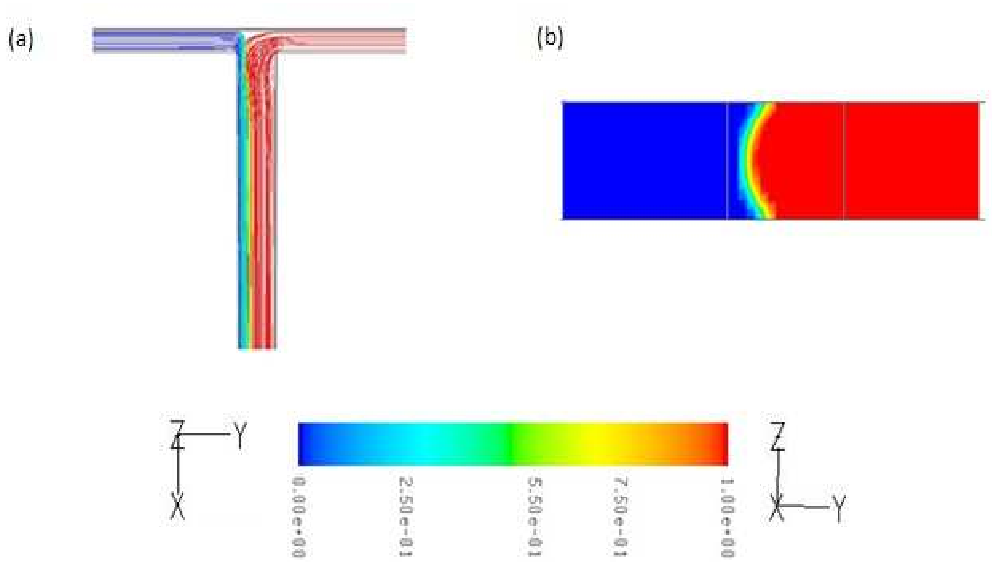

Fig. 4.12. (a) Pathlines along of the mixing channel, (b) mass fraction contour plot of one species at the entrance cross section for W=2×10 $^{-4}$m, H=×10 $^{-4}$m, Re=10 and inlet flow rate ratio β=20.

4.3.4 Effect of Inlet Flow rate Ratios

When the flow rates in the two inlet channels, $\dot{V}_1$ and $\dot{V}_2$, are different from each other, with $\beta = \dot{V}_1 / \dot{V}_2$, the velocity and concentration profiles are obviously asymmetric, therefore enhancing mixing. In particular, in the stratified flow regime, the minority fluid never crosses the centerline of the mixing channel (Fig. 4.12a and b, with a flow rate ratio β=20), while in the vortex and engulfment flow regimes this transfer occurs (Fig. 4.13 a-g), with a consequent increase of the degree of mixing. In table 1 the degree of mixing for three types of geometry and flow regimes (stratified flow, with Re=10; vortex flow, with Re=150 and engulfment flow, with Re= 300) are reported.

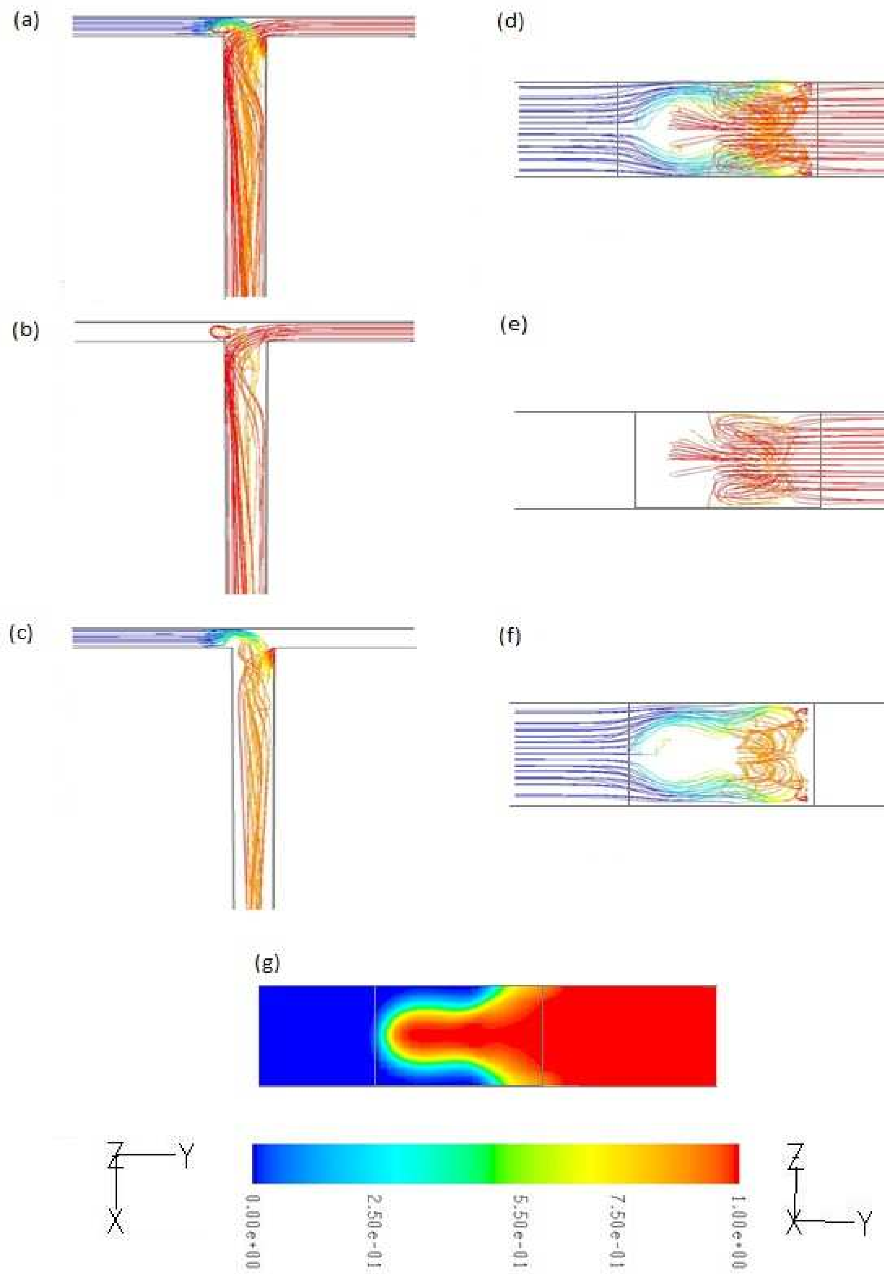

Fig. 4.13. (a) and (d): Pathlines along the mixing channel and at the entrance cross section for Re= 300 and flow rate ratio β=20; (b) and (e): trajectories of the fluid with a higher flow rate along the mixing channel and at the entrance cross section; (c) and (f): trajectories of the fluid with a lower flow rate. The difference between the inlet flow rates causes the minority fluid to cross the centerline; (g) mass fraction contour plot of one of the fluids at the entrance cross section.

Table. 4.1 Degree of mixing δ_m at the outlet of the micro T-mixer for different inlet flow rate ratios β and different width, W, at fixed height, $H=\times 10^{-4}$m .

	Degree of mixing (δ_m%)											
Re	10				150				300			
$\beta=\dot{V}_1/\dot{V}_2$	1	5	10	20	1	5	10	20	1	5	10	20
$W=75\times10^{-6}$m	14	21	30	60	16	60	63	73	20	73	73	80
$W=2\times10^{-4}$m	6	15	23	27	19	63	72	77	24	85	78	81
$W=3\times10^{-4}$m	4	12	20	22	30	58	70	77	66	68	79	81

4.3.5 Effect of Mixing angles

Simulations were also performed to investigate whether the mixing angle has any effect on the degree of mixing. Therefore, we let the mixing angle α vary from 25° to 150° (Fig. 4.14), keeping the channel width and height fixed at $H = 2\times10^{-4}$m and $W = 2\times10^{-4}$m .

Results for different mixing angles are shown in figure 4.15. We see that in the stratified flow regime the mixing angle has only a marginal effect on the degree of mixing; on the other hand, in the vortex and engulfment flow, the degree of mixing first increases as the mixing angle is increased, until it reaches a maximum value; after that, increasing α will dampen the vortices and therefore the degree of mixing decreases, until engulfment is induced again and the degree of mixing increases. (Fig.4.15) As usual, the transition between different regimes depends on the Reynolds number.

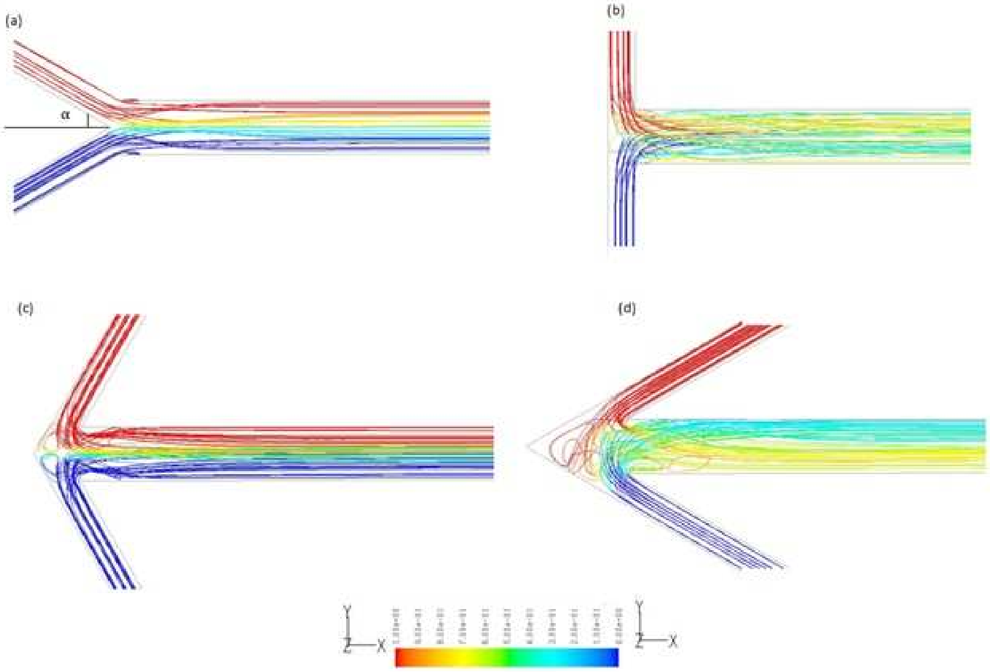

Fig. 4.14. Pathlines along the mixing channel for for Re=200 while W=2×10 $^{-4}$m , H = 10 $^{-4}$m and different mixing angles, (a) α=30°; (b) α=90°; (c) α=120°; (d) α=150°.

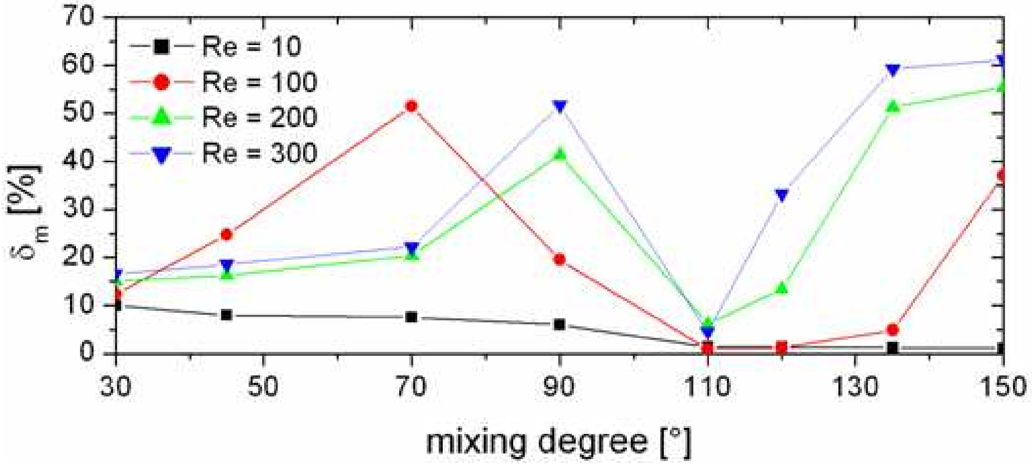

Fig. 4.15. Degree of mixing δ_m as a function of the mixing angle, α, for W=2×10 $^{-4}$m and H=×10 $^{-4}$m

4.4 Summary

Flow dynamics and mixing characteristics of liquids flows in T-type micromixers were investigated, aiming at optimizing these devices. The mixing process was simulated with various operating and design parameters by means of computational fluid dynamics. Simulation results proved that the development of vortices is essential for good mixing performance. Furthermore, it was shown that the development and occurrence of vortices depends strongly on both volume flow rates and geometrical parameters of the mixer such as its aspect ratio and mixing angle. In particular, good mixing requires that the Reynolds number is large enough to enhance transverse convection, while the channel width (and, to a smaller extent, the channel height) must be large enough to avoid vortex damping, due to shear stresses at the wall.

Chapter 5

Mixing of Binary Mixtures in Microdevices

5.1 Introduction

The previous works on T-shaped micromixers were directed towards analyzing mixing for a wide range of Reynolds numbers, corresponding to various flow regimes. It is well known that mixing is mainly governed by molecular diffusion and it depends on the residence time of the fluid particles that are located near the interfaces separating the two fluids. Accordingly, at very low Reynolds number, the mixing efficiency is relatively high due to a long residence time of the fluids. Then, as the Reynolds number increases, at first the mixing length decreases, due to a decrease in the residence time of the fluids; then, beyond a certain critical Reynolds number, this effect is reversed, due to the appearance of vortices in the mixing region. Exploring a way to increase the mixing performances for the range of Reynolds numbers where low mixing is depicted is an interesting and important issue.

A possible way to accelerate mixing is to use perfectly miscible fluids at the inlet. In fact, in that case, the chemical potential difference between the two fluids could induce a diffusive material flux that is higher than that occurring in the case of two identical inlet fluids. Two-fluid mixing is an essential process in many microfluidic devices. For example, various biomedical and biochemical processes involve the mixing of two fluids, including DNA purification, polymerase chain reaction (PCR), enzyme reaction, and protein folding. The performance of such processes relies on effective and rapid mixing of samples and reagents. Accordingly, the present study focuses on the comparison between the case where the two inlet fluids are both water and that when they consist of water and ethanol, using a T-type passive micro-mixer and with Reynolds numbers ranging from 1 to 300. To do that, a commercial Computational Fluid Dynamic (CFD) code, FLUENT 6.3 by Ansys Inc., was used to solve the three-dimensional flow and mass transfer equations in the proposed geometrical configurations.

5.2 Numerical Modeling

We considered a reference case, consisting of a T-shaped microchannel with 3 branches, i.e. 2 inlets and 1 outlet (Fig. 5.1). Both inlet branches have a 10^{-4} m$\times10^{-4}$ m cross section, while the mixing channel is 2×10^{-4} m wide and 10^{-4} m deep, corresponding to a hydraulic diameter of 133×10^{-6} m. The length of the inlet (L_{in}) and mixing channels (L) are 5×10^{-4} m, which are sufficient for mixing zone.

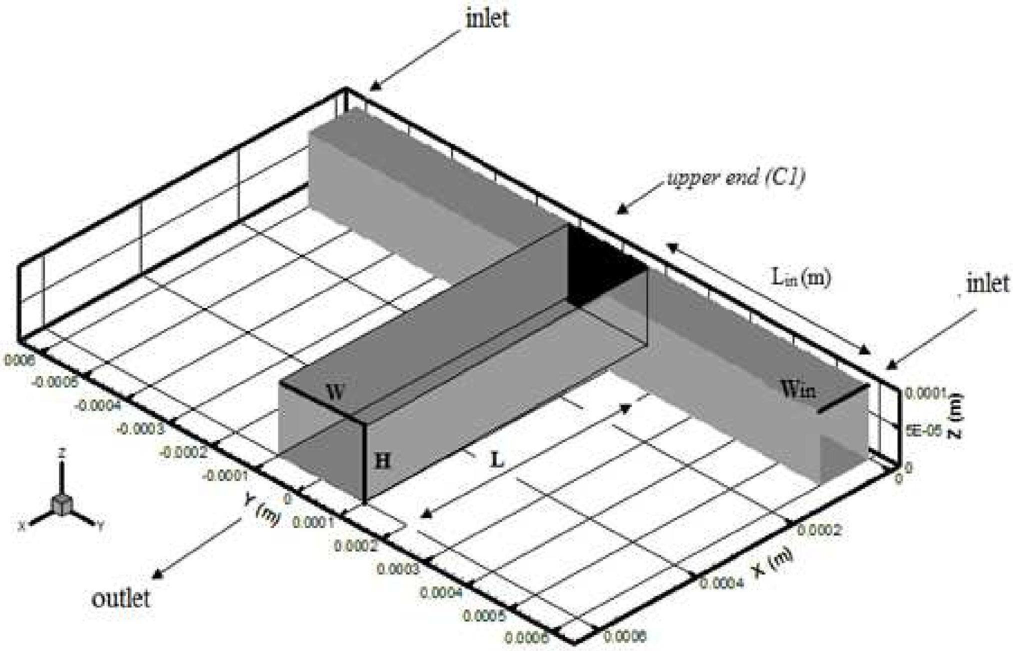

Fig. 5.1 Schematics of the T-mixer.

We should be aware that the inlet channels should be sufficiently long to ensure that the fluid flow can reach fully developed conditions before entering the mixing zone.

Simulation and theoretical results show that this is so, even at Re = 100. In fact, the length of our inlet channels satisfies the conditions given by several previous investigators[126]-[132]-[133]-[134] In addition, in Fig. 5.2 we see that at the end of the inlet channels the velocity profile is indeed fully developed. For higher Reynolds numbers up to 300 we used fully developed velocity profile in each inlets.

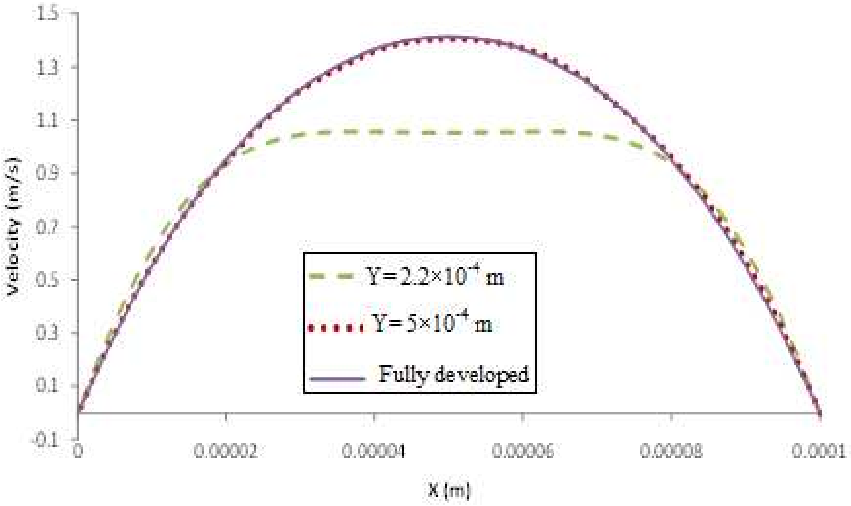

Fig. 5.2. Velocity profile for Re=100 at the centerline of different cross sections, y, in the inlet channel, with y denoting the distance from the center of the mixing channel (see Fig.5 1). The purple line represents the fully developed theoretical profile.

Another important issue is whether the mixing channel length, L, is long enough to make sure that the boundary conditions at the outlet do not influence the mixing process occurring at the confluence of the inlet flows. As shown in Fig. 5.3, there is no difference between our results, where L = 6×10^{-4}m, and those obtained with L = $1{,}6\times10^{-4}$m, i.e. using the same geometry as in[135] Bothe et al. Clearly, the length of the mixing channel should be larger if we considered flows at higher Reynolds numbers, so that the morphology of the engulfment flow (which is absent in our case) could be fully resolved[136]-[137]

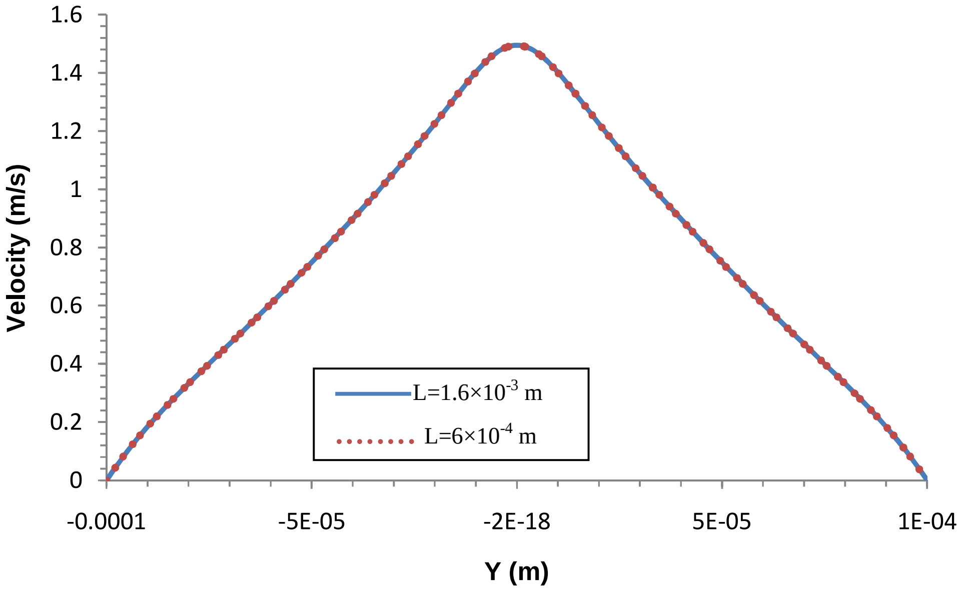

Fig. 5.3. Velocity profile for Re = 100 at cross section x=0.2 mm in the mixing channel, where x is defined in Fig. 5.1.

The grid independence check was performed at Re = 100 and for both velocity and concentration profiles, as shown in Fig. 5.4. From the results of this test, a 3μm mesh size was selected, as it ensured that the complete flow field could be resolved.

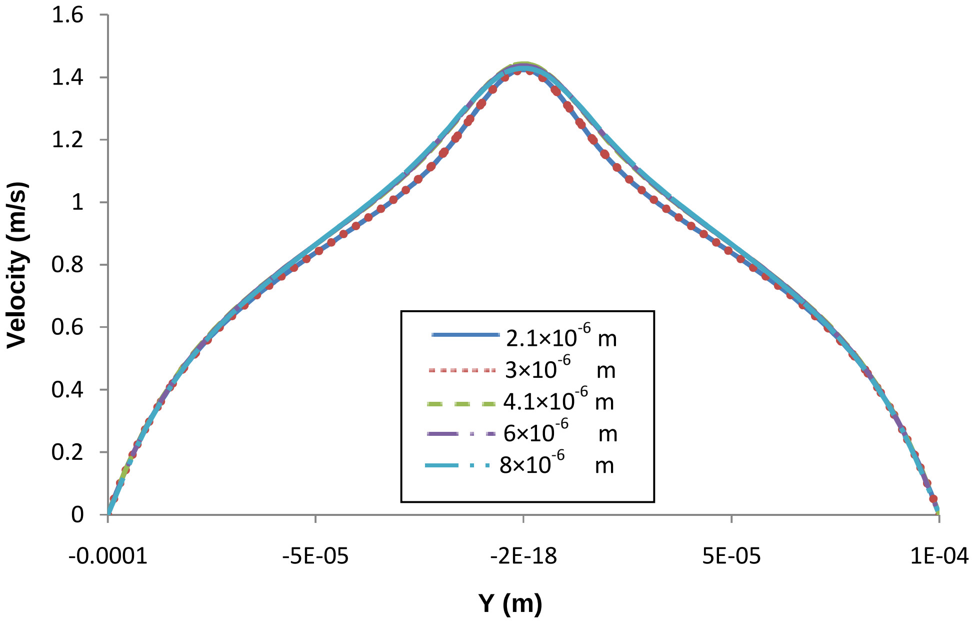

Fig. 5.4. Velocity distribution grid independency for Re = 100 at cross section x=0.2 mm in the mixing channel

A second order discretization scheme was used to solve all equations; using FLUENT 6.3 by Ansys Inc. Simulations were typically considered converging when the normalized residuals for velocities fell below 1×10^{-6}. The steadiness of the solution with iterations was also assessed by checking the concentration field in the outlet section of the mixing channels at different iterations. The values of density and viscosity were set equal to 10^3 kg m^{-3} and 10^{-3} kg m^{-1} s^{-1} for water and 789 kg m^{-3} and 1.2×10^{-3} kg m^{-1} s^{-1} for ethanol, respectively , while the diffusion coefficient was set equal to $D = 3.23\times 10^{-10}$ m^2 s^{-1}, corresponding to that of a water(ethanol) - ink mixture , as this value is very close to the self- diffusivity of pure water and of ethanol as well.

5.3 Results and Discussions

The water-water case is compared to the water-ethanol case, presenting them side by side. For sake of clarity, the comparison has been performed keeping the inlet volumetric flow rates fixed, i.e. using the same mean inlet velocity $\bar{u}$, irrespectively whether we refer to the water or to the ethanol stream. In the same way, the Reynolds number is defined using the mean inlet velocity, $\bar{u}$, the hydraulic diameter D_h of the mixing channel and the kinematic viscosity of water (any other choice would be as arbitrary as ours, because we should consider the properties of the mixture in the mixing region, which therefore change as we move down the channel). Blue and red colors represent fluid "A" and fluid "B", respectively, which means that blue and red contours correspond to mass fractions 0 and 1, respectively, while green shading represents a mixture with a mass fraction of 0.5.

5.3.1 Simulation Results

5.3.1.1 Equal Inlet Velocity

At small flow rates, as wall shear stresses are small, the two streams behave in the same way, so that the velocity profile is symmetric along the y-direction (i.e. along channel width), both near the walls and at the center of the conduit (Fig. 5.5a). In fact, at small Reynolds number ($Re < 30$), the flow patterns in water-water systems is very similar to those in water-ethanol systems (see Fig. 5.5b and 5.5c), so that mixing occurs mainly by mass diffusion and it is therefore very slow.

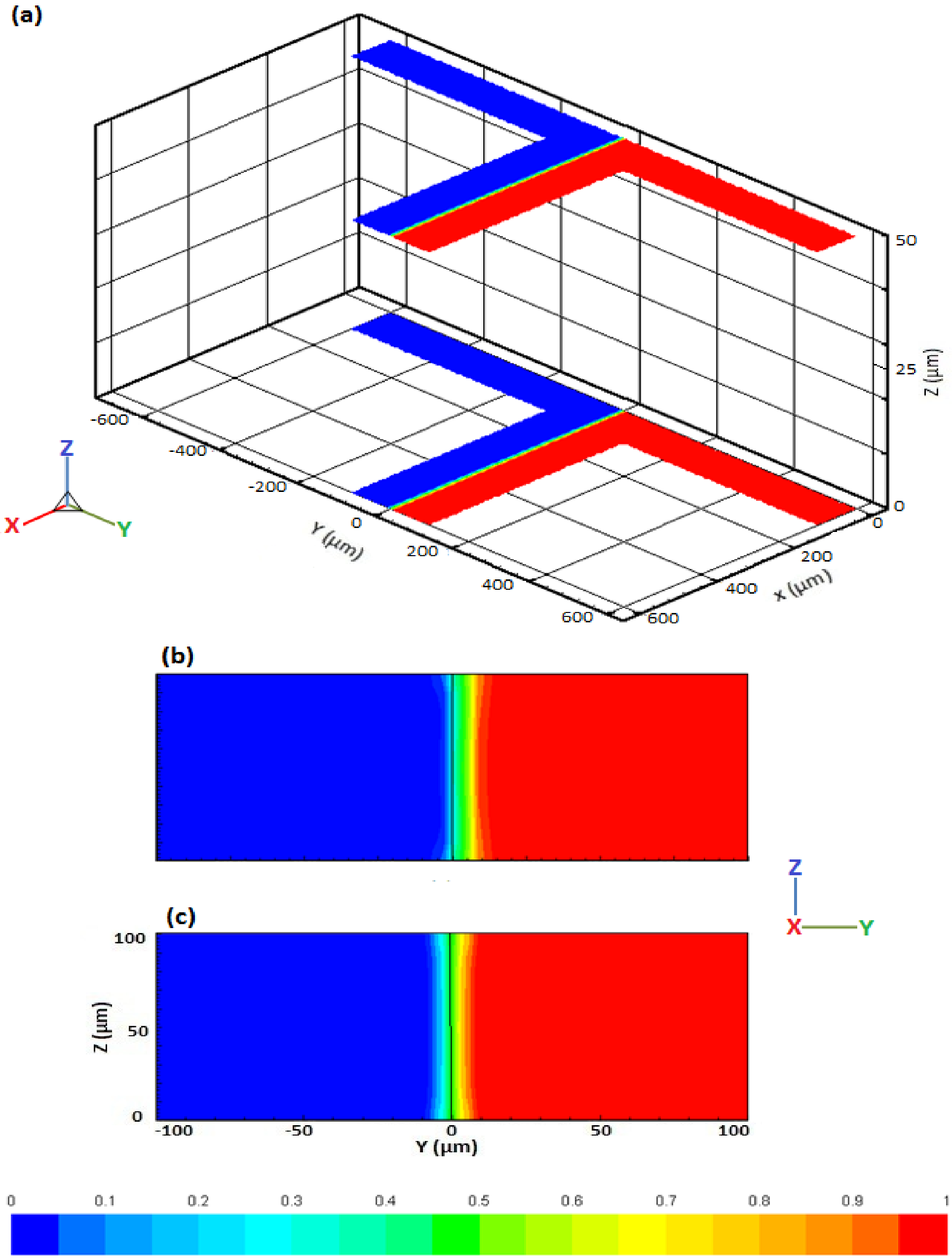

Fig. 5.5. Mass fraction contour plots at *Re* =10. a) Water-ethanol system along the mixing channel close to the bottom wall and in the channel center; water-water systems present a very similar pattern; b) and c) water-ethanol and water-water systems, respectively, at the outlet cross section.

At larger Reynolds numbers, we see changes in the flow patterns. In fact, as the pressure drops of the two fluid streams along the mixing channel must be equal to each other, ethanol moves slower than water, to compensate for its larger viscosity. This causes the water moving towards the channel center, while ethanol is driven to the walls. This phenomenon is more evident near the walls, because of higher wall shear stresses (Fig. 5.6). Note that the fact that the two fluids have different residence times does not favor mixing by diffusion along the y-direction, and hence the water-ethanol degree of mixing in smaller than its water-water counterpart.

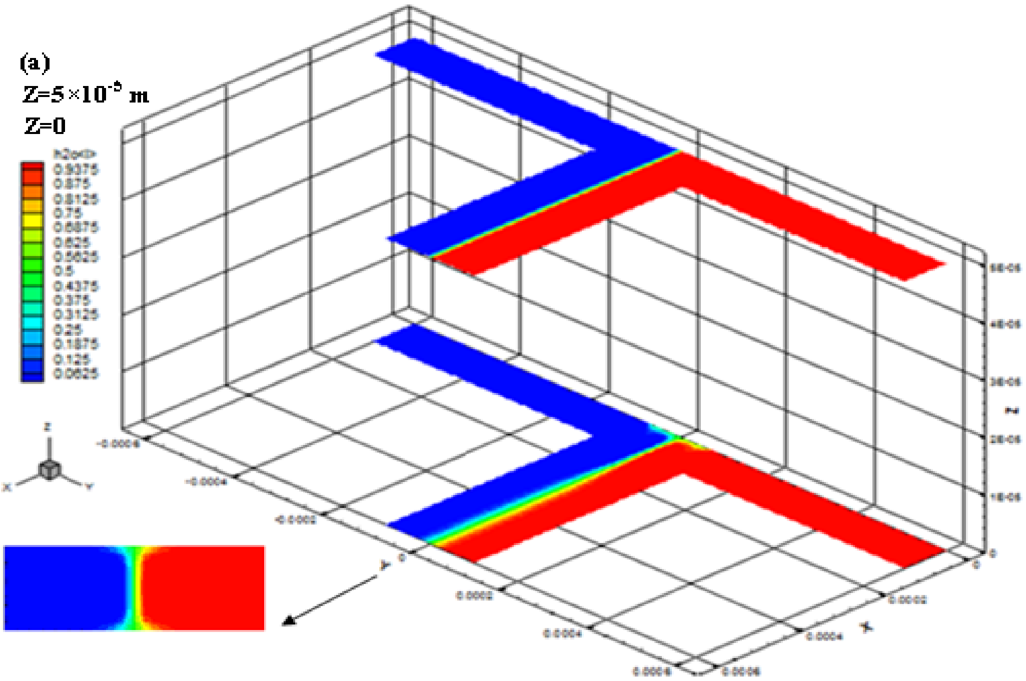

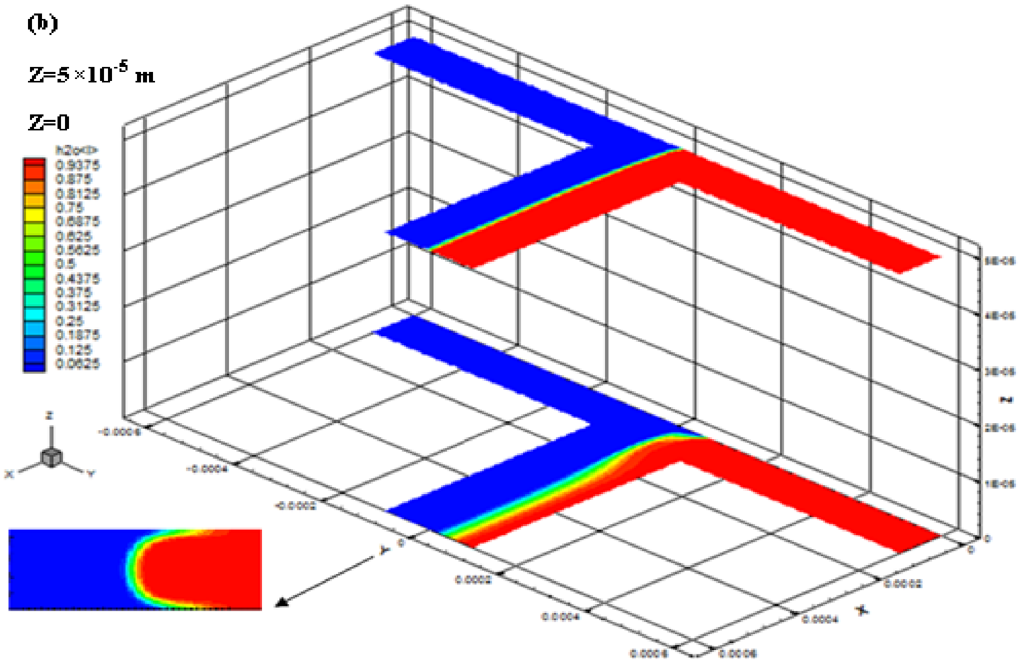

Fig. 5.6. Mass fraction contour plots at along the mixing channel close to the bottom wall and in the channel center and at the outlet cross section at Re =50. a) water-water and b) water-ethanol systems.

At further higher Reynolds numbers, we saw a significant difference in flow patterns and degree of mixing. In fact, as it is evident from figure. 5.7, in water-water systems, as we move from Re =100 to Re =200, we see the appearance of symmetric vortices and engulfment flows, thus confirming the results by Bothe et al[131].

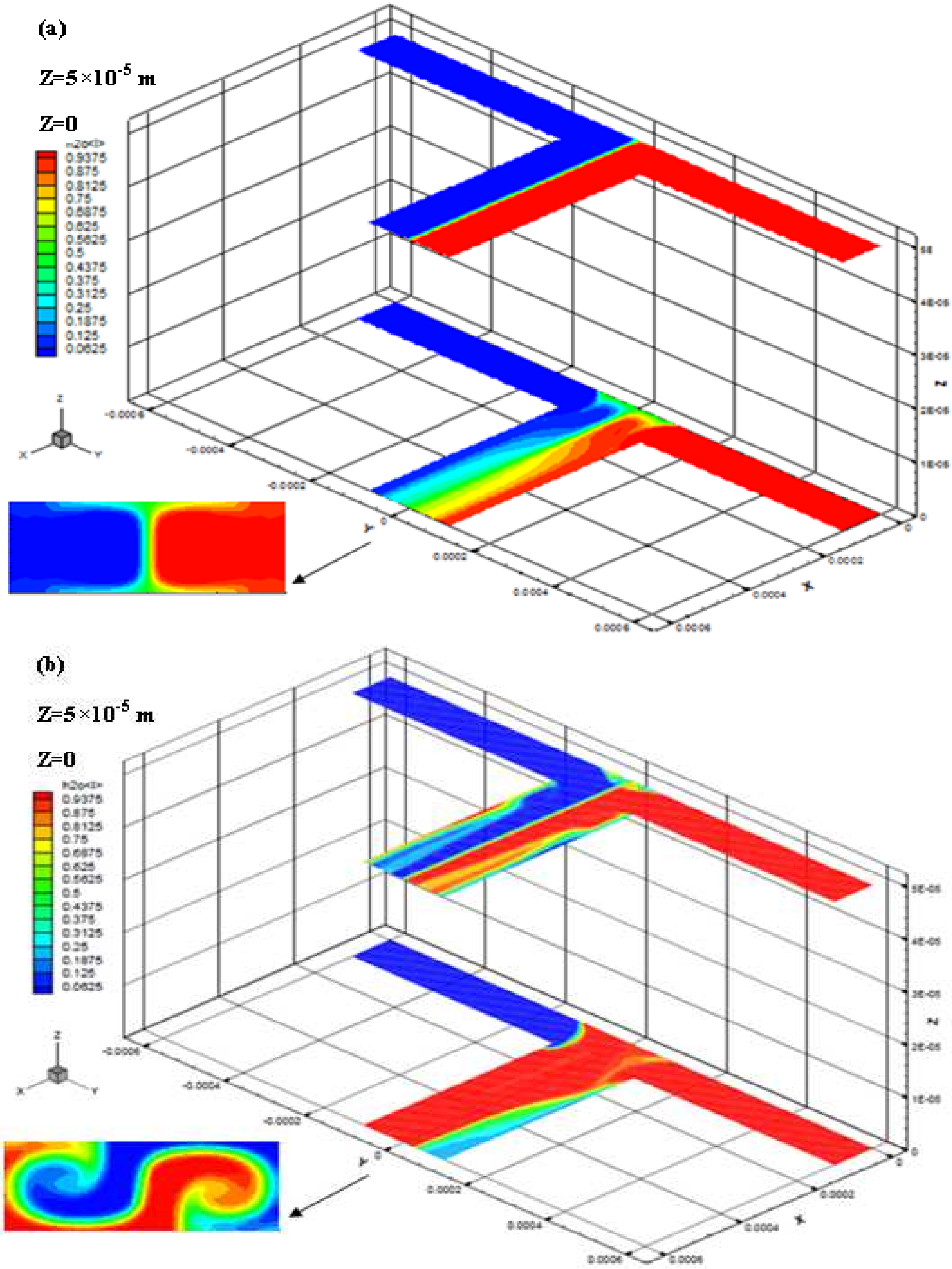

Fig. 5.7 Mass fraction contour plots along the mixing channel (close to the wall and in the channel center) and at the outlet cross section for water-water systems at a) Re = 100 and b) Re=200.

On the other hand, as shown in figure. 5.8, for water–ethanol systems the onset of the engulfment regime occurs at a higher Reynolds number, ranging from 200 to 300. Concomitantly, in table 5.1 we see that the two systems exhibit a very large difference in the degree of mixing δ_m and the wall shear stresses at the outlet of the micro T-mixer. Finally, it should be added that, even if the Reynolds number was defined based on the kinematic viscosity of a well mixed mixture, the Reynolds number corresponding to the onset of engulfment is larger than in the water-water case.

Table 5.1 Degree of mixing δ_m and wall shear stresses at the outlet of the micro T-mixer for water-water and water-ethanol systems at different Reynolds numbers for equal velocity inlets.

	W+W			W+E				
Re_{mix}	δ_m %	τ(shear stress, mixing)(Pa)		δ_m %	τ(inlet channel)		τ(mixing channel)	
		τ_0 (z=0)	τ_c(center)		τ_{0Water}	$\tau_{0Ethanol}$	τ_0	τ_c
1	4	0.47	0.05	3.2	0.57	0.63	0.514	0.056
10	2	4.7	0.51	1.2	5.31	6.33	5.16	0.57
20	-	-	-	1.6	10.4	12.7	10	1.1
30	-	-	-	2	16.3	19.7	15.8	1.66
40	-	-	-	2.2	22.1	26	21.4	2.2
50	3.6	25	2.5	2.4	28	32.7	27	2.8
100	10	57.4	5.11	5.8	68.5	60	61	5.6
200	26.4	142	12	8.9	133	149	148.4	12
300	41	-	-	31	218	235	248	21

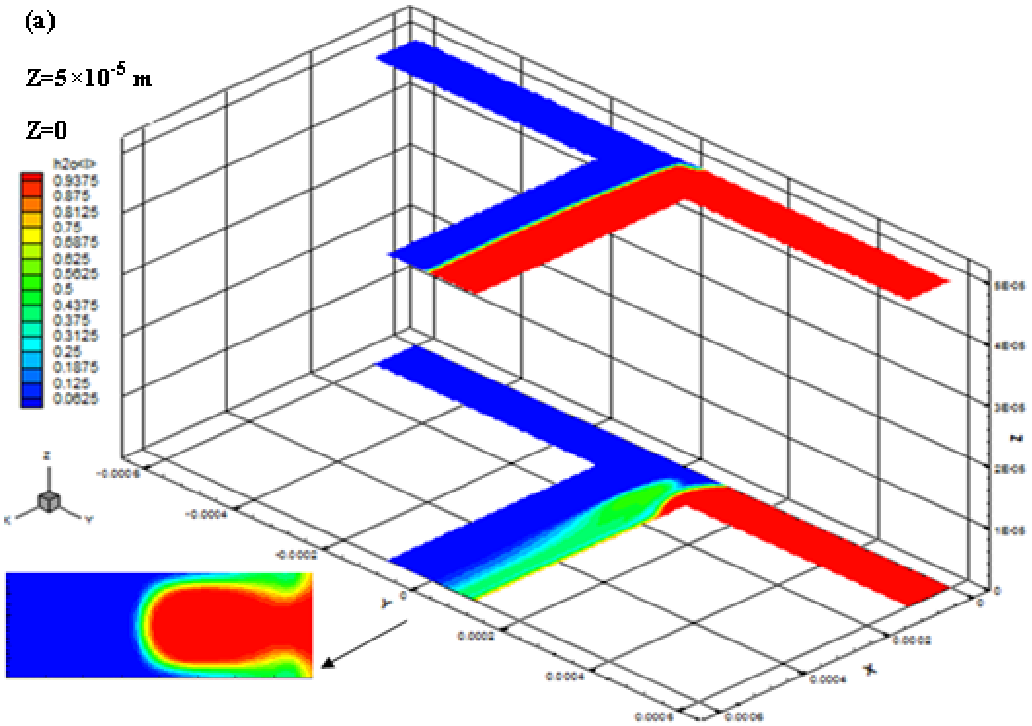
(a)
Z=5×10^{-5} m
Z=0
h2o<l>
0.9375
0.875
0.8125
0.75
0.6875
0.625
0.5625
0.5
0.4375
0.375
0.3125
0.25
0.1875
0.125
0.0625
Z
X
Y
-0.0006
-0.0004
-0.0002
0
0.0002
0.0004
0.0006
0
0.0002
0.0004
0.0006
X
0
1E-05
2E-05
3E-05
4E-05
5E-05
Z

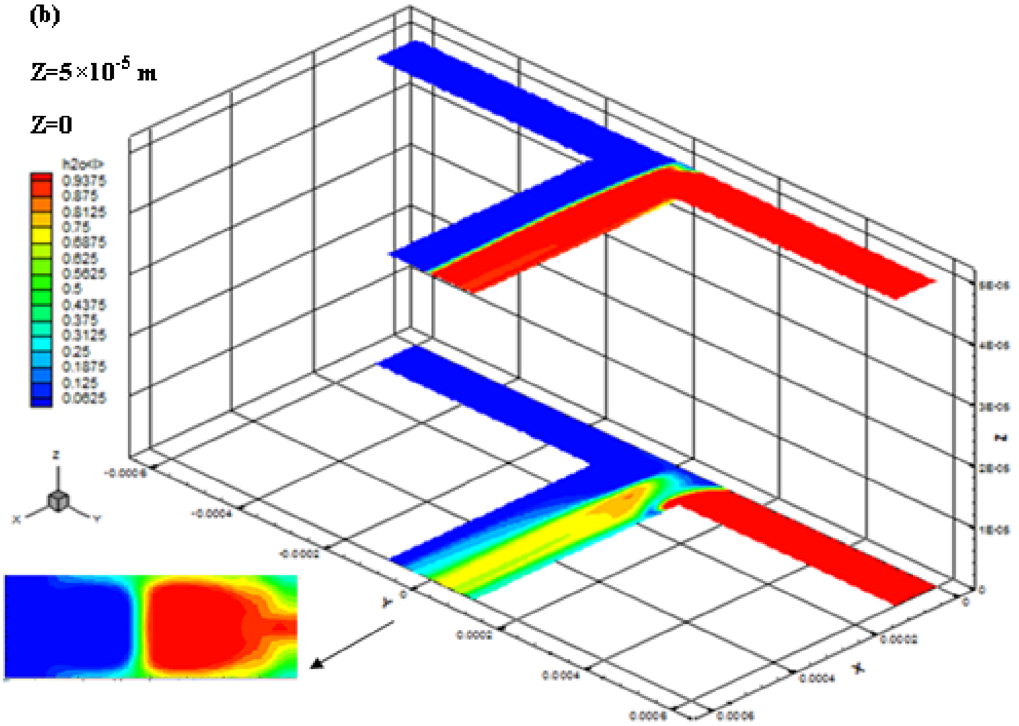
(b)
Z=5×10^{-5} m
Z=0
h2o<l>
0.9375
0.875
0.8125
0.75
0.6875
0.625
0.5625
0.5
0.4375
0.375
0.3125
0.25
0.1875
0.125
0.0625
Z
X
Y
-0.0006
-0.0004
-0.0002
0
0.0002
0.0004
0.0006
0
0.0002
0.0004
0.0006
X
0
1E-05
2E-05
3E-05
4E-05
5E-05
Z

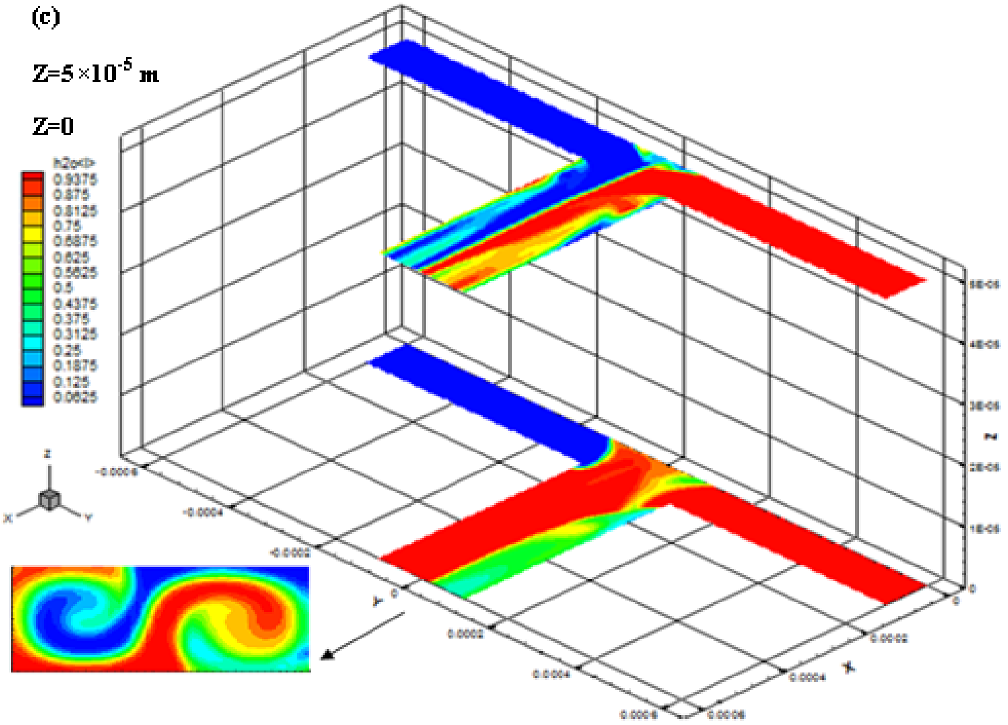

Fig. 5.8 Mass fraction contour plots along the mixing channel (close to the bottom wall and in the channel center) and at the outlet cross section for water-ethanol systems at a) *Re* =100, 200 and 300, a, b and c respectively.

5.3.1.2 Unequal Inlet Velocity

For unequal velocity studies, a velocity ratio between the two inlet streams of 5 was used. When the two inlet streams have different velocities (and flow rates as well), the mixing process is radically different, depending on whether the fluid with the larger velocity is water or ethanol. First, let us consider the behavior of a water-water system. At low Reynolds number, when the velocity of the two streams are different from each other, the interface moves towards one of the walls, where the velocity is lower than that at the centerline (which corresponds to the velocity experienced by the interface region in the equal velocity case) (Fig. 5.9a and 5.9c). Accordingly, as the diffusion time is larger than that in the equal velocity case, the mixing degree increases also. Then, at larger Reynolds numbers, in figure. 5.9b and 5.9d we see that the faster fluid stream hops to the opposite side of the mixing channel, leaving the slower fluid close to the walls, resulting in an increase of a mixing efficiency.

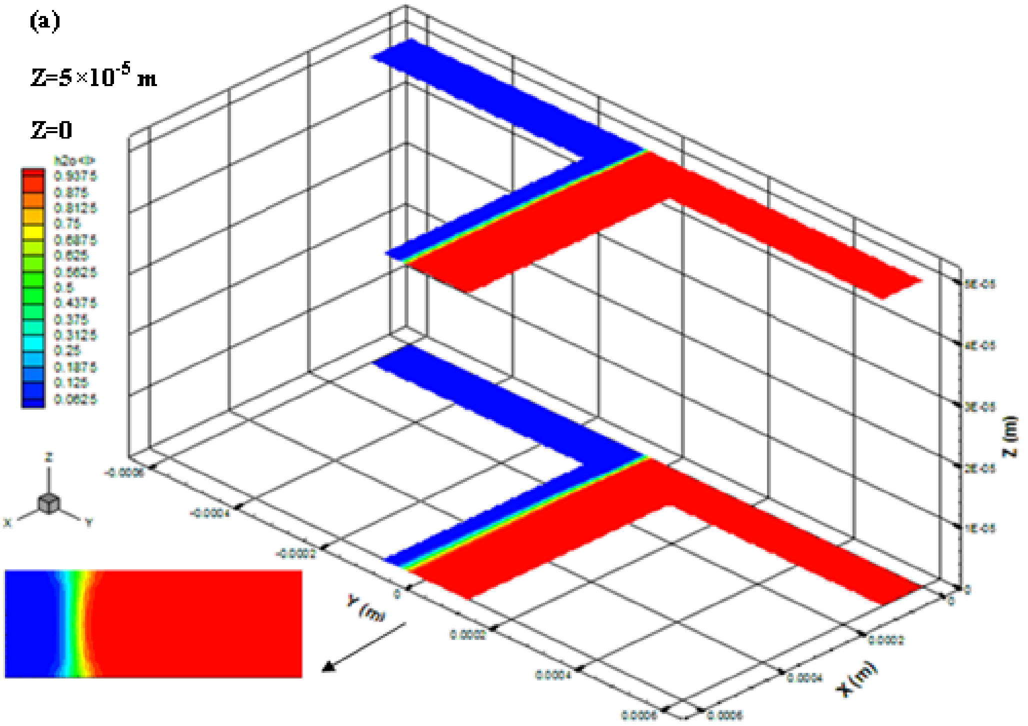

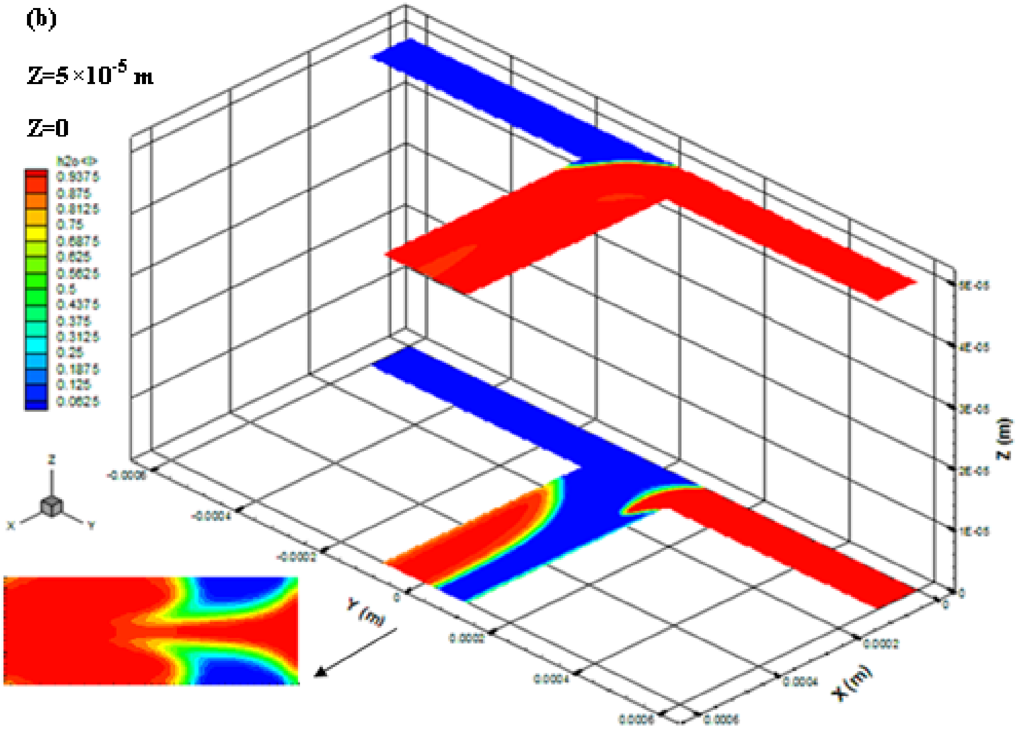

Fig. 5.9 Mass fraction contour plots of water-water systems at a velocity ratio $V_1/V_2 = \beta = 5$ along the mixing channel (close to the bottom wall and in the channel center) and at the outlet cross section for a) *Re* =1; b) Re=100.

In water-ethanol systems, when the water stream is faster, we observe a behavior that is very similar to that of water-water systems, although, as shown in table 2, the degree of mixing is smaller, both at small and at larger Re. On the other hand, when ethanol is the faster stream, the behavior is radically different, as shown in figure. 5.10. In fact, in this case, comparing figure. 5.9d with 5.10d, we see that at high Reynolds number, the faster stream, i.e. ethanol, now tends to hop to the opposite side even more easily, generating a phase pattern that is quite different. Also at low Reynolds number, comparing figure 5.9c with 5.10c, we see that the interface region is thicker and therefore the degree of mixing is higher. These observations are summarized in table 5.2.

Table 5.2 Degree of mixing δ_m at the outlet of the micro T-mixer for water-water and water-ethanol systems at different Reynolds numbers and inlet velocity ratios.

Systems		W+W		W+E	
Re		1	100	1	100
δ_m %	V1/V2=5	9.5	28	-	-
	Vw/Ve=5	-	-	5.7	23
	Ve/Vw=5	-	-	15.8	27

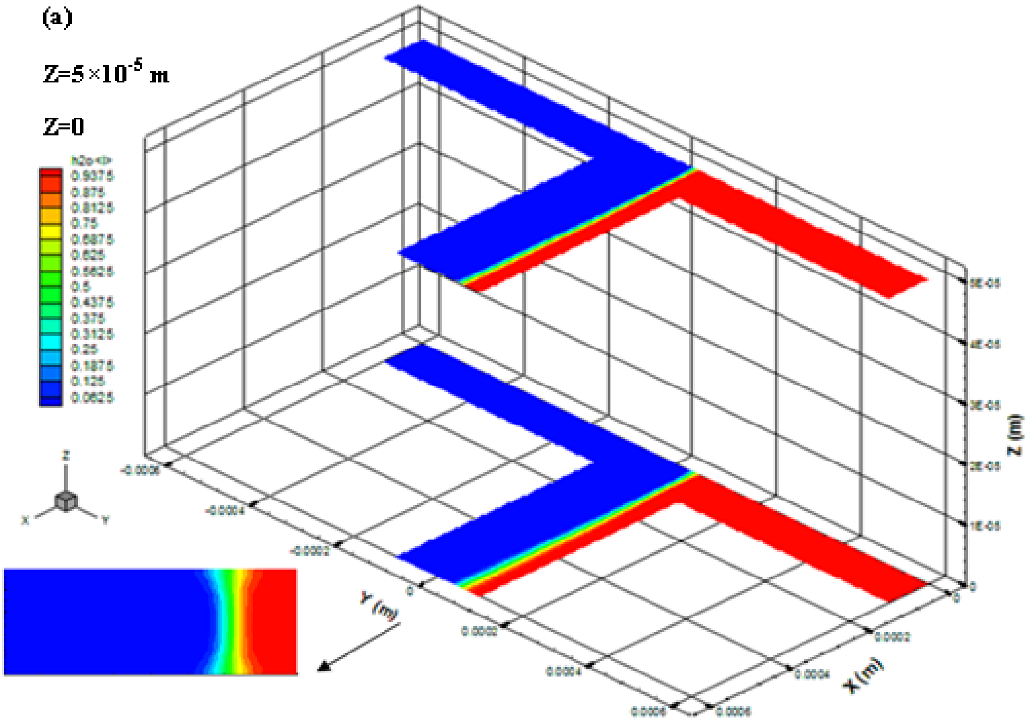

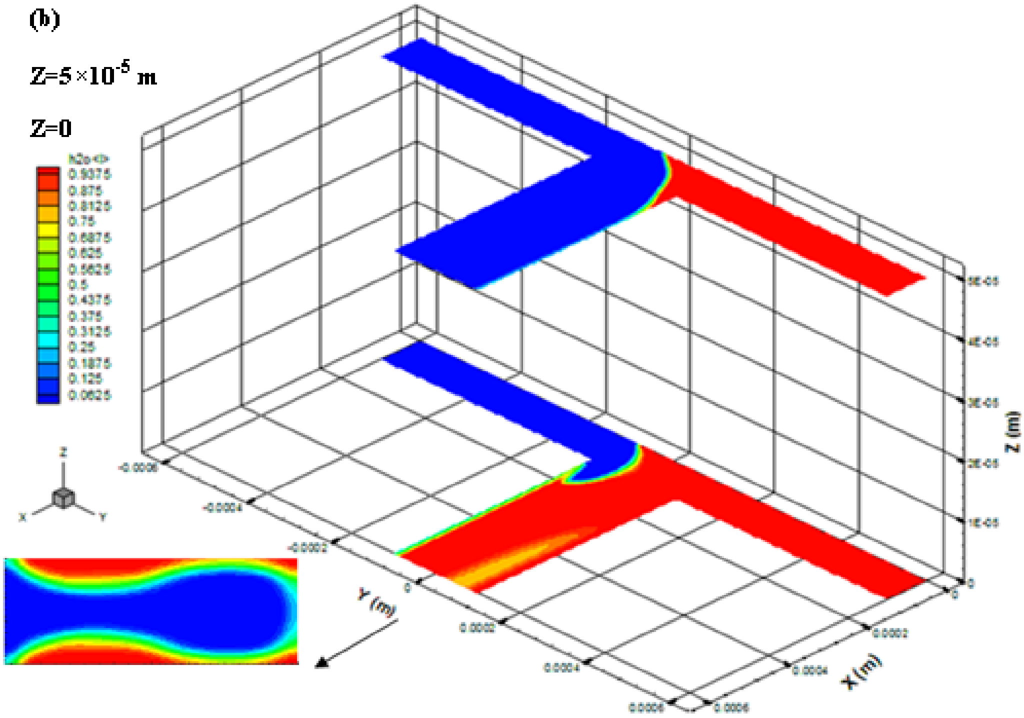

Fig. 5.10 Mass fraction contour plots of water-ethanol systems at a velocity ratio $V_e/V_w = \beta=5$ along the mixing channel (close to the bottom wall and in the channel center) and at the outlet cross section for a) Re = 1 and b) Re =100.

5.3.2 Experimental Section

Flow visualization experiments were carried out to verify the simulation predictions of the earlier section. Our objective is to conduct experiments on the mixing of two miscible fluids and qualitatively verify the numerical predictions of the simulations of the previous section.

5.3.2.1 Experimental set-up

A schematic drawing of the experimental set-up is presented in Fig. 5.11. KDS Gemini 88 syringe pump was connected to the mixer by 1.0mm inner diameter PTFE tubing. Similar PTFE tubing was also connected to the outlet of the mixer. In all the experiments, the total flow rate was in the range between 0.0408 and 4.08 ml min−1.

This range corresponds to Reynolds numbers between 1 and 100 in the mixing chamber.

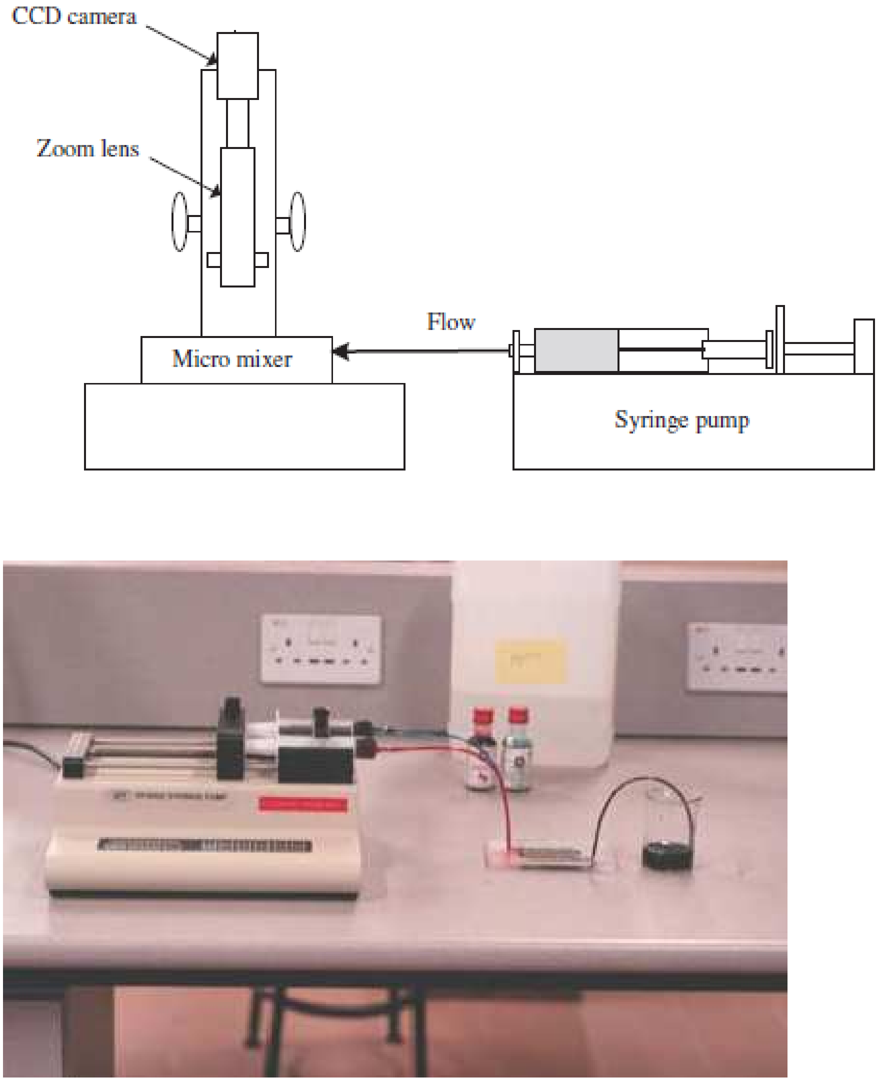

Fig. 5.11. The experimental set-up for the mixing experiments

5.3.2.2 Experimental procedure

As shown in Fig. 5.11, two feed streams were used. One feed stream contained ethanol blue food dye color and the other de-ionized water with red food dye color (in Water-Water case we have just water with red and blue food dye color in each inlet respectively). All the experiments were carried out at 293 K. The feed streams were pumped into the mixer and samples were taken from the outlet of the mixers.

5.3.2.3 Experimental results

Experimental results, representing the mixing efficiency of micromixers, are shown in Fig. 5.12 to Fig 5.15 for both water-water and water ethanol systems. This experimental observation is consistent with the numerical finding that the mixing efficiency of water-ethanol systems is lower than the corresponding water-water case. In figure 5.12 (a-c) and Figure 5.13 (a-c) we can see clearly thicker interface at small Re in w-w case rather than w-e systems also the vortex generation and therefore mixing performance depend not only on Reynolds number, but also on inlet fluids and initial conditions, so we can see these effects in figure 5.12d and 5.13d. and appearing the vortex just for w-w case at Re=100.

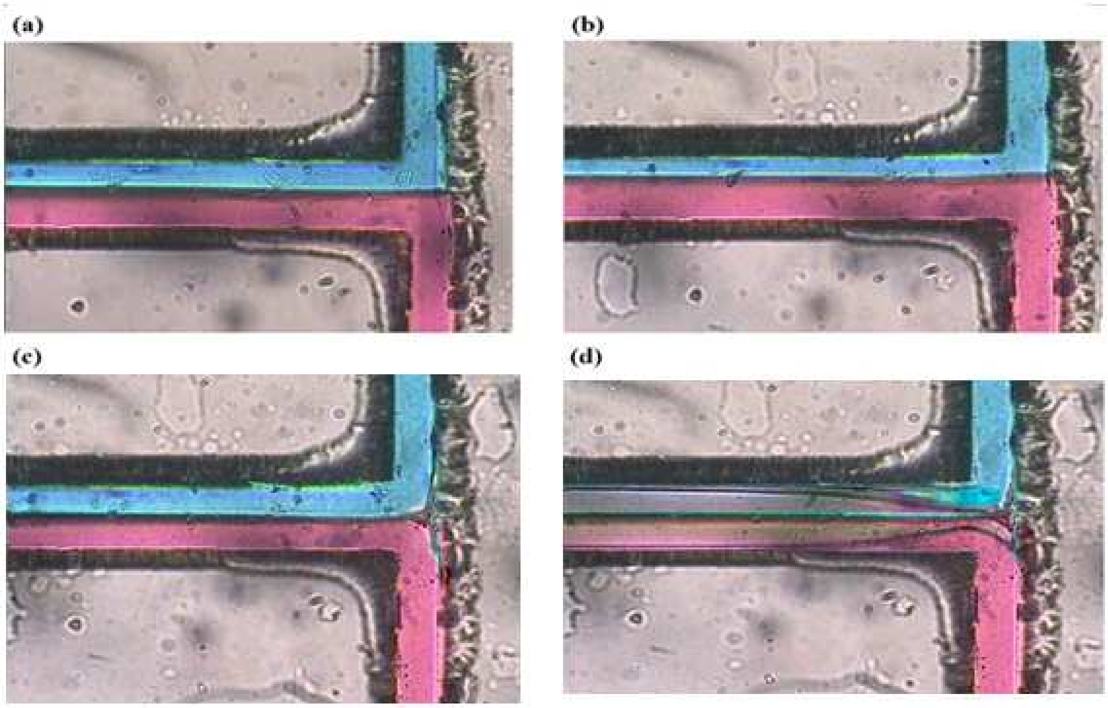

Fig. 5.12. The observations of the mixing process at the junction of micro T-mixer for water-water systems while we use equal flow rate in each inlets at different applied Re (a) 1, (b) 10, (c) 50 and (d) 100.

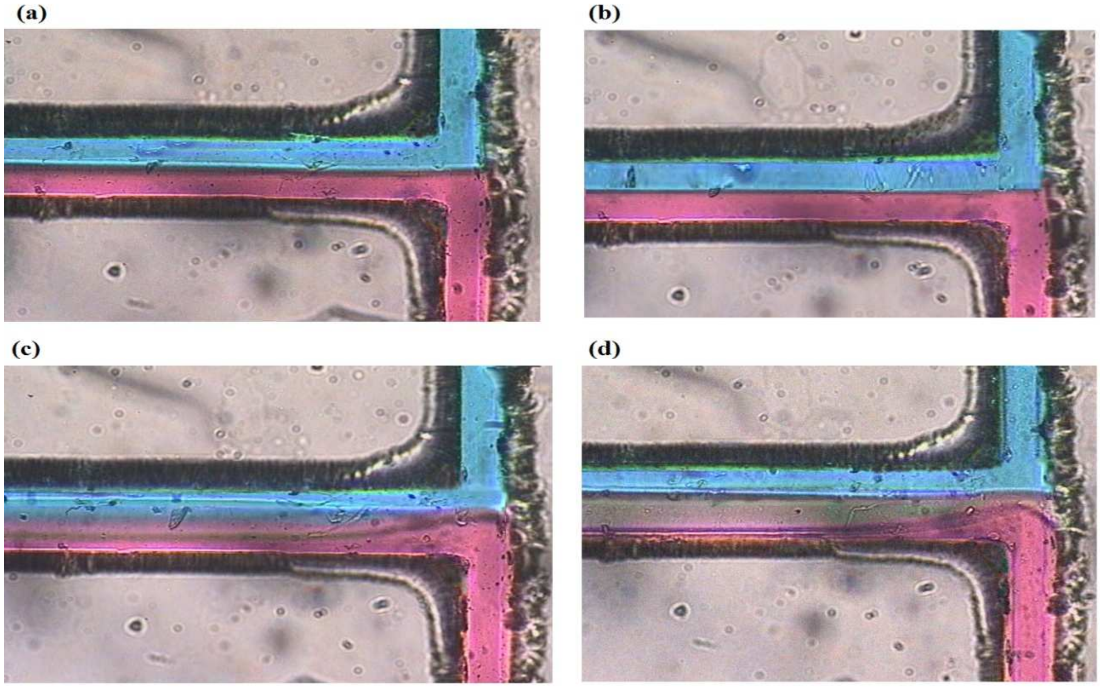

Fig. 5.13. The observations of the mixing process at the junction of micro T-mixer for water-ethanol systems while we use equal flow rate in each inlets at different applied Re (a) 1, (b) 10, (c) 50 and (d) 100.

For unequal inlet flow rates we see again the same behavior like simulation results. At Re=1 (Fig. 5.14a and Fig. 5.15.a and b), the interface in w-w case is thicker than w-e case while Vw>Ve and is thinner while Ve>Vw. This view can emphasis our simulation results.

At Re=100, the flow patterns for both w-w and w-e case are similar and the mixing efficiency are really close to each other as we have seen in simulation.

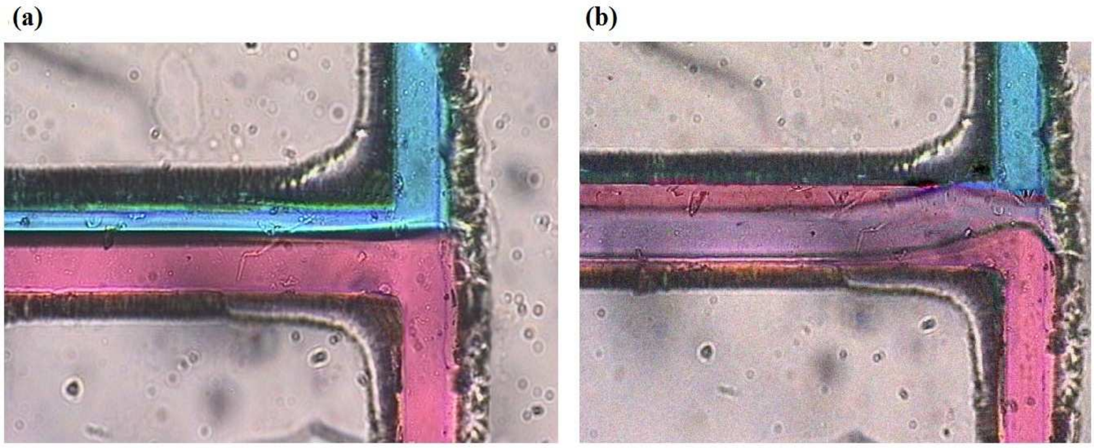

Fig. 5.14. The observations of the mixing process at the junction of micro T-mixer for water-water systems at (a) Re=1, $V_1/V_2=5$ and (b) Re=100, $V_1/V_2=5$.

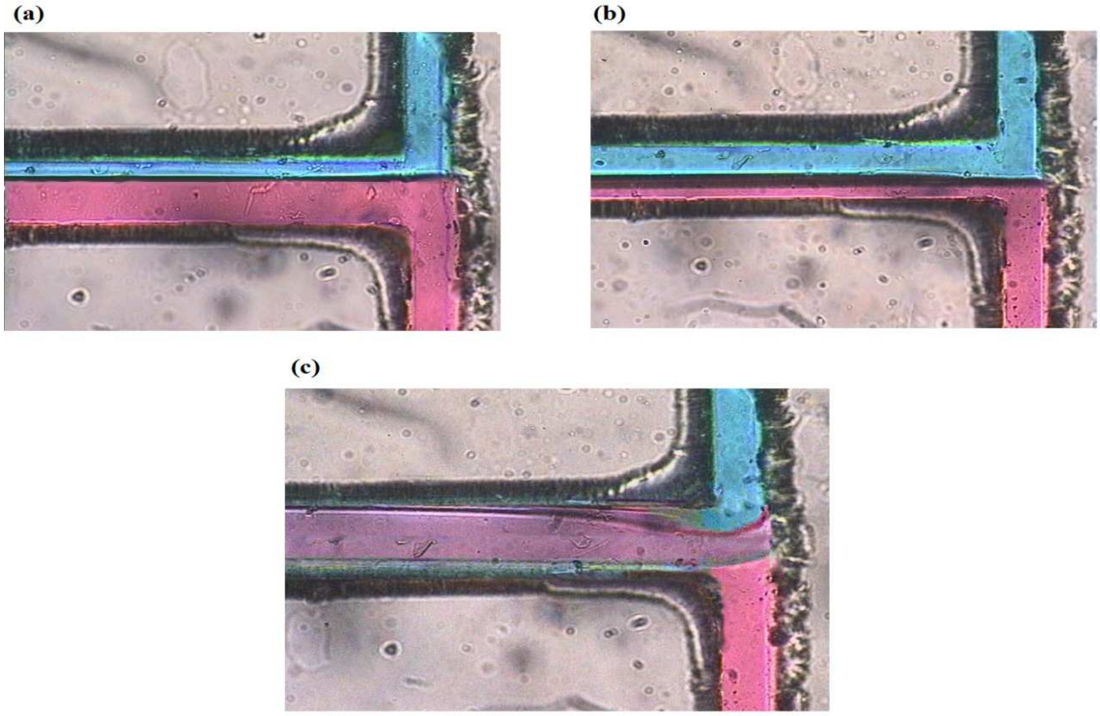

Fig. 5.15. The observations of the mixing process at the junction of micro T-mixer for water-ethanol systems at (a) Re=1, $V_w/V_e=5$, (b) Re=1, $V_e/V_w=5$ and (c) Re=100, $V_e/V_w=5$.

5.4 Summary

Three-dimensional numerical simulations and experimentals were performed to study the flow dynamics and mixing characteristics of liquids flows inside T-shaped micromixers, when the two inlet fluids are either both water or water and ethanol. In particular we showed that, contrary to what one could think beforehand, the mixing efficiency of water-ethanol systems is lower than the corresponding water-water case.

The experimental observation is consistent with the numerical finding that interface position and thickness, the vortex generation and therefore mixing performance depend not only on Reynolds number, but also on the type of fluids and initial conditions.

Chapter 6

Split T-Micromixer

6.1 Introduction

In this work, we study the mixing process in T-micromixers at low and moderate Reynolds number, when Re = 1 or Re = 100, as these cases are highly relevant to medicine and biology. Typical low-Reynolds-number biomedical and biological flow systems include flow in the lower airways, cerebrospinal fluid flows, flows in the eye and the inner ear (balance sense, hearing), microcirculation and red blood cell transport, propulsion and collective behavior of micro-organisms, and biomedical micro-devices (e.g. filters, pumps, micro-robots). Accordingly, although it is well known that at higher Reynolds number engulfment flow strongly enhances mixing, here we want to show that similar effect can be achieved in the creeping flow regime, by choosing clever appropriate geometries. In fact, in this work new micromixer designs are proposed, presenting a split into the inlet channels that enhance their mixing performances, even at small Reynolds number. Detailed numerical studies of the new micromixer designs are presented based on a thorough characterization of the mixing process that is achieved via computational modeling.

6.2 Numerical Modeling

We considered a reference case from previous chapter, consisting of a T-shaped microchannel with 3 branches, i.e. 2 inlets and 1 outlet (Fig. 5.1). Both inlet branches have a 10^{-4} m $\times 10^{-4}$ m cross section, while the mixing channel is 2×10^{-4} m wide and 10^{-4} m deep, corresponding to a hydraulic diameter of 133×10^{-6} m. The length of the inlet (L_{in}) and mixing channels (L) are 5×10^{-4} m, which are sufficient for mixing zone while the fully developed velocity profile used in each inlets.

Figure. 6.1 shows vertical and horizontal schematics of split flow T-micromixers. The split inlet channels are 5×10^{-5} m wide 10^{-4} m deep in the vertical splitting scheme, and 10^{-4} m wide - 5×10^{-5} m deep for the horizontal splitting scheme. In all cases, the outlet channel is 2×10^{-4} m wide and 10^{-4} m deep.

We considered two flow regimes, where the merged flow has average velocity 6.8×10^{-3} m/s and 6.8×10^{-1} m/s, corresponding to Reynolds numbers of 1 and 100, respectively. A new grid independency study was performed, showing that a 1.9×10^{-6} m mesh size in the inlet channel is necessary to capture the flow feature. This mesh was gradually increased up to 1.9×10^{-6} m (i.e. the same as in the simple T-shape device) in the mixing channel.

Other effects, such as chemical reaction and heat transfer, are not included in our numerical simulation[138]-[139]-[140]-[141]-[142]. We considered two cases. In the former (case a), we injected the red fluid into inlets R1 and L1 and the blue fluid into R2 and L2; in the latter (case b), we injected the red fluid into inlets R1 and L2 and the blue fluid into R2 and L1.

A second order discretization scheme was used to solve all equations; using FLUENT 6.3 by Ansys Inc. Simulations were typically considered converging when the normalized residuals for velocities fell below 1×10^{-6}. The steadiness of the solution with iterations was also assessed by checking the concentration field in the outlet section of the mixing channels at different iterations. The values of density and viscosity were set equal to 10^{3} kg m^{-3} and 10^{-3} kg m^{-1} s^{-1} for water and, while the diffusion coefficient was set equal to $D = 3\times 10^{-10}$ m^{2} s^{-1}, corresponding to that of a water ink mixture, as this value is very close to the self- diffusivity of pure water as well.

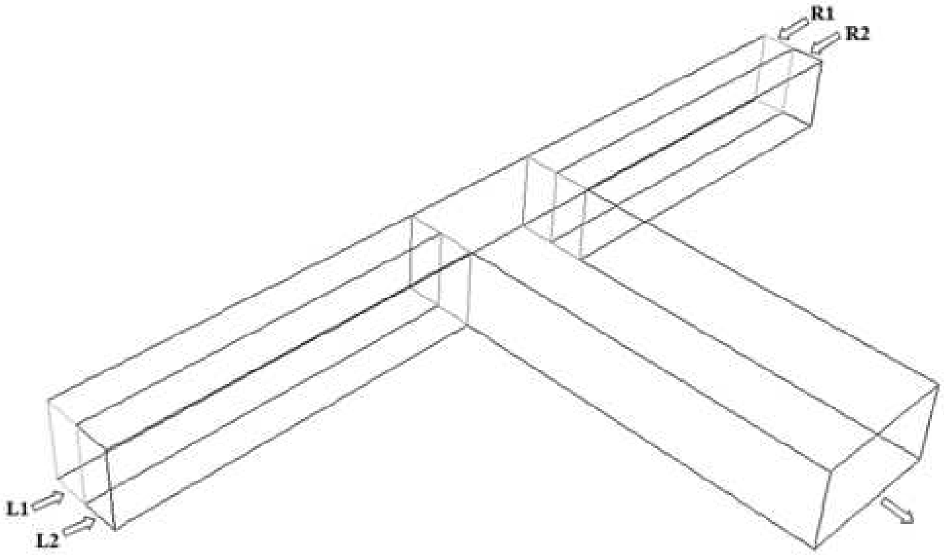

Vertical Splitting

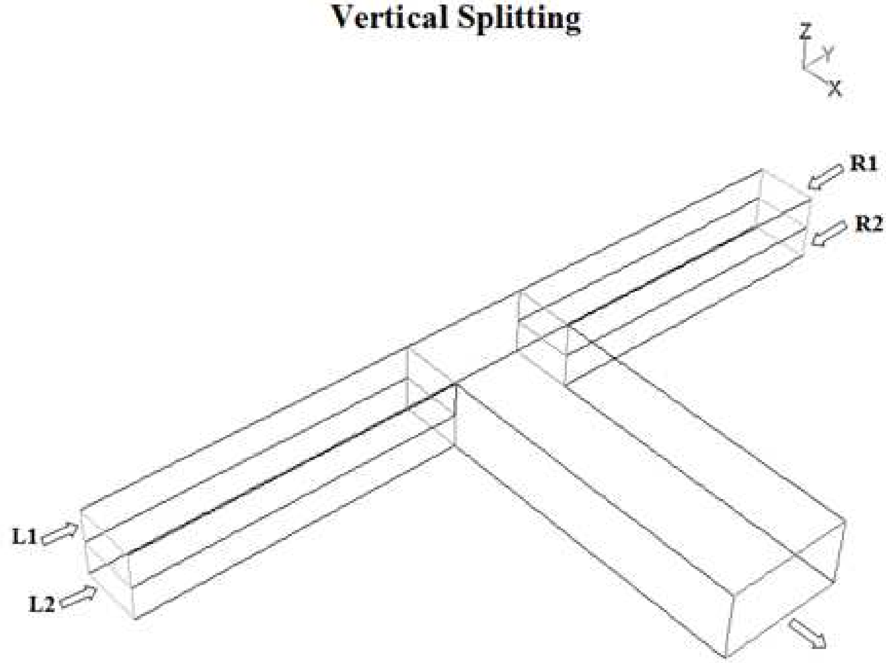

Horizontal Splitting

Fig. 6.1. Schematics of inlet splitting

6.3 Results and Discussions

6.3.1 Equal Inlet Flow Rates

First, we imposed that each of the four inlet branches have the same flow rate. In this case, the contour plots and the degree of mixing at the outlet are described in Figure 6.2 and Table 6.1, respectively. Fig. 6.2 shows clearly that the main effect of the split inlets is an increase of the number of interfaces, which in turn causes an increase of the degree of mixing, as it appears in Table 6.1, when we compare column T (simple T-micromixer) with columns 2T (split T-micromixer). In fact, at Re = 1, mixing depends mainly on the residence time of the fluid particles located near the interfaces; accordingly, it is not surprising that, as shown in Table 6.1, the degree of mixing achieved with vertical split is larger than that with horizontal split.

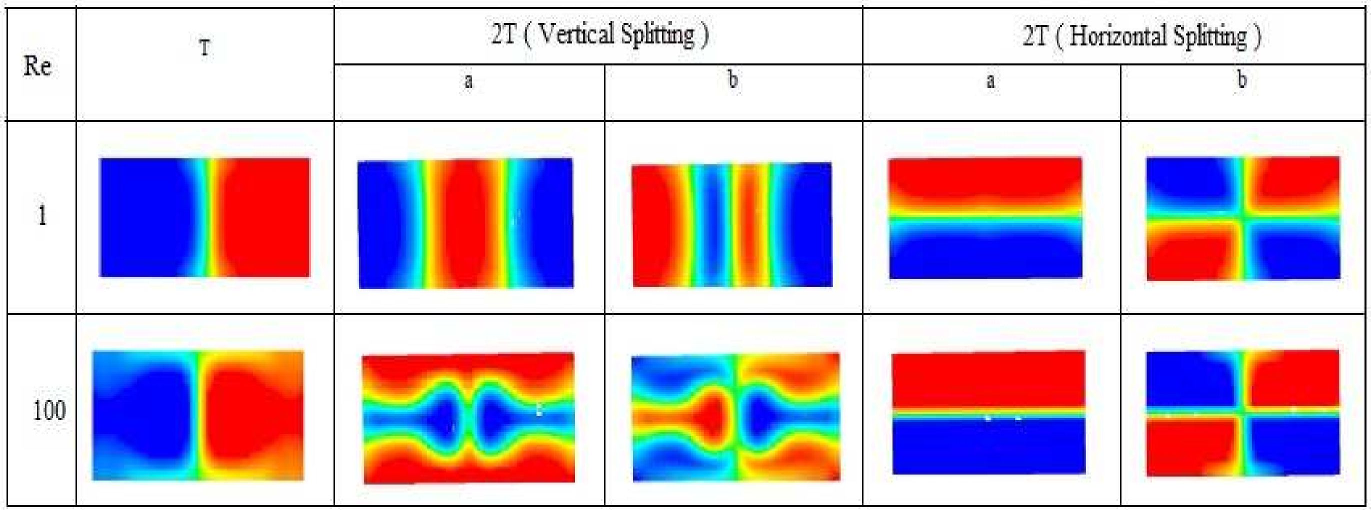

Fig.6.2. Mass fraction contour plots at the outlet cross section of T micromixers, without and with flow splitting, both horizontal and vertical, with equal inlet flow rates, corresponding to two different injection systems, *a* and *b*, as indicated in the text

Table 6.1 Degree of mixing at the outlet cross section of T micromixers, without and with flow splitting, both horizontal and vertical, with equal inlet flow rates, corresponding to two different injection systems, *a* and *b*, as indicated in the text.

Re	T	2T (Vertical)		2T (Horizontal)	
		a	b	a	b
1	4.0	14.0	16.0	7.0	10.0
100	10.6	21.4	24.6	0.2	3.6

When Re = 100, though, the result is much less predictable. In that case, with vertical splits we see the appearance of fluid overlapping, as shown in Fig. 6.3a, which, together with the convection-induced vortices seen in Fig. 6.3b, causes an increase of the degree of mixing that is larger than that occurring in simple T shape devices (where we just have vortices, with no fluid overlapping[143]).On the other hand, with horizontal splits we see the same patterns as for the Re = 1 case, with no vortices nor fluid overlapping (see Fig. 6.4), inducing a very small degree of mixing at the outlet, due to the fact that the residence time is much shorter. Actually, since the height of the inlet channels enhances vortex formation, vortices in horizontal split geometry, i.e. with smaller inlet channel heights, are much weaker than in simple T micromixers, so that the degree of mixing is predictably smaller. This effect is evident in Fig. 6.3 and 6.4, where we show the streamlines, along the axial direction and within the C_1 cross section (see Fig. 6.1) at the upper end of the mixing channel, for both vertical and horizontal geometries, respectively. In fact, with a horizontal split geometry and type (b) injection system, the fluids that are injected in the four inlet channels hardly mix, resulting in a degree of mixing δ_m = 3.6%. On the other hand, in Fig. 6 we see that with a vertical split geometry, the fluids that are injected in inlets R1 and R2 form vortices, and eventually fluids R1 and R2 (and fluids L1 and L2 as well) engulf each other, resulting in a degree of mixing which is almost 7 times larger (24.6% vs. 3.6%). When we use the type (a) injection system, the difference is even larger, as we obtain δ_m = 20% for the horizontal split geometry and δ_m = 21.4% for the vertical case. Here, the surprisingly low degree of mixing in the horizontal split geometry stems from the combination of absence of vortices and large velocity at the interface.

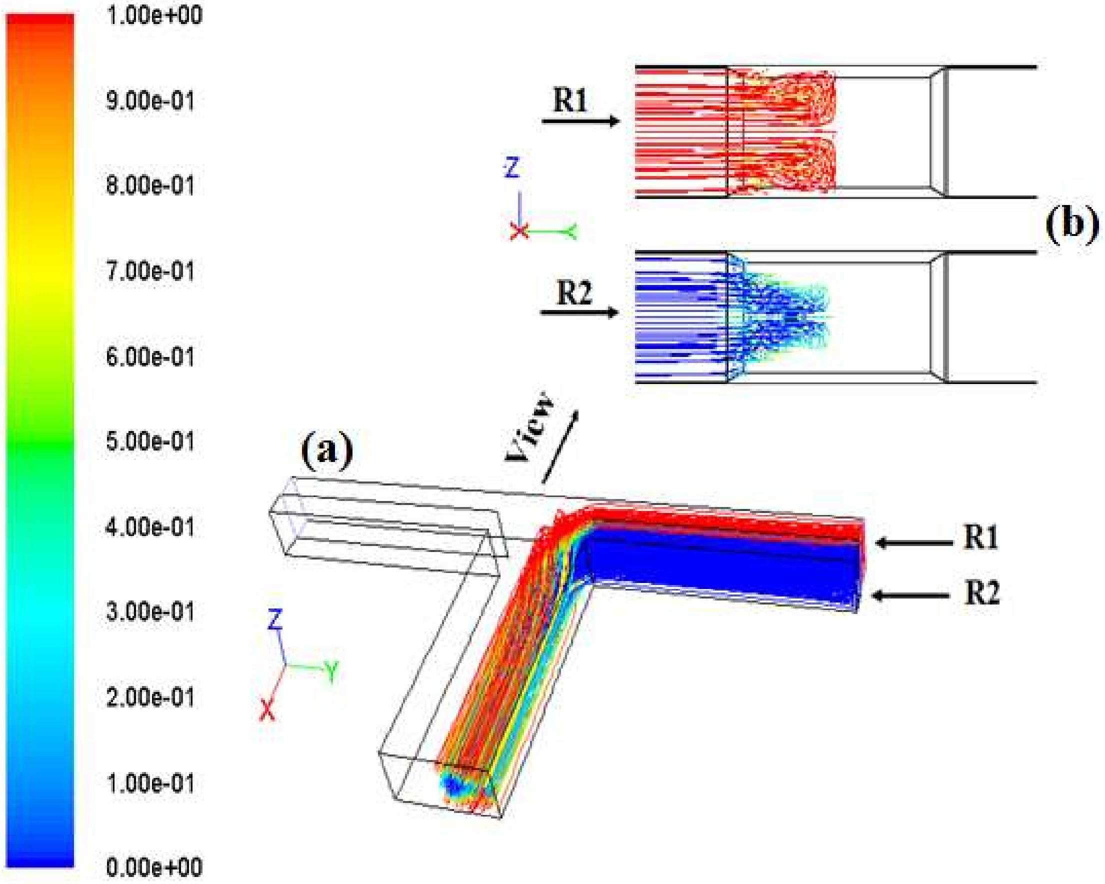

Fig. 6.3. Streamlines for vertical splitting geometry at *Re*=100 (a) along the microchannel axis (b) within the C_1 cross section and. Each color shows fluids injected from different inlets.

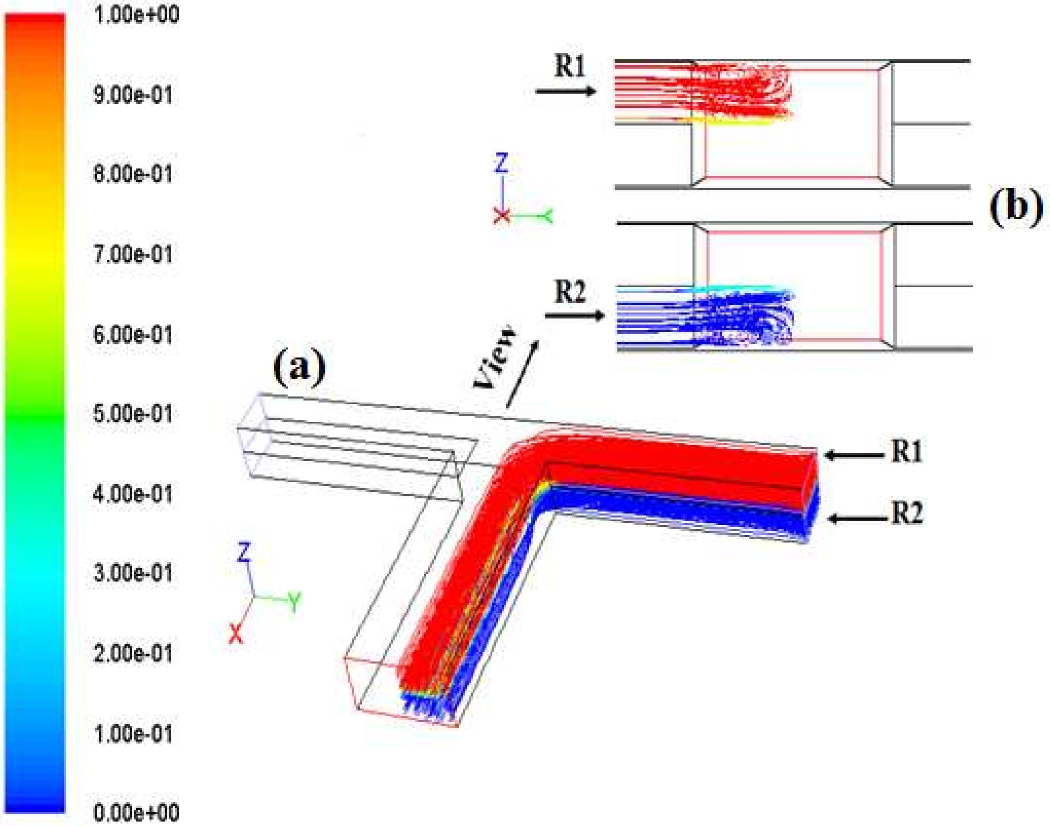

Fig. 6.4 Streamlines in a horizontal splitting geometry at *Re*=100 (a) along the microchannel axis and (b). within the C_1 cross section. Each color shows fluids injected from different inlets

6.3.2 Unequal inlet flow rates

Now we consider the case where, provided that the total inlet flow rates injected on the right and on the left are equal to each other, we allow the flow rates injected in the inlet split sub-channels to change. Predictably, the mixing performance of the micromixer is a function of the sub-channel flow rate ratio.

In Fig. 6.5 we see the contour plots for Re = 1 and Re=100 and when $V_{R1} = 5\ V_{R2}$, $V_{L1} = 5\ V_{L2}$ and $V_{R1} = V_{L1}$ (first raw), $V_{R2} = 5\ V_{R1}$, $V_{L2} = 5\ V_{L1}$ and $V_{R1} = V_{L1}$ (second raw), $V_{R1} = 5\ V_{R2}$, $V_{L2} = 5\ V_{L1}$ and $V_{R1} = V_{L2}$ (third raw). In all cases, the sub-channel flow rate ratio is equal to 5, while the total flow rate on the left inlet channel is equal to that on the right inlet channel, i.e., $V_{R1} + V_{R2} = V_{L1} + V_{L2}$. The results are shown together with the contour plot obtained with a simple T-shaped micromixer with a right-left flow rate ratio of 5 (see left column). As indicated in Table 6.2, the degree of mixing in these cases can either increase or decrease as compared to the equal inlet velocity case. In general, we see that the horizontal split geometry is beneficial towards better mixing, while the vertical split geometry corresponds to lower values of the degree of mixing.

Table 6.2. Degree of mixing at the outlet cross section of T micromixers for *Re* = 1, without and with flow splitting, both horizontal and vertical, with unequal inlet flow rates, corresponding to two different injection systems, *a* and *b*, as indicated in the text. The results refer to the water-water system and (within bracket) the water-ethanol system.

	T	2T (vertical)		2T (horizontal)	
		a	b	a	b
$V_L = V_R$	4	14	16	7	10
$V_{R1} = 5\ V_{R2}$ $V_{L1} = 5\ V_{L2}$	9.6	17.6	17.6	21.5	27.5
$V_{R2} = 5\ V_{R1}$ $V_{L2} = 5\ V_{L1}$		10	10.6		
$V_{R1} = 5\ V_{R2}$ $V_{L2} = 5\ V_{L1}$		13	30	14	37

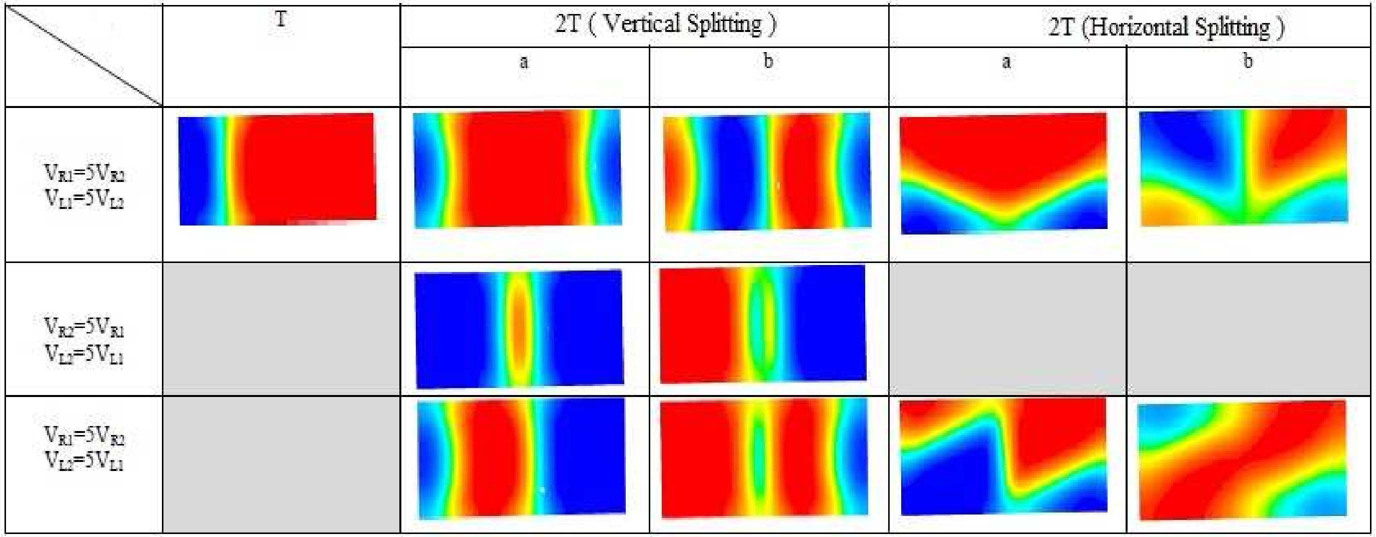

Fig. 6.5. Mass fraction counter plots at the outlet cross section of T micromixers at *Re* = 1, without and with flow splitting, both horizontal and vertical, with unequal inlet flow rates, corresponding to three different injection systems, as indicated in the text. The subcases a and b refer to two different injection systems, as indicated in the text

	T	2T (Vertical Splitting)		2T (Horizontal Splitting)	
		a	b	a	b
$V_{R1}=5V_{R2}$ $V_{L1}=5V_{L2}$	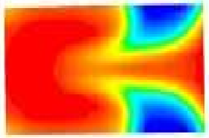	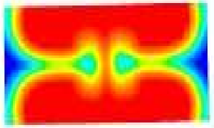	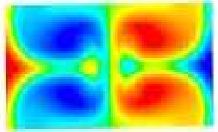	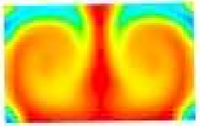	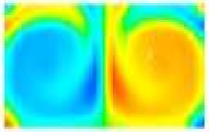
$V_{R2}=5V_{R1}$ $V_{L2}=5V_{L1}$		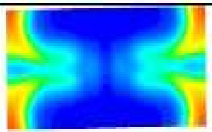	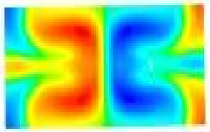		
$V_{R1}=5V_{R2}$ $V_{L2}=5V_{L1}$		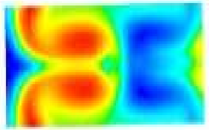	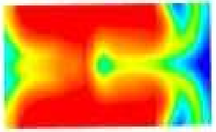	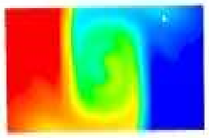	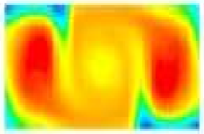

Fig. 6.6 Mass fraction counter plots at the outlet cross section of T micromixers at *Re* = 100, without and with flow splitting, both horizontal and vertical, with unequal inlet flow rates, corresponding to three different injection systems, as indicated in the text. The subcases a and b refer to two different injection systems, as indicated in the text.

As in the equal flow rate case, when Re = 100 we may experience the formation of vortices, fluid swapping and overlapping, which will enhance the mixing process. For example, for the vertical split geometry, comparing the equal flow rate case of Fig. 6.2 with the unequal flow rate case shown in Fig. 6.6: In the latter case, we see the formation of a vortex pair (Fig. 6.7a), fluid swapping (Fig.6.7c) and fluid overlapping (Fig. 6.7b), causing a significant increase in the degree of mixing δ_m, growing from 20% to 40%, approximately.

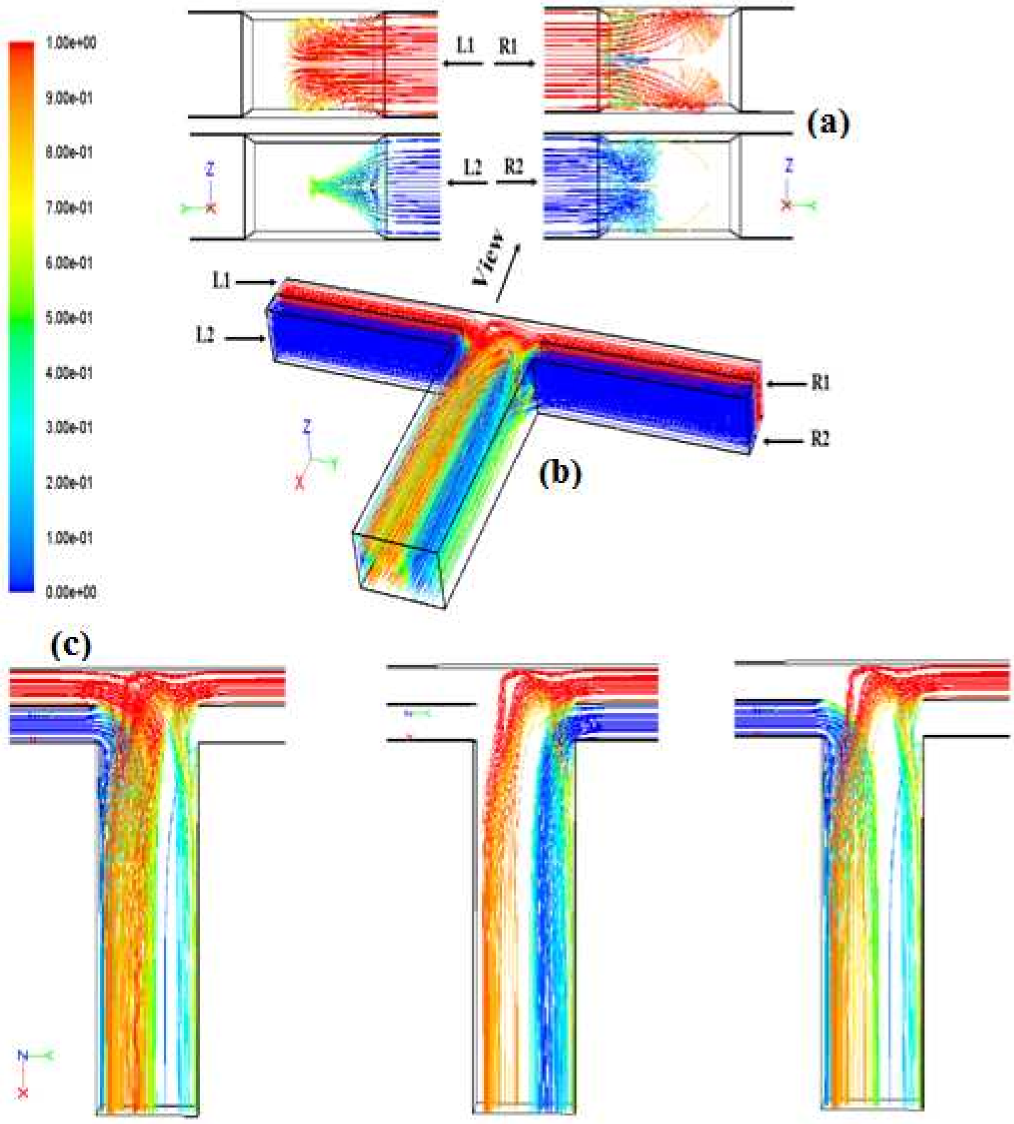

Fig. 6.7 Streamlines at *Re = 100* in a vertical split T-microchannel (a) within the C_1 cross section (b) 3D view and (c) upper view when $V_{R1} = 5\ V_{R2}$ and $V_{L2} = 5\ V_{L1}$.

Mixing appears to be even more efficient with a horizontal split geometry, when we see four pairs of engulfment flow (Fig. 6.8a) with large overlapping (Fig. 6.8b and c), obtaining, consequently, a the degree of mixing, δ_m ~ 60%, which is higher than that of the vertical split T-mixer. There is one exception to this trend, corresponding to the flow pattern shown in Fig. 6.6 (third raw, case a), with no vortices, so that the interface region occupies the center of the channel, where the velocity is large, thereby decreasing the residence time, yielding δ_m ~ 22% (see Tab. 6.3).

We may conclude that, compared to the simple T shaped case and equal flow rates where the degree of mixing is δ_m ~ 10%, for unequal inlet flow rates we obtain δ_m ~ 40% with a vertical split, and δ_m ~ 60% with a horizontal split.

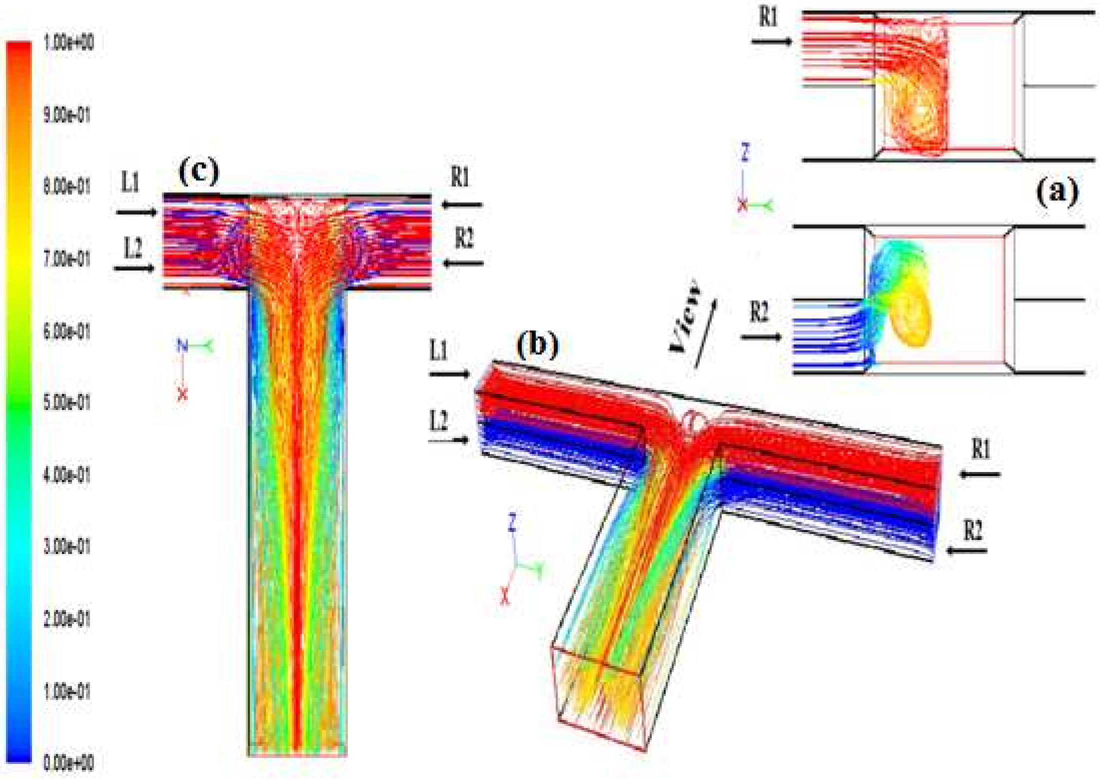

Fig. 6.8. Streamlines at *Re = 100* in a vertical split T-microchannel (a) within the C_1 cross section (b) 3D view and (c) upper view when $V_{R1} = 5\ V_{R2}$ and $V_{L1} = 5\ V_{L2}$.

Table 6.3. Degree of mixing at the outlet cross section of a T micromixer for Re = 100, without and with inlet flow splitting, both horizontal and vertical, with unequal inlet flow rates, corresponding to two different injection systems, *a* and *b*, as indicated in the text.

	T	2T (Vertical)		2T (Horizontal)	
		a	b	a	b
$V_L = V_R$	10.6	21.4	24.6	0.2	3.6
$V_{R1} = 5\ V_{R2}$ $V_{L1} = 5\ V_{L2}$	28.0	28.4	28.0	58.0	54.2
$V_{R2} = 5\ V_{R1}$ $V_{L2} = 5\ V_{L1}$	-	38.0	41.4	-	-
$V_{R1} = 5\ V_{R2}$ $V_{L2} = 5\ V_{L1}$	-	41.5	39.0	22.0	58.5

6.4 Summary

In this work we studied numerically the mixing process of two low diffusivity fluids in a micromixer, proposing a split T-shaped geometry to enhance the process. When Re = 1, mixing is purely due to molecular diffusion and therefore it depends on the residence time of the fluid particles that are located near the interfaces. Accordingly, in those conditions the mixing efficiency of a split T-micromixer is better than that of a simple T-micromixer. On the other hand, when Re = 100, mixing may be strongly enhanced by the formation of complex patterns, such as vortex pairs, fluid swapping and overlapping, which, however, need to have enough room to form. Accordingly, for equal flow rates in the inlet sub-channels, vortex formation is enhanced in vertical split geometry, with the degree of mixing increasing by a factor *2* as compared to the no-split case. On the other hand, in the horizontal split geometry, vortices are damped, resulting in a mixing efficiency which is several times lower than both the no-split and the Re = 1 cases. Finally, for unequal flow rates in the inlet sub-channels, at Re = 100 fluid vortices, swapping and overlapping occur for both vertical and horizontal case, resulting in a strong increase of the degree of mixing, especially in the horizontal case, where we have engulfment.

Chapter 7

Swirling Micrimixer

7.1 Introduction

In the previous chapters, it was found that the geometric topology of a microchannel could create useful disturbance for microfluidic mixing. On the other hand one micromixer has different behavior while we use just one kind of fluid or two different fluids.

In this chapter we present a general strategy for creating transverse flows in swirling microchannels whose geometry is illustrated in Fig. 7.1, that can be used to induce chaotic stirring at low Re ($1<Re< 100$). A numerical study of the mixing of two fluids (pure water and a solution of glycerol in water) in a microchannel was carried out. By varying the glycerol content of the glycerol/water solution, the variation in mixing behavior with changes in the difference in the properties of the two fluids (e.g., viscosity, density and diffusivity) was investigated. We examine the influence of difference in the properties of two mixing fluids on the mixing behavior. The mixing of two miscible fluids, i.e., pure water and a water-glycerol solution was studied numerically. In the systems studied, the difference in the properties of the two mixing fluids was adjusted by varying the amount of glycerol in the glycerol/ water solution. The mixing performance of the two liquids was tested in two types of micromixer: a three-dimensional stair mixer and a T- mixer. The mixing of the two fluids inside these micromixers was simulated at $Re =1$, 10 and 100. Three values of mass fraction $\emptyset$, were chosen in the present study, $\emptyset= 0$, 0.25 and 0.5.

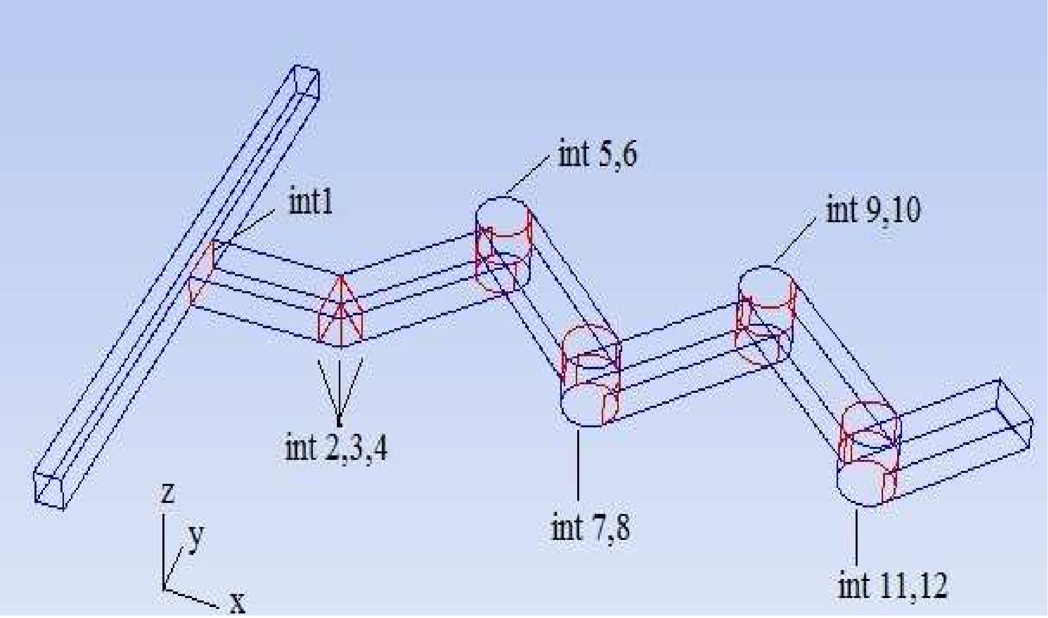

Fig. 7.1. Geometry of three-dimensional swirling micromixer.

7.2 Numerical Modeling

Flows in which two fluids, pure water and a solution of glycerol in water in the present case, are mixing can be simulated by solving the following general transport equation[144](Cussler, 1997):

$$\nabla \cdot [\rho(\emptyset)\emptyset\mathbf{u}] = \nabla \cdot [D(\emptyset)\nabla\emptyset] \tag{7.1}$$

where ρ is density of mixture, D is mass diffusivity, **u** is the velocity vector. As mentioned earlier, $\emptyset$ is the mass fraction of glycerol in the fluid.

$$\emptyset = \dot{m}_g/(\dot{m}_g + \dot{m}_w) \tag{7.2}$$

where $\dot{m}_g$ and $\dot{m}_w$ are the mass flow rate of glycerol and water in the mixed solution, respectively. A Neumann boundary condition is applied at the solid surface and outlet. The governing equations of continuity and three dimensional momentum can be expressed as follows:

$$\nabla \cdot [\rho(\emptyset)\mathbf{u}] = 0 \qquad (7.3)$$

$$\nabla \cdot [\rho(\emptyset)\mathbf{u}] = -\nabla \cdot \mathrm{p} + \nabla \cdot [\mu(\emptyset)\nabla\mathbf{u}] \qquad (7.4)$$

where μ is dynamic viscosity of the fluid. During the mixing of two fluids, we would like to express the properties of the fluid mixture as functions only of $\emptyset$ however, Eqs. (7-1) - (7-4) are fully coupled with different properties. To decouple them, the equations of continuity and momentum based on an initially assumed $\emptyset$, μ ($\emptyset$) and D ($\emptyset$) fields were solved first, and then the transport equation of each species based on the intermediate velocity field and D ($\emptyset$) was solved. The properties ρ ($\emptyset$), μ ($\emptyset$) and D ($\emptyset$) were updated by the calculated $\emptyset$ field. All the equations were iteratively solved by the above procedure.

As mentioned before, Computational fluid dynamics simulation was carried out with the commercial code FLUENT 12.0 (ANSYS Inc.). The model used considers laminar mixing of the species in a T-type micromixer. A fully developed velocity profile was assumed at the inlets and the pressure at the exit was assumed to be fixed to the local atmospheric pressure. A no-slip boundary condition at the side walls was applied. The SIMPLE-consistent algorithm [145](Vandoormaal and Raithby, 1984) was implemented for pressure–velocity coupling. The solution is considered to attain convergence when the relative difference of adjacent variables in consecutive iterations is less than 10^{-6}.

A grid dependency test has been carried out to find the optimal number of grids and to ensure that the solution is independent of the grid size four different structured grid systems with the number of grids ranging from 480×10^3 to 212×10^4 were tested. The distribution of the velocity (Fig. 7.3) and variance of the mass fraction along the serpentine channel were evaluated with an increasing number of grids. The grid distribution was checked and adjusted in each case due to the complicated geometry of the channel. The density of the grid was maintained higher at cylindrical bend regions in order to capture the flow structure precisely in the region where the flow changes rapidly. Finally, from the results of the grid dependency test, 135×10^4 was selected as the optimum number of grids. An example of the structured grid system employed in this work is shown in Fig. 7.2.

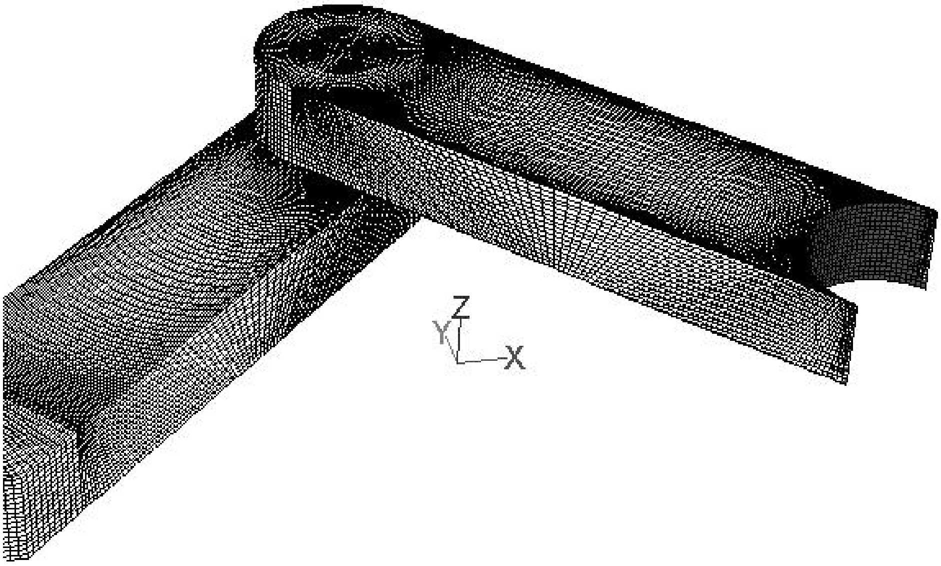

Fig. 7.2. Example of structured grid system in one cylindrical bend.

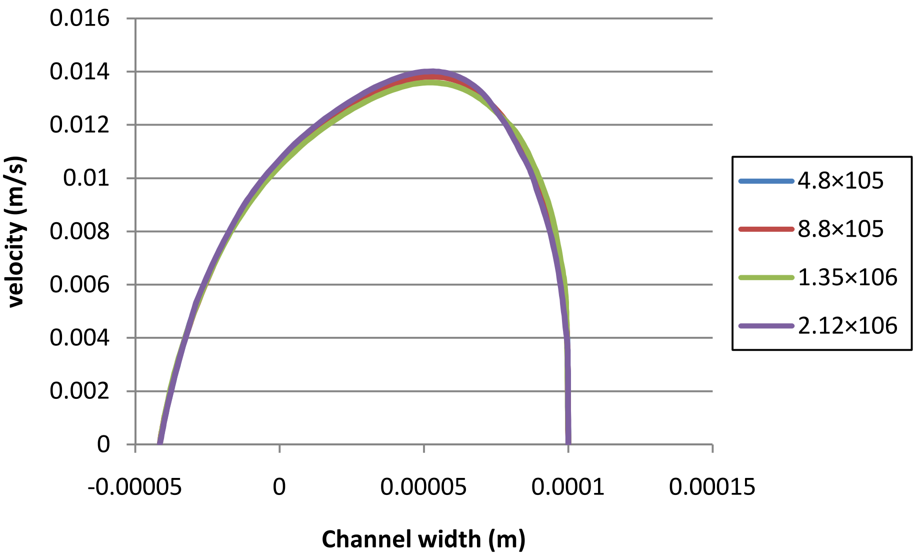

Fig. 7.3. Velocity distribution grid independency for Re = 1 at interior 8 (unit2 exit) in the mixing channel.

The changes in the viscosity and diffusivity of the water–glycerol mixture [146](Cohen et al., 2000) with increasing $\emptyset$ are shown in Fig.7.4. Both the diffusivity and viscosity of the mixture are very sensitive to $\emptyset$, with the diffusivity decreasing and the viscosity increasing with increasing $\emptyset$ the diffusivity varies approximately inversely with viscosity, showing a large drop on going from the dilute, $\emptyset = 0$, to the concentrated solution. Schematic diagrams of three dimensional swirling mixer are shown in Fig. 7.1.

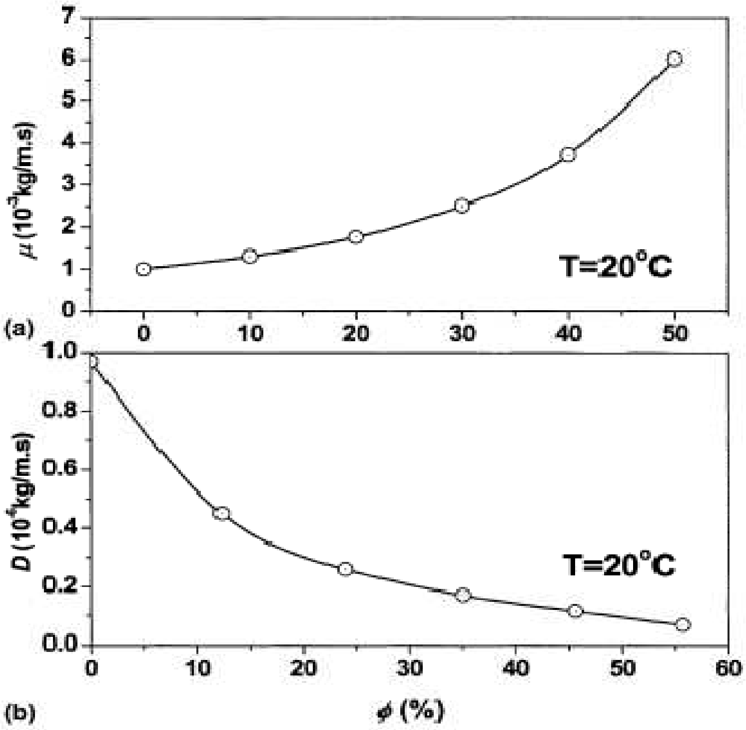

Fig. 7.4. Dependence of viscosity and diffusivity of mixture on mass fraction of glycerol: (a) viscosity; (b) diffusivity.

Equal volume streams of two fluids were injected into the micromixers at the same condition: one fluid was glycerol dissolved in water and the other one was pure water.

7.3 Results and Discussions

7.3.1 Mixing Distributions

First, we carried out numerical simulations of the mixing of two fluids with zero gradient of ∅ at Re = 1 and 10. To investigate the dependence of mixing performance on ∅, three mixing cases are considered (∅= 0, 0.25 and 0.5). We now consider the two-fluid flow inside the three dimensional stair mixer at Re = 1, 0.25 and 0.5.

Fig. 7.5 shows the variation in mixing uniformity with distance through the mixer at the three values of ∅.

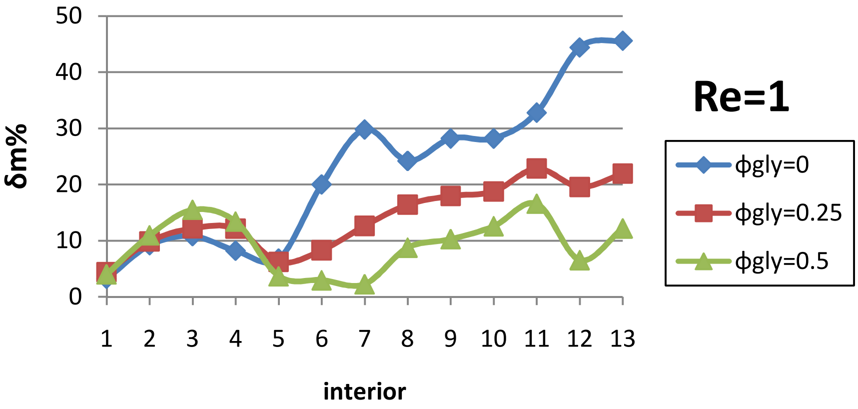

Fig. 7.5. Mixing performance of three-dimensional stair mixer at Re = 1.

The mixing uniformity decreases with increasing ∅ with the discrepancy in mixing uniformity for systems with different ∅ becoming larger as the fluids move downstream. Fig. 7.6 shows cross-sectional visualizations of the flows in the mixing of the systems with ∅= 0, 0.25 and 0.5 at various downstream distances.

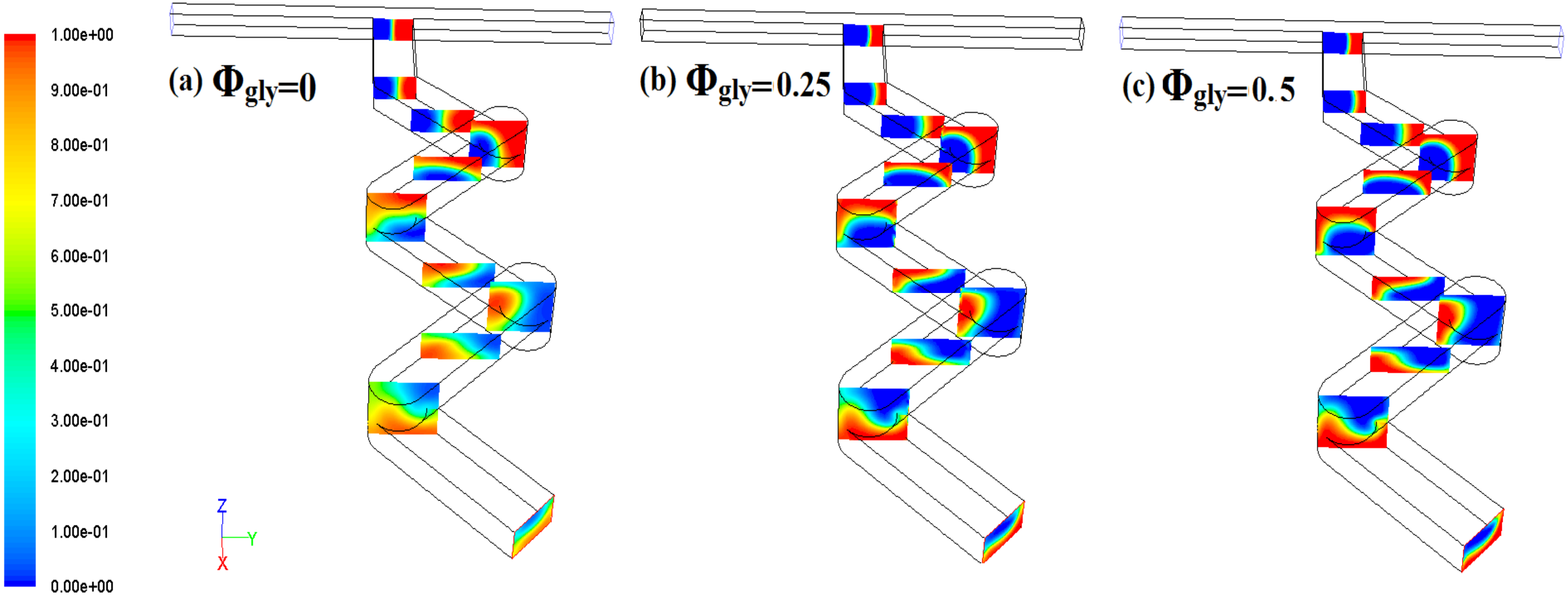

Fig. 7.6. Cross-section mixing photograph of three-dimensional swirling mixer at Re = 1.

As shown in Fig.7.6, the mixing behavior of the glycerol-containing solution (the left fluid) at each cross-section is similar at the three values of $\emptyset$. The glycerol-containing solution is quickly rotated in counter clock wise in the first cylindrical unit, and then appears as a thumb shape. In the subsequent cylindrical units, the glycerol-containing solution continues rotating and enlarges further into the other fluid (pure water). In the straight channel, the glycerol-containing solution slows down due to its higher viscosity. The occupation of more space by the glycerol-containing solution at higher $\emptyset$ has the effect of pushing the bottom fluid, increasing its flow velocity. As the value of $\emptyset$ increases at inlet, the deformation of the slowly moving thumb-shaped configuration of the glycerol-containing solution becomes more pronounced. The interface between two fluids is then enlarged at every cross-section of the serpentine channel.

It is known that pure mixing of two fluids occurs through a combination of flow advection and molecular diffusion. At a fixed Re (Re = 1), the residence time of fluids inside the mixer decreases with increasing $\emptyset$. Given the previous observation of no chaotic advection at Re = 1, we conclude that molecular diffusion, which is proportional to the residence time of the fluids, is the dominant factor in two-fluid mixing inside the swirling mixer.

The mixing behavior inside the swirling mixer at Re = 10 is considered. Fig. 7.7 shows the mixing uniformity of the two fluids inside the mixer for systems with $\emptyset_{gly}$ = 0, 0.25 and 0.5.

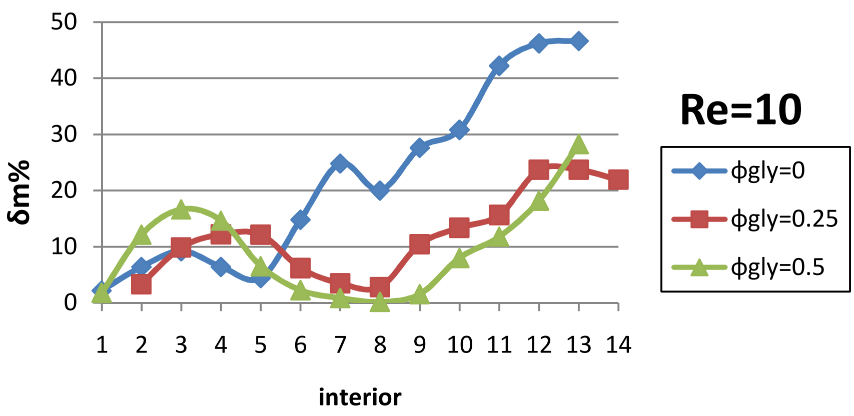

Fig. 7.7. Mixing performance of three-dimensional swirling mixer at Re = 10

The mixing uniformity is higher at Re = 10 than at Re = 1 due to small chaotic advection. However, at Re = 10 the mixing performance before cylindrical at every cross-section decreases with increasing ∅ which is the same of the behavior observed at Re = 1 (Fig. 7.5). The corresponding mixing is visualized in Fig.7.8.

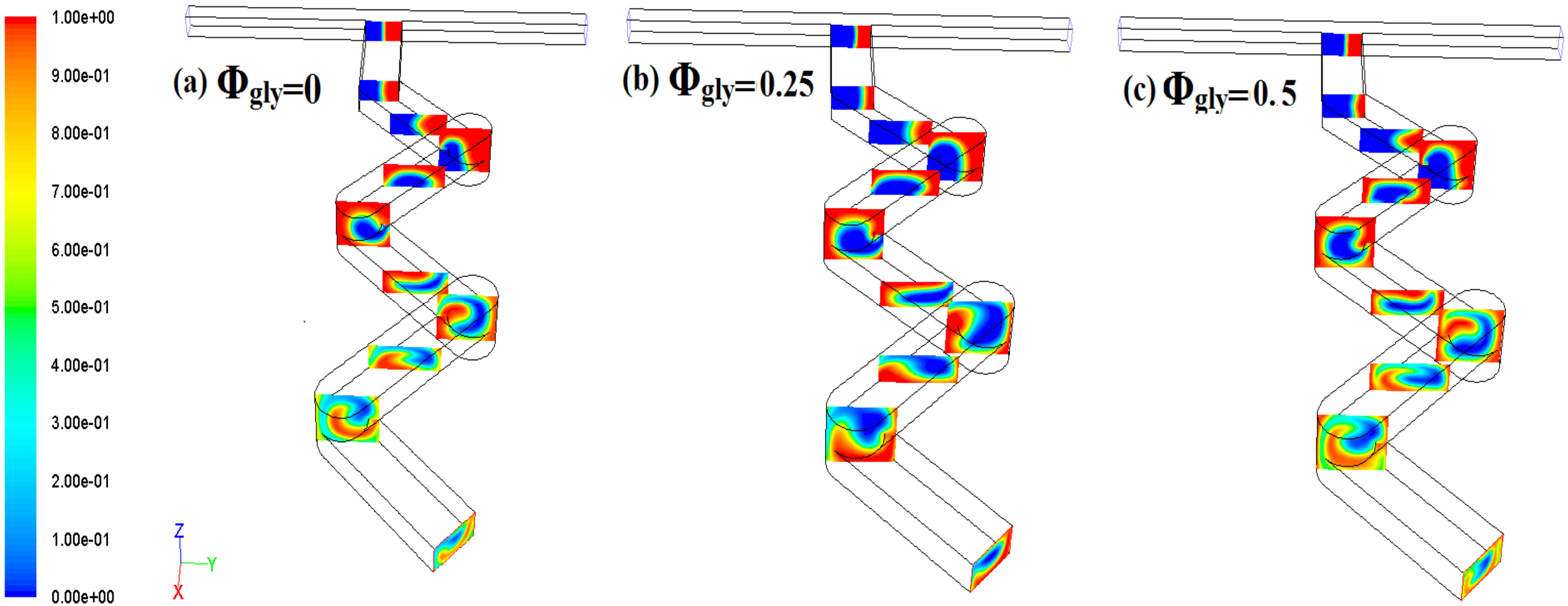

Fig. 7.8. Cross-section mixing photograph of three-dimensional swirling mixer at Re = 10.

The variation in mixing behavior with increasing ∅ is similar to that observed at Re = 1, except that the thumb-shaped configuration of the glycerol-containing solution is deformed to be very slender after the first cylindrical units. At both ∅= 0.25 and 0.5, the glycerol-containing solution detaches from the left surface and moves to a central location at the outlet.

The switch in the behavior of the mixing uniformity on going from Re = 1 to 10 (Figs.7.5 and 7.7) can be attributed to a shift from the dominance of molecular diffusion at Re = 1 to the dominance of advection at Re = 10.

The mixing behavior inside the stair mixer at Re = 100 is considered in Fig. 7.9. As the Reynolds number increases, however, the vertical interfacial line is deformed to a curved one before the first cylindrical units. At an even higher Reynolds number, Re = 100, the interface becomes more complicated by the combined effect of rotational flows and back flows due to inertia (Fig. 7.10). The complex flow pattern occurring in Re = 100 is thought to be the main cause of enhanced mixing in this mixing device.

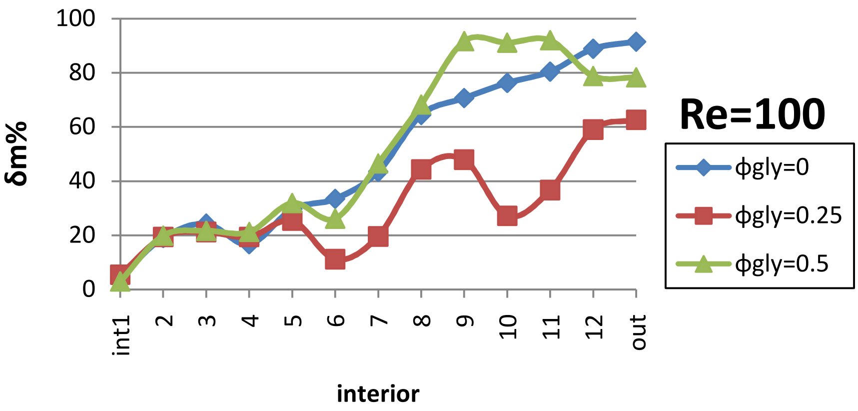

Fig. 7.9. Mixing performance of three-dimensional swirling mixer at Re = 100.

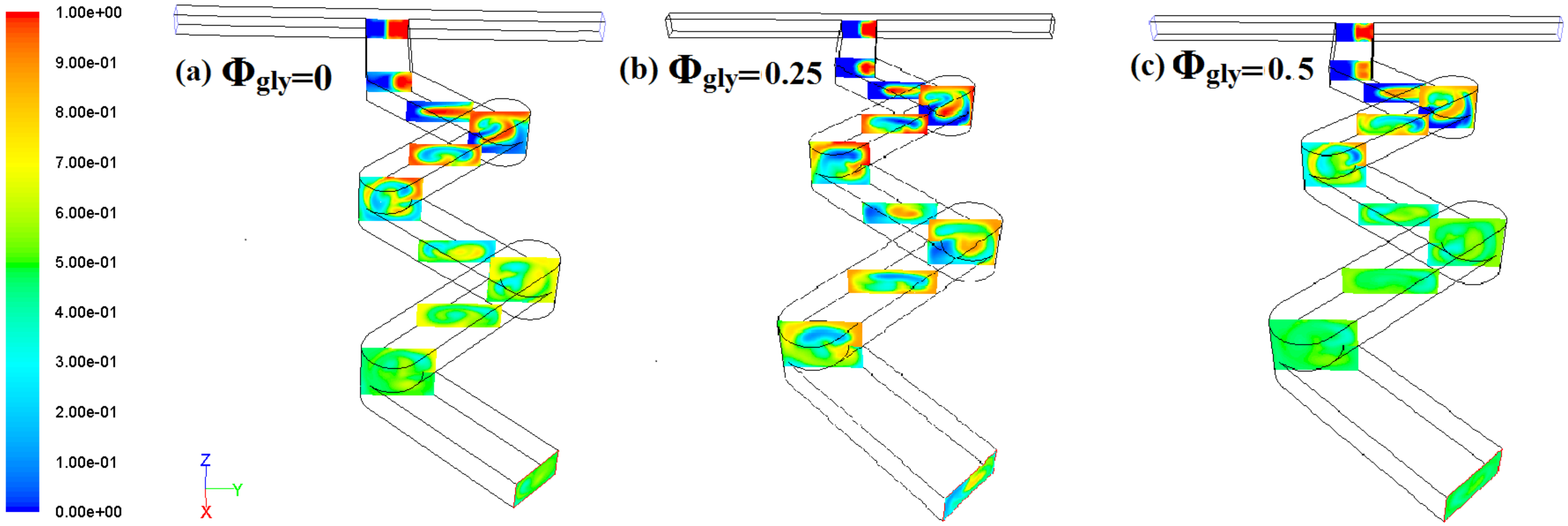

Fig. 7.10. Cross-section mixing photograph of three-dimensional swirling mixer at Re = 100.

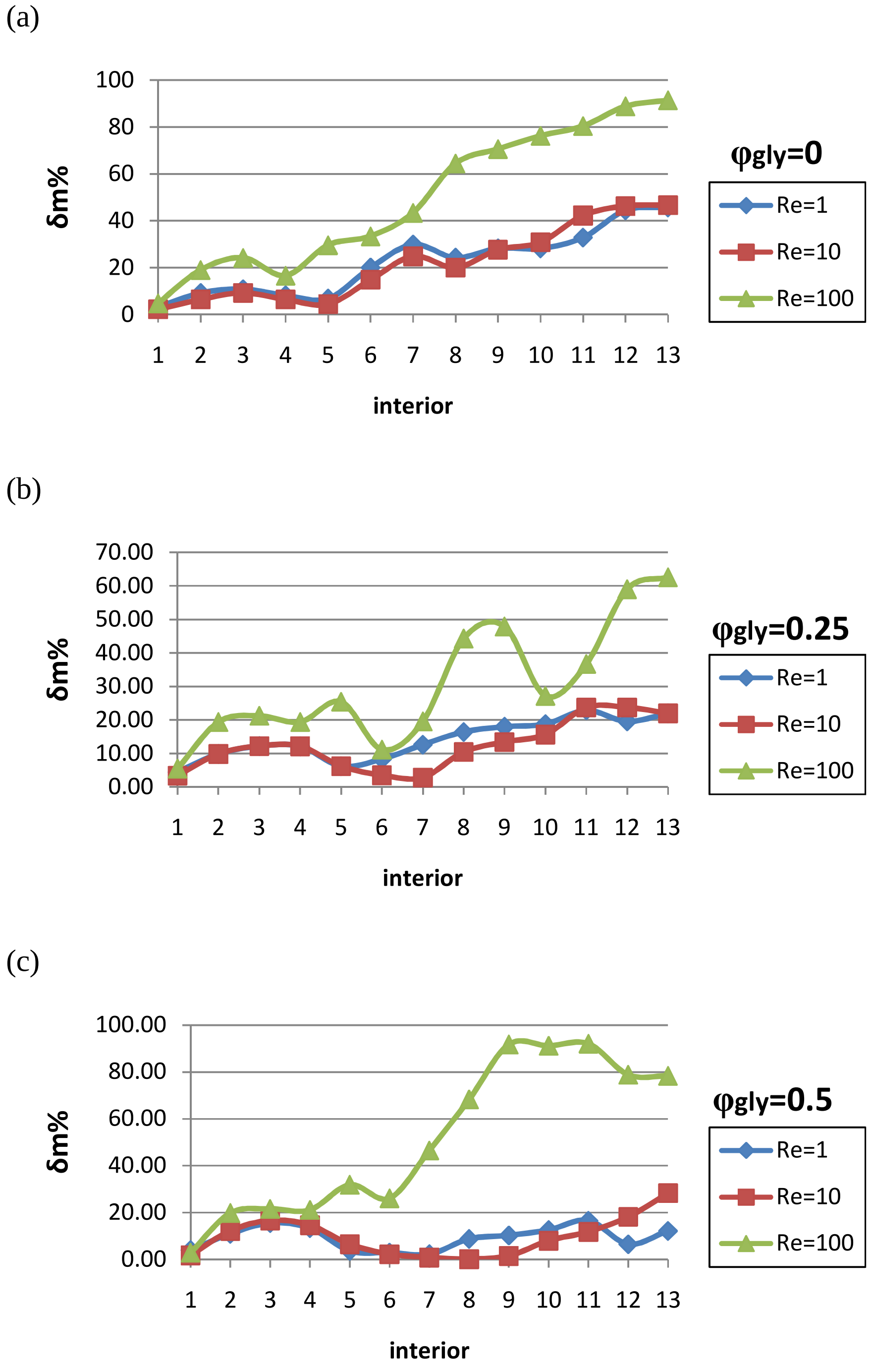

Fig. 7.11. Mixing performance of three-dimensional stair mixer at different φ (a) Re=1, (b) Re=10 and (c) Re=100.

We study the progress of mixing for the three Reynolds numbers, Re = 1, 10 and 100. Figure 7.5, 7.7 and 7.9 shows the progress of mixing visualized by the concentration along the channel positions for the three Reynolds numbers. As the Reynolds number increases, stretching and folding of interfaces become more vigorous. It is evident that the flow at Re = 100 is capable of producing the best mixing among the three cases, while at the lowest Reynolds number, Re = 1, one cannot mix the two fluids at all. The onset of chaos in the whole cross-section requires a minimum cross-over Reynolds number.

7.3.2 Swirling Intensity and Fluid Distribution

The swirling intensities in the first cylindrical unite are shown in Fig. 7.12. Two working fluids are fully developed before entering the serpentine channel with no swirling. This effect is more evident at higher Reynolds number and $\emptyset$ (Fig. 7. 11 and 7.12). When Re = 100, swirling flow with reduced strength is generated, while in the laminar flow regime, i.e., when Re = 1, no such swirling flow is observed due to insufficient advection effect, (Fig 7.12a and b) where there is no vortex streamlines unlike Fig. 7.12 e and 7.12 f the three-dimensional secondary flow effect of stair-type micromixers become effective for high Re regime. The swirling flow alone will result in a stretching effect only, thus existence of chaotic mixing may not be assured. However, will give rise to the stretching and folding mechanism which is typical of chaotic mixing.

On the other hand the mixing index curves discussed in Fig. 7.5, 7.7 and 7.9 shows the presence of oscillations along channel length especially after first cylindrical units. This can be explained with reference to Fig. 7.6, 7.8 and 7.10 which shows mass fraction distribution of glycerin on zy-plane for three different conditions.

The flow velocity has three effects on fluid mixing: the flow velocity determines the residence period—a flow with sufficient residence has improved diffusion; a large flow velocity in a cylindrical units induces an adverse pressure and vortex flow—the interfacial area of the fluids greatly increases if the vortex involves both fluids, and the velocity difference makes fluids with disparate densities separate. For the flow of two fluids with disparate densities, the rotating flow induces a centrifugal force. The centrifugal force is proportional to the density and to the square of velocity. Accompanied by a varied density of fluids, this force makes them separate At smaller Reynolds number, as the centrifugal force is decreased, the density difference has little effect on the separation (Fig 7.11, Re = 1, 10). The effect of centrifugal force may change the proportion of two fluids. This might be the cause for the varying proportion of mass fraction in “cylindrical-shaped” units along channel, and hence shows oscillating curve for mixing index.

This result suggests that three-dimensional secondary flows in the swirling region due to inertia effect can favorably work out to improve the mixing performance by enhancing the stretching and folding of the fluid elements as Re increases But beside this positive effect we may have interface separation at each unite that cause increasing in mixing in cylindrical unites which increases by increasing Re especially after the first unit. The positive effect of increasing the interfacial area exceeds the negative effect of the interface separation; the mixing performance improves with an increasing velocity of flow along the mixing channel.

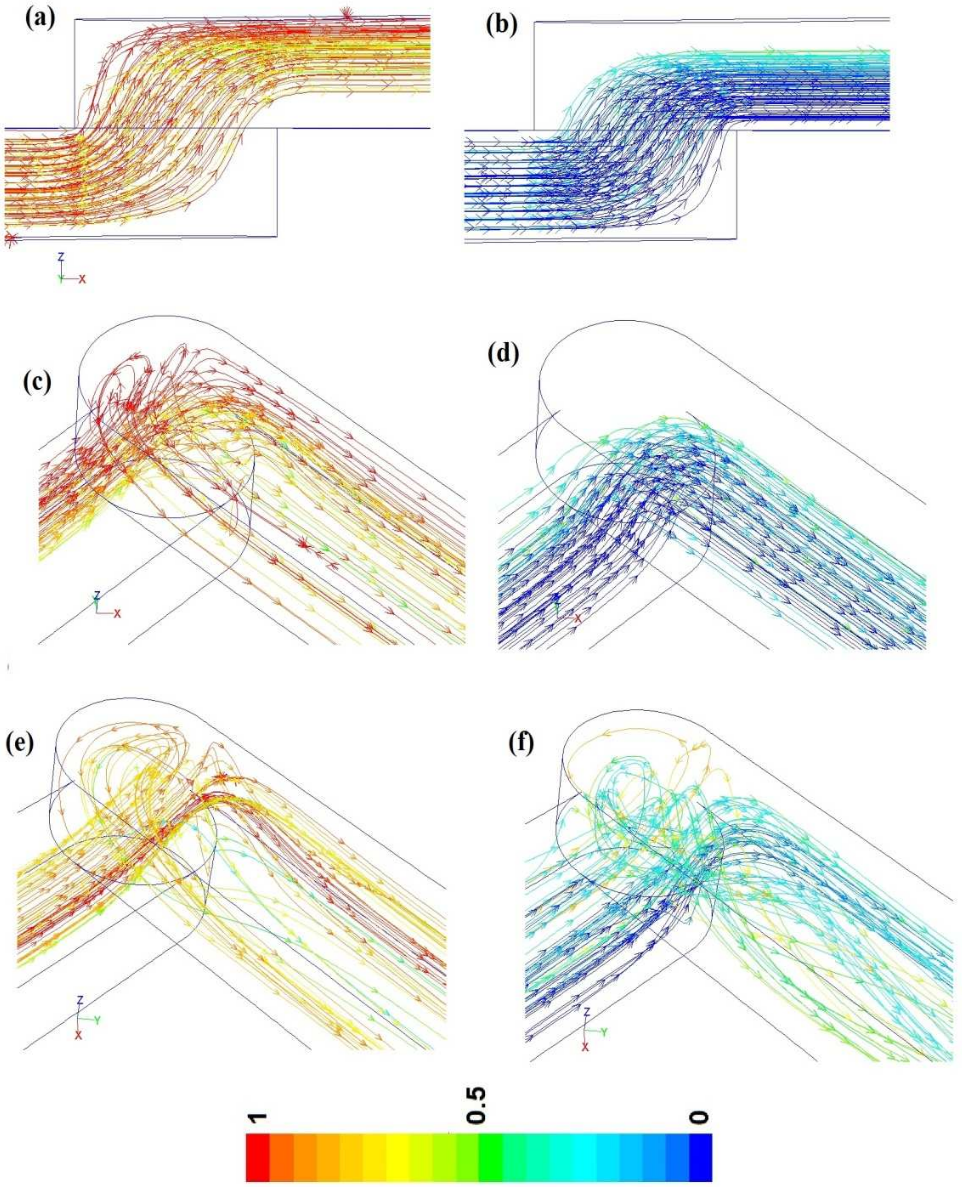

Fig. 7.12. streamlines at first cylindrical unites while $\emptyset_{gly}$=0.5 at (a) and (b) Re=1, (c) and (d) Re=10 , (e) and (f) Re=100. Red and blue colors show water and glycerin fluids respectively.

7.4 Summary

The mixing of two fluids was numerically modeled for a three-dimensional swirling mixer with cylindrical units. In these calculations, the mixing of pure water with a water-glycerol solution was investigated for three different mass fractions of glycerol ($\emptyset_{gly}$= 0, 0.25 and 0.5). These fluids were chosen to test the mixing behavior of fluids with different properties and a large concentration gradient. The dependence of the mixing performance on $\emptyset$ at Re = 1, 10 and 100 was examined. At Re = 1, the mixing performance of both mixers varied inversely with the mass fraction of glycerol due to the dominance of molecular diffusion.

As the flow velocity becomes rapid enough to induce an adverse pressure gradient, a secondary flow of vortices occurs. The threshold velocity becomes diminished on incorporating alternating the cross-sectional area. Vortices increase the interfacial area of fluids by repeatedly stretching and folding in a spiral manner.

At Re = 10 the contact area of the solutions is increased, but the performance of fluid mixing is not improved more because of the smaller period of residence. When the positive effect of increasing the interfacial area exceeds the negative effect of the decreased residence period, the mixing performance improves with an increasing velocity of flow. We can see this situation at Re = 100 with high vortices and swirling. This change in behavior was attributed to the enhancement of flow advection and degree of mixing.

Chapter 8

Conclusions

8.1 Overview

This study has investigated the ability of various geometric configurations to improve the performance of microfluidic mixing, by using computational fluidic dynamic (CFD) simulations and experimental. This chapter presents the findings, contributions and limitations of this research on passive mixing in microchannels. The last section makes recommendations to extend this study on microfluidic mixing.

8.2 Contributions of the Research

8.2.1 Mixing Patterns in T-Micromixers

Three-dimensional numerical simulations were performed to study the flow dynamics and mixing characteristics of liquid flows inside T-type micromixers. The effects of various operating and design parameters on the flow dynamics and the mixing quality were investigated in order to optimize the mixing process. Due to the simple fabrication technology of passive T-shaped micromixers and its easy implementation in complex microfluidic systems, flow mixing mechanisms in this type of mixers were the focus of many investigations. The present study focuses on improving the mixing efficiency of T-micromixers by investigating the effects of different flow parameters, such as the inlet flow velocity, the diffusion coefficient and several geometrical parameters such as the width, height and inlet angle of the mixing channel. To do that, a commercial Computational Fluid Dynamic (CFD) code, i.e.

FLUENT 6.3 by Ansys Inc., was used to solve the three-dimensional flow and mass transfer equations in the proposed geometrical configurations.

It was shown that the development and occurrence of vortices depends strongly on both volume flow rates and geometrical parameters of the mixer such as its aspect ratio and mixing angle. In particular, good mixing requires that the Reynolds number is large enough to enhance transverse convection, while the channel width (and, to a smaller extent, the channel height) must be large enough to avoid vortex damping, due to shear stresses at the wall.

8.2.2 Mixing of Binary Mixtures in Microdevices

The previous work on T-shaped micromixers was directed towards analyzing mixing for a wide range of Reynolds numbers, corresponding to various flow regimes.

A possible way to accelerate mixing is to use perfectly miscible fluids at the inlet. In fact, in that case, the chemical potential difference between the two fluids could induce a diffusive material flux that is higher than that occurring in the case of two identical inlet fluids. Two-fluid mixing is an essential process in many microfluidic devices. For example, various biomedical and biochemical processes involve the mixing of two fluids, including DNA purification, polymerase chain reaction (PCR), enzyme reaction, and protein folding. The performance of such processes relies on effective and rapid mixing of samples and reagents. Accordingly, the present study focuses on the comparison between the case where the two inlet fluids are both water and that when they consist of water and ethanol, using a T-type passive micro-mixer and with Reynolds numbers ranging from 1 to 300. To do that, a commercial Computational Fluid Dynamic (CFD) code, FLUENT 6.3 by Ansys Inc., was used to solve the three-dimensional flow and mass transfer equations in the proposed geometrical configurations.

Three-dimensional numerical simulations and experimentals were performed to study the flow dynamics and mixing characteristics of liquids flows inside T-shaped micromixers, when the two inlet fluids are either both water or water and ethanol. In particular we showed that, contrary to what one could think beforehand, the mixing efficiency of water-ethanol systems is lower than the corresponding water-water case.

The experimental observation is consistent with the numerical finding that interface position and thickness, the vortex generation and therefore mixing performance depend not only on Reynolds number, but also on the type of fluids and initial conditions.

8.2.3 Split T-Micromixers

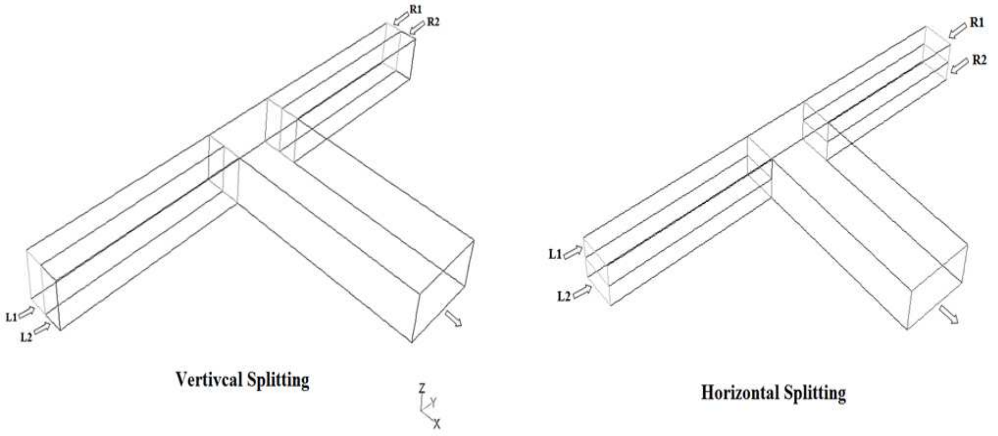

Vertivcal Splitting

Horizontal Splitting

Fig. 8.1 Schematics of inlet splitting

In this work, we study the mixing process in T-micromixers at low and moderate Reynolds number, when Re = 1 or Re = 100, as these cases are highly relevant to medicine and biology. Typical low-Reynolds-number biomedical and biological flow systems include flow in the lower airways, cerebrospinal fluid flows, flows in the eye and the inner ear (balance sense, hearing), microcirculation and red blood cell transport, propulsion and collective behavior of micro-organisms, and biomedical micro-devices (e.g. filters, pumps, micro-robots). Accordingly, although it is well known that at higher Reynolds number engulfment flow strongly enhances mixing, here we want to show that similar effect can be achieved in the creeping flow regime, by choosing clever appropriate geometries. In fact, in this work new micromixer designs are proposed, presenting a split into the inlet channels that enhance their mixing performances, even at small Reynolds number. Detailed numerical studies of the new micromixer designs are presented based on a thorough characterization of the mixing process that is achieved via computational modeling.

We studied numerically the mixing process of two low diffusivity fluids in a micromixer, proposing a split T-shaped geometry to enhance the process. When Re = 1, mixing is purely due to molecular diffusion and therefore it depends on the residence time of the fluid particles that are located near the interfaces. Accordingly, in those conditions the mixing efficiency of a split T-micromixer is better than that of a simple T-micromixer. On the other hand, when Re = 100, mixing may be strongly enhanced by the formation of complex patterns, such as vortex pairs, fluid swapping and overlapping, which, however, need to have enough room to form. Accordingly, for equal flow rates in the inlet sub-channels, vortex formation is enhanced in vertical split geometry, with the degree of mixing increasing by a factor *2* as compared to the no-split case. On the other hand, in the horizontal split geometry, vortices are damped, resulting in a mixing efficiency which is several times lower than both the no-split and the Re = 1 cases. Finally, for unequal flow rates in the inlet sub-channels, at Re = 100 fluid vortices, swapping and overlapping occur for both vertical and horizontal case, resulting in a strong increase of the degree of mixing, especially in the horizontal case, where we have engulfment.

8.2.4 Swirling Micromixer

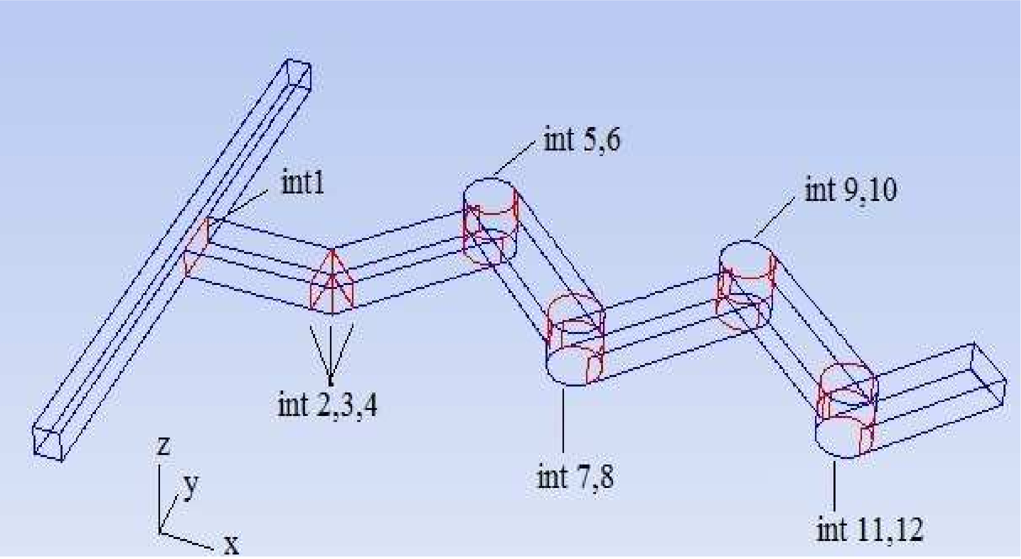

Fig. 8.2. Schematics of swirling micromixer

In the previous parts, it was found that the geometric topology of a microchannel could create useful disturbance for microfluidic mixing. On the other hand one micromixer has different behavior while we use just one kind of fluid or two different fluids.

In this study we presented a general strategy for creating transverse flows in swirl microchannels (Fig. 8.2) that can be used to induce chaotic stirring at low Re ($1<Re< 100$). A numerical study of the mixing of two fluids (pure water and a solution of glycerol in water) in a microchannel was carried out. By varying the glycerol content of the glycerol/water solution, the variation in mixing behavior with changes in the difference in the properties of the two fluids (e.g., viscosity, density and diffusivity) was investigated. We examined the influence of difference in the properties of two mixing fluids on the mixing behavior. The mixing of two miscible fluids pure water and a solution of glycerol in water was studied numerically. In the systems studied, the difference in the properties of the two mixing fluids was adjusted by varying the amount of glycerol in the glycerol/ water solution. The mixing performance of the two liquids was tested in two types of micromixer: a three-dimensional stair mixer and a T- mixer. The mixing of the two fluids inside these micromixers was simulated at Re =1, 10 and 100. Three values of mass fraction (∅) were chosen in the present study, ∅= 0, 0.25 and 0.5.

The dependence of the mixing performance on ∅ at Re = 1, 10 and 100 was examined. At Re = 1, the mixing performance of both mixers varied inversely with mass fraction of glycerol due to the dominance of molecular diffusion.

As the flow velocity becomes rapid enough to induce an adverse pressure gradient, a secondary flow of vortices occurs. The threshold velocity becomes diminished on incorporating alternating the cross-sectional area. Vortices increase the interfacial area of fluids by repeatedly stretching and folding in a spiral manner.

At Re=10 the contact area of the solutions is increased, but the performance of fluid mixing is not improved more because of the smaller period of residence. When the positive effect of increasing the interfacial area exceeds the negative effect of the decreased residence period, the mixing performance improves with an increasing velocity of flow. We can see this situation at Re=100 with high vortices and swirling. This change in behavior was attributed to the enhancement of flow advection and degree of mixing.

8.3 Summary

In this research, passive mixing using geometric and initial conditions variations in microchannels were studied due to its advantages over active mixing in terms of simplicity and ease of fabrication. Because of the nature of laminar flow in a microchannel, the geometric variations were designed to improve lateral convection to increase cross-stream diffusion. Previous research using this approach was limited, and a detailed research program using computational fluid dynamic (CFD) solvers, various shapes, sizes and layouts of geometric structures was undertaken for the first time. Mixing efficiency was evaluated by using mass fraction distributions.

Different types of geometric and initial conditions variations were researched. First, Structures were used to investigate the effect channel geometry on fluid mixing and flow patterns. Secondly, we applied different initial velocity in each inlet to see the effect of Reynolds number applied on mixing behavior. Third, we applied different kind of fluid in each inlet to visualize the effect of viscosity and finally we create new split and stair geometries to enhance the mixing efficiency.

References

---

[1] S. C. Terry, J. H. Jerman, and J. B. Angell, “A gas chromatographic air analyzer fabricated on a silicon wafer,” *IEEE Trans. on Elec. Dev*., **26**, 1880-1886, 1979.

[2] E. Bassous, H. H. Taub, and L. Kuhn, “Ink jet printing nozzle arrays etched in silicon,” *Appl. Phys. Lett*., **31**, 135-137, 1977.

[3] A. Manz, N. Graber, and H. M. Widmer, “Miniaturized total chemical-analysis systems: a novel concept for chemical sensing,” *Sens. Actuators B*, **1**, 244-248, 1990.

[4].N. T. Nguyen, and S. T. Wereley, *Fundamentals and Applications of Microfluidics*,Boston, MA, USA: Artech House, 2002.

[5] S. Latta, “Miniaturization, parallel processing come to lab devices,” *The Scientist*, **11**, 1-7, 1997.

[6] M. Stephan, “Survival in the microfluidics market,” *The Scientist*, **18**, 38-40, 2004.

[7] J.Knight, “Honey, I shrunk the lab,” *Nature*, **418**, 474-475, 2002.

[8] M. Freemantle, “Downsizing Chemistry,” *Chem. Eng. News*, **8**, 27-36, 1999.

[9] S. Borman, “Microchips Deliver on Command,” *Chem. Eng. News*, **5**,. 30-31, 1999.

[10] A. G. Hadd, D. E. Raymond, J. W. Halliwell, S. C. Jacobson, and J. M. Ramsey, “Microchip device for performing enzyme assays,” *Anal. Chem*., **69**, 3407-3412, 1997.

---

[11] S. C. Jacobson, and J. M. Ramsey, “Integrated microdevice for DNA restriction fragmentanalysis,” *Anal. Chem.*, **68**, 720-723, 1996.

[12] I. Kheterpal, and R. A. Mathies, “Capillary array electrophoresis DNA sequencing,” *Anal. Chem.*, **71**, 31A-37A, 1999.

[13] J. Khandurina, T. E McKnight, S. C. Jacobson, L. C. Waters, R. S. Foote, and J. M.Ramsey, “Integrated system for rapid PCR-based DNA analysis in microfluidic devices,”*Anal. Chem.*, **72**, 2995-3000, 2000.

[14] M. Kopp, A. D. Mello, and A. Manz, “Chemical amplification: continuous-flow PCR on a chip,” *Science*, **280**, 1046-1048, 1998.

[15] P. Belgrader, M. Okuzumi, F. Pourahmadi, D. A. Borkholder, and M. A. Northrup, “Amicrofluidic cartridge to prepare spores for PCR analysis,” *Biosens. Bioelectron.*, **14**,. 849-852, 2000.

[16] D. J. Harrison, K. Fluri, K. Seiler, Z. Fan, C. S. Effenhauser, and A. Manz,“Micromachining a miniaturized capillary electrophoresis-based chemical analysis system on a chip,” *Science*, **261**, 895-897, 1993.

[17] S. B. Cheng, C. D. Skinner, J. Taylor, S. Attiya, W. E. Lee, G. Picelli, and J. D. Harrison,“Development of a multichannel micro fluidic analysis system employing affinitycapillary electrophoresis for immunoassay,” *Anal. Chem.*, **73**, 1472-1479, 2001.

---

[18] L. C. Waters, S. C. Jacobson, N. Kroutchinina, J. Khandurina, R. S. Foote, and M. J. Ramsey, “Microchip device for cell lysis, multiplex PCR amplification and electrophoretic sizing,” *Anal. Chem.*, **70**, 158-162, 1998.

[19] I. K. Glasgow, H. C. Zeringe, D. J. Beebe, S. J. Choi, J. T. Lyman, N. G. Chan, and M. B.Wheeler, “Handling individual mammalian embryos using microfluidics,” *IEEE. Trans. Biomed. Eng.*, **48**, 570-578, 2001.

[20] J. Yang, Y. Huang, X. B. Wang, F. F. Becker, and P. R. C. Gascoyne, “Cell separation on microfabricated electrodes using dielectrophoretic/gravitational field-flow fractionation,” *Anal. Chem.*, **71**, 911-918, 2001.

[21] A. Folch, B. H. Jo, O. Hurtado, D. J. Beebe, and M. Toner, “Microfabricated elastomericstencils for micropatterning cell cultures,” *J. Biomed. Mater*. Res., **52**, 346-353, 2000.

[22] E. M. Purcell, “Life at low Reynolds number,” *Am. J. Phys.*, **45**, 3– 11, 1977.

[23] W. Pan, Engineering Fluid Dynamics, *Tsing Hua University Press*, 1988.

[24] B. R. Bird, W. E. Stewart and E. N. Lightfoot, “Transport Phenomena,” *John Wiley & Sons, Inc.*, USA. 1960.

[25] I. Papautsky, T. Ameel and A. B. Frazier, “A review of laminar single-phase flow in microchannels,” In Proc. *Int. Mech. Eng. Cong. Expos. ASME,* USA, 1-9, 2001.

---

[26] .S. W. Ma and F. M. Gerner, “Forced convection heat transfer from microstructures,” *J. Heat* Transfer, **115**, 872-880, 1993.

[27] J. Pfahler, j. Harley, H. Bau, and J. Zemal, “gas and Liquid Flow in Small Channel,” *Am. Soc. Mech. Eng., Dynam. Syst. Control Division*, **32**, 49-60, 1991.

[28] K. F Jensen, “Microreaction engineering – is small better?,” *Chem. Eng. Sci.*, **56**, 293-303, 2001.

[29] K. A. Alfadhel and M. V. Kothare, “Microfluidic modeling and simulation of flow in membrane microreactors,” *Chem. Eng. Sci,.* ***6*0**, 2911-2926, 2005.

[30] S. Waelchli and P. R. Von Rohr, “Two-phase flow characteristics in gas-liquid microreactors,” *Int. J. Multiphase Flow*, **32**, 791-806, 2006.

[31] X. F. Peng and G. P. Peterson, “Convective heat transfer and flow friction for water flow in mirochannel structures,” *Int. J. Heat Mass Transfer*, **39,** 2599-2608, 1996.

[32] M. Gad-el Hak, “Fluid mechanics of microdevices-the Freeman scholar lecture,” ASME *J. Fluid Eng.*, **121**, 5–33, 1999.

[33] B. Steinhaus, A. Q. Shen, and R. Sureshkumar, “Dynamics of Viscoelastic Fluid Filaments in Microfluidic Devices,” *Phys. Fluids*, **19**, 73-103, 2007.

[34] J. Eggers, “Nonlinear Dynamics and Breakup of Free-Surface Flows,” *Rev. Mod. Phys.*, **69**, 865–929, 1997.

---

[35] S. H. Spiegelberg, D. C. Ables, and G. H. McKinley, “The Role of End Effects on easurements of Extensional Viscosity in Filament Stretching Rheometers,” *J. Non-Newtonian Fluid Mech*., **64,** 229–267, 1996.

[36] F. Tay, “Microfluidics and BioMEMS Applications,” 1st ed. *Springer*, *Kluwer Academic Publishers,* Boston, 3–24, 2002.

[37] J. G. Smits, “Piezoelectric Micropump with Three Valves Working Peristaltically,” *Sens. Actuators A, Phys.,* **21**,.203-206, 1990.

[38] C. Grosjean and Y. C. Tai “A Thermopneumatic Peristaltic Micropump,” in *Proc. Int. Conf. on Solid-State Sensors and Actuators*, Japan, 1776–1779. 1999.

[39] M. A. Unger, H. P. Chou, T. Thorsen, A Scherer and S. R. Quake, “Monolithic Microfabricated Valves and Pumps by Multilayer Soft Lithography,” *Science*, **288**, 113–116, 2000.

[40] H. P. Chou, M. A. Unger and S. R. Quake, “A Microfabricated Rotary Pump,” *Biomed. Microdevices,* **3**, 323–330, 2001.

[41] J. M. Berg, R. Anderson, M. Anaya, B. Lahlouh, M. Holtz and T. Dallas, “A Two-stage Discrete Peristaltic Micropump,” *Sen. Actuators A-Phys.*, **104**, 6–10, 2003.

[42] J. Xie, J. Shih and Y. C. Tai, “Integrated Parylene Electrostatic Peristaltic Pump,” in *Proc. 7t h Int. Conf. on Micro Total Analysis System*, Squaw Valley, 865–868, 2003.

---

[43] S. Bohm, W. Olthuis and P. Bergveld, “A Bi-directional Electrochemically Driven Micro Liquid Dosing System with Integrated Sensor/Actuator Electrodes,” in *Proc. 13th IEEE Int. Conf. on Micro Electro Mechanical Systems*, Japan, 92–95, 2000.

[44] S. W. Lee, W. Y. Sim and S. S. Yang, “Fabrication and InVitro Test of a Microsyringe,” *Sen. Actuators A-Phys.*, **83**, 17–23, 2000.

[45] P. Griss, H. Andersson, and G. Stemme, “Liquid Handling Using Expandable Microspheres,” in *Proc. 15th IEEE Int. Conf. on Micro Electro Mechanical Systems*, Las Vegas, 117–120, 2002.

[46] H. Suzuki and R. Yoneyama, “A Reversible Electrochemical Nanosyringe Pump and Some Considerations to Realize Low-power Consumption,” *Sen. Actuators B-Chem.*, **86**, 242–250, 2002.

[47] Y. H. Choi and S. S. Lee, “Novel Micropump Actuated by Drying of Gel,” in *Proc. 7th Int. Conf. on MicroTotal Analysis Systems*, CA, 219–222, 2003.

[48] J. Xie, Q. He, Y. C. Tai, J. Liu and T. Lee, “Electrolysis-based on-chip Dispensing System for ESIMS,” in *Proc. 16th IEEE Int. Conf. on Micro Electro Mechanical Systems*, Japan, 443–446, 2003.

[49] Y. H. Choi, S. U. Son. S. S. Lee, “A Micropump Operating with Chemically Produced Oxygen Gas,” *Sen. Actuators A-Phys.*, **111**, 8–13, 2004.

[50] J. M. Ottino, and S. Wiggins, “Introduction: Mixing in microfluidics,” *Philos. Trans. R. Soc. London Ser. A,* ***362***, 923-935, 2004.

---

[51] M. A. Stremler, F. R. Haselton, and H. Aref, “Designing for chaos: applications of chaotic advection at the microscale,” *Philos. Trans. R. Soc. London Ser. A, 362*, 1019-1036, 2004.

[52] N. T. Nguyen, and Z. *J*. Wu, “Micromixers—a review,” Micromech. *Microeng.,***15**, 1-16, 2005.

[53] S. Hardt, K. S. Drese, V. Hessel, and F. Schönfeld, “Pssive micromixers for applications in the microreactor and μ TAS fields,” *Microfluid. Nanofluid.,* **1**,108-118, 2005.

[54] A. J. Demello, “Control and detection of chemical reactions in microfluidic systems,” *Nature, **442***, 394-402. 2006.

[55] M. H. Oddy, J. G. Santiago, and J. C. Mikkelsen, “Electrokinetic Instability Micromixing,” *Anal. Chem.,*. **73**, 5822-5832, 2001.

[56] L. H Lu, and K. S. R. Liu,“A magnetic microstirrer and array for microfluidic mixing,” *J. Microelectromechan. Syst.,* **11**, 462-469, 2002.

[57] R. H. Liu, J. Yang, M. Z. Pindera, M. Athavale, and P. Grodzinski, “Bubble-induced acoustic micromixing,” *Lab Chip.,. **2***, 151-157, 2002.

[58] Z. Yang, H. Goto, M. Matsumoto, and R. Maeda, “Ultrasonic Micromixer for Microfluidic,” Systems. *Electrophoresis., **21***, 116- 119, 2000.

---

[59] A. A. Deshmukh, D. Liepmann, and A. P. Pisano, “Continuous micromixer with pulsatile micropumps,” *Tech. Digest IEEE Solid State Sensor and Actuator*, Island, 73-76, 2000.

[60] A. A. Deshmukh, D. Liepmann, and A. P. Pisano, “Characterization of a micromixing, pumping, and valving system,” *Proc. Transducers’01, 11th Int. Conf. on Solid-State Sensors Actuators*, Germany, 779, 2001.

[61] T. Fujii, Y. Sando, K. Higashino, and Y. Fugii, “A plug and play microfluidic device,” *Lab. Chip.*, **3,** 193, 2003.

[62] I. Glasgow, and N. Aubry, “Enhancement of microfluidic mixing using time pulsing,” *Lab. Chip*, **3**, 114, 2003.

[63] X. Z. Niu, and Y. K. Lee, “Efficient spatial–temporal chaotic mixing in microchannels,” *J. Micromech. Microeng.*, **13**, 454, 2003.

[64] J. Evans, D. Liepmann, and A. P. Pisano, “Planar laminar mixer," *Proc. MEMS’97, 10th IEEE Int. Workshop Micro Electro Mechanical System (Nagoya, Japan)*, 96, 1997.

[65] F Okkels, and P. Tabeling, “Spatiotemporal resonances in mixing of open viscous fluidis,” *Phys. Rev. Lett.*, **92,** 038-301, 2004

[66] H. Suzuki, and C. M. Ho, “A magnetic force driven chaotic micro-mixer,” *Proc. MEMS’02, 15th IEEE Int. Workshop Micro Electro Mechanical System (Las Vegas, Nevada)*, 40, 2002.

---

[67] L. H. Lu, K. S. Ryu, and C. A. Liu, “magnetic microstirrer and array for microfluidic mixing,” *J. Microelectromech. Syst.*, **11,** 462, 2002.

[68] A. O. El Moctar, N. Aubry, and J. Batton, “Electro–hydrodynamic micro-fluidic mixer,” *Lab Chip*, **3,** 273, 2003.

[69] J. Deval, P. Tabeling, and C. M. Ho, “A dielectrophoretic chaotic mixer,” *Proc. MEMS’02, 15th IEEE Int. Workshop Micro Electro Mechanical System (Las Vegas, Nevada)*, 36, 2002.

[70] Y. K. Lee, J. Deval, P. Tabeling, and C. M. Ho, “Chaotic mixing in electrokinetically and pressure driven micro flows,” *Proc. MEMS’01, 14th IEEE Int. Workshop on Micro Electro Mechanical System (Interlaken, Switzerland)*, 483, 2001.

[71] S. C. Jacobson, T. E. McKnight, and J. M. Ramsey, “Microfluidic devices for electrokinematically driven parallel and serial mixing,” *Anal. Chem.*, **71,** 4455, 1999.

[72] G. L. Lettieri, A. Dodge, G. Boer, J. Lichtenberg, E. Verpoorte, and N. F. de Rooij, “Consequences of opposing electrokinetically and pressure-induced flows in microchannels of varying geometries,” *Proc. MEMS’00, 13th IEEE Int. Workshop Micro Electro Mechanical System* (Enschede, NL), 351, 2000.

[73] M. H. Oddy, J. G. Santiago, and J. C. Mikkelsen, “Electrokinetic instability micromixing,” *Anal. Chem.*, **73**, 5822, 2001.

---

[74] Z. Tang, S. Hong, D. Djukic, V. Modi, A. C. West, J. Yardley, and R. M Osgood, “Electrokinetic flow control for composition modulation in a microchannel,” *J. Micromech. Microengg.*, **12**, 870, 2002.

[75] H. H. Bau, J. Zhong, and M. Yi, “A minute magneto hydro dynamic (MHD) mixer,” *Sensors Actuators B.*, **79**, 207, 2001.

[76] R. M. Moroney, R. M. White, and R. T. Howe, “Ultrasonically induced microtransport,” *Proc. MEMS’91, 3rd IEEE Int. Workshop Micro Electro Mechanical System (Nara, Japan),* 277, 1991.

[77] X. Zhu, and E. S. Kim, “Acoustic-wave liquid mixer,” *Microelectromechanical Systems (MEMS), ASME, Dynamic Systems and Control Division (Publication),* Fairfield, NJ, **62,** 35, 1997.

[78] J. C. Rife, M. I. Bell, J. S. Horwitz, M. N. Kabler, R. C. Y. Auyeung, and W. J. Kim, “Miniature valveless ultrasonic pumps and mixers,” *Sensors Actuators A.*, 86, 135, 2000

[79] V. Vivek, Y. Zeng, and E. S. Kim, “Novel acoustic-wave micromixer,” *Proc. MEMS’00, 13th IEEE Int. Workshop Micro Electro Mechanical System (Miyazaci, Japan),* 668, 2000.

[80] P. Woias. K. Hauser, and E. Yacoub-George, “An active silicon micromixer for μTAS applications, van den Berg. A., Olthuis. W., Bergveld. P.,” *(Eds.), Micro Total Analysis Systems,* Kluwer Academic Publishers, Drodecht, 277, 2000.

---

[81] K. Yasuda, “Non-destructive, non-contact handling method for biomaterials in micro-chamber by ultrasound,” *Sensors Actuators B.*, **64**, 128, 2000.

[82] Z. Yang, H. Goto, M. Matsumoto, and R Maeda, “Active micromixer for microfluidic systems using lead-zirconate-titanate(PZT)-generated ultrasonic vibration,” *Electrophoresis*, **21**, 116. 2000.

[83] Z. Yang, S. Matsumoto, H. Goto, M. Matsumoto, and R Maeda, “Ultrasonic micromixer for microfluidic systems,” *Sensors Actuators A.*, **93**, 266, 2001.

[84] R. H. Liu, J. N. Yang, M. Z. Pindera, M. Athavale, and P. Grodzinski, “Bubble induced acoustic micromixing,” *Lab Chip*, 2, 151, 2002.

[85] R. H. Liu, R. Lenigk, R. L. Druyor-Sanchez, J. Yang, and P. Grodzinski, “Hybridization enhancement using cavitation microstreaming,” *Anal Chem.*, **75,** 1911, 2003.

[86] G. G. Yaralioglu, I. O. Wygant, T. C. Marentis, and B. T. Khuri-Yakub, “Ultrasonic mixing in microfluidic channels using integrated transducers,” *Anal. Chem.,*. **76,** 3694, 2004.

[87] H. Mao, T. Yang, and P. S. Cremer, “A microfluidic device with a lineartemperature gradient for parallel and combinatorial measurements,” *J. Am. Chem. Soc.*, 124, 4432, 2002.

[88] J. H. Tai, and L. Lin, “Active microfluidic mixer and gas bubble filter driven by thermal bubble pump,” *Sensors Actuators A.*, **665**, 97–98, 2002.

---

[89] A. E. Kamholz, B. H. Weigl, B. A. Finlayson, and P. Yager, “Quantitative analysis of molecular interaction in a microfluidic channel: the T-Sensor,” *Anal. Chem.*, **71**, 5340, 1999.

[90] A. E. Kamholz, and P. Yager, “Molecular diffusive scaling laws in pressure-driven microfluidic channels: deviation from one-dimensional Einstein approximations,” *Sensors Actuators B.*, **82,** 117, 2002.

[91] R. F. Ismagilov, A. D. Stroock, P. J. A. Kenis, G. Whitesides, H. A. Stone, “Experimental and theoretical scaling laws for transverse diffusive broadening in two-phase laminar flows in microchannels.” *Appl. Phys. Lett.*,. **76**, 2376, 2000.

[92] M. Yi, and H. H. Bau, “The kinematics of bend-induced mixing in micro-conduits,” *Int. J. Heat Fluid Flow*., **24,** 645, 2003.

[93] S. H. Wong, M. C. L. Ward, and C.W. Wharton, “Micro T-mixer as a rapid mixing micromixer,” *Sensors Actuators B.*, **100,** 365, 2004.

[94] J. Branebjerg, P. Graveson, J. Krog, and C. Nielsen, “Fast mixing by lamination,” *Proc. MEMS '96, 9th IEEE Int. Workshop on Micro Electro Mechanical Systems, (San Diego, CA),* 441, 1996.

[95] N. Schwesinger, T. Frank, and H. Wurmus, “A modular microfluidic system with an integrated micromixer,” *J. Micromech. Microeng.*, **6,** 99, 1996.

[96] B. L. Gray, D. Jaeggi, N. J. Mourlas, B. P. van Drieënhuizen, K. R. Williams, N. I. Maluf, and G. T. Kovacs, “A. Novel interconnection technologies for integrated microfluidic systems,” *Sensors Actuators A.*, **77**, 57, 1999.

---

[97] M. S. Munson, and P. Yager, “Simple quantitative optical method for monitoring the extent of mixing applied to a novel microfluidic mixer,” *Ana. Chim. Acta.*, **507**, 63, 2004.

[98] B. He, B. J. Burke, X. Zhang, R. Zhang, and F. E. Regnier, “A picoliter-volume mixer for microfluidic analytical systems,” *Anal. Chem.*, **73**, 1942, 2001.

[99] J. Melin, G. Gimenez, N. Roxhed, W. van der Wijngaart, and G. Stemme, “A fast passive and planar liquid sample micromixer,” *Lab Chip,* **4**, 214. 2004.

[100] R. Miyake, T. S. J. Lammerink, and M. Elwenspoek, “micromixer with fast diffusion,” *Proc. IEEE Micro Electro Mechanical Systems Workshop*; San Diego, CA, 248-253., 1993.

[101] J. Voldman, M. L. Gray, and M. A. Schmid, “An Integrated Liquid Mixer /Valve,” *J. Microelectromechan. Syst.,* **9**, 295-302, 2000.

[102] H Wang, P. Iovenitti, E. Harvey, and S. Masood, “Optimizing layout of obstacles for enhanced mixing in microchannels,” *Smart Mater. Struct.*, **11,** 662, 2002.

[103] Y. Lin. G. J. Gerfen, D. L. Rousseau, and S. R. Yeh, “Ultrafast microfluidic mixer and freeze-quenching device,” *Anal. Chem.*, **75,** 53-81, 2003.

[104] C. C. Hong, J. W. Choi, and C. H. Ahn, “A novel in-plane microfluidic mixer with modified tesla structures,” *Lab. Chip,* **4**, 109-113, 2004.

---

[105] R. H. Liu et al., “Passive mixing in a three-dimensional serpentine microchannel,” *J. Microelectromech. Syst.*, **9,** 190-197, 2000.

[106] T. J .Johnson, D. Ross, and L. E. Locascio, “Rapid microfluidic mixing,” *Anal. Chem.,*. **74**, 45-51, 2002

[107] A. D. Stroock, S. K. Dertinger, A. Ajdari, I. Mezic, and H. A. Stone, G. M. Whitesides, “Chaotic mixer for microchannels,” *Science,*. **295**, 647-651, 2002.

[108] A. D. Stroock, and G. M. Whitesides, “Controlling flows in microchannels with patterned surface charge and topography,” *Acc. Chem. Res.*, **36,** 597-604, 2003.

[109] H. Wang. P. Iovenitti, E. Harvey, and S. Masood, “Numerical investigation of mixing in microchannels with patterned grooves,” *J. Micromech. Microeng.*, **13,** 801, 2003.

[110] D. S. Kim, S. W. Lee, T. H. Kwon, and S. S. Lee, “A barrier embedded chaotic micromixer,” *J. Micromech. Microeng.*, **14**, 798,.2004.

[111] K. Hosokawa, T. Fujii, and I. Endo, “Droplet-based nano/picoliter mixer using hydrophobic microcapillary vent,” *Proc. MEMS’99, 12th IEEE Int. Workshop Micro Electro Mechanical System (Piscataway, NJ)*, 388, 1999.

[112] K. Handique, and M. A. Burns, “Mathematical modeling of drop mixing in a slit type microchannel,” *J. Micromech. Microeng.*, **11**, 548, 2001.

[113] P. Paik, V. K. Pamula, and R. B. Fair, “Rapid droplet mixers for digital microfluidic systems,” *Lab Chip,*. **3**, 253, 2003.

---

[114] H. Song, M. R. Bringer, J. D. Tice, C. J. Gerdts, and R. F. Ismagilov, “Experimental test of scaling of mixing by chaotic advection in droplets moving through microfluidic channels,” *Appl. Phys. Lett.,*. **83,** 46-64, 2003.

[115] J.D Tice.., A.D Lyon.., R.F Ismagilov.. Effects of viscosity on droplet formation and mixing in microfluidic channels. *Anal. Chim. Acta.* 2003. **507:** 73.

[116] J. G. Santiago, S. T. Wereley, C. D. Meinhart, D. J. Beebe, and R. J. Adrian, “A article Image Velocimetry System for Microfluidics,”*Experiments in Fluids,*. **25**, 316–319, 1998.

[117] Q. Li, N. Wang, and D. Yi, Numerical analyses, 3rd. ed., Huazhong: University of Science and Technology Press, 215–222. 2000.

[118] L. Shui, J. C. T, Eijkel, and A. van den Berg, “Multiphase flow in micro- and nanochannels,” *Sensor and Actuator B,* **121,** 263-276, 2007.

[119] G. Rosengarten, J. Cooper-White, and G. Metcalfe, “Experimental and analytical study of the effect of contact angle on liquid convective heat transfer in microchannels,” i*nternational Journal of Heat and Mass Transfer,* **49**, 4161-4170, 2006.

[120] D. Tretheway, X. Liu, and C. Meinhart, “Analysis of slip flow in microchannels,” *In: 11th International Symposium on Applications of Laser Techniques to Fluid Mechanics, Lisbon,* 2002.

[121] N. Nguyen, and Z. Wu, “Micromixers – A Review” *J. Micromech. Microeng.,* **15**, R1-R16, 2005.

---

[122] J. L. Tan, W. Liu, C. M. Nelson, S. Raghavan, and C. S. Chen, “Simple Approach to Micropattern Cells on Common Culture Substrates by Tuning Substrate Wettability,” *Tissue Eng.*, **10**, 865-872, 2004.

[123] J. G. Santiago, S. T. Wereley, C. D. Meinhart, D. J. Beebe, R. J. Adrian, and A. Particle, “Image Velocimetry System for Microfluidics,” *Experiments in Fluids.,* **25**, 316–319, 1998.

[124] R. C. Reid, J. M. Prausnitz, and B. E. Poling, “*The Properties of Gases and Liquids*,” 4th edn, McGraw-Hill, Inc. 1987.

[125] J. Hussong, R. Lindken, M. Pourquie, J. Westerweel, in *IUTAM Symposium on Advances in Micro- and Nanofluidics* (Eds: M. Ellero et al.), Springer **2009**, pp. 191-205.

[126] A. Soleymani, H. Yousefi, W. Ratchananusorn, and I. Turunen, “Pressure drop in micro T-mixers,” *J. Micromech . Microeng*, 20, 15-29, 2010.

[127] P. C. Chatwin and P. J. Sullivan, “The effect of aspect ratio on the longitudinal diffusivity in rectangular channels,” J. Fluid Mech. 120, 347-358, 1982.

[128] J. Happel and H. Brenner, “Low Reynolds Number Hydrodynamics,” Springer, Sijthoff and Noordhoff, Amsterdam, 1973

[129] J. P. Van Doormal, and G. D. Raithby, “Enhancements of the SIMPLE method for predicting incompressible fluid flows,” *Numerical Heat Transfer*, **7**, 147–163, 1984.

[130] P. V. Danckwerts, “The definition and measurement of some characteristics of mixtures,” *Appl. Sci.* Res., **3**, 279-96, 1952.

---

[131] S. Middleman, “An Introduction to Mass and Heat Transfer,” *Wiley*, 217-218. 1998.

[132] K. V. Price, R. M. Storn, and J. and A. Lampinen, “Differential Evolution: A Practical Approach to Global Optimization,” *Springer*, Berlin, 2005.

[133] R. Storn and K. V. Price, “Differential evolution: A simple and efficient adaptive scheme for global optimization over continuous spaces,” *Int. Comput. Sci. Instit.*, Berkeley, CA, Tech. Rep. TR-95-012, 1995.

[134] N. Dombrowski, E. A. Foumeny, S. Ookawara, and A. Riza, “The influence of Reynolds number on the entry length and pressure drop for laminar pipe flow, *Can. J. Chem. Eng*.**71**, 472–476, 1993.

[135] D. Bothe, C. Sternich, and H. J. Warnecke, “Fluid mixing in a T-shaped micro-mixer,” *Chem. Eng. Sci*.**, 61**. 2950–2958, 2006.

[136] S. Thomas, and T. Ameel, “An Experimental Investigation of Low-Reynolds Number Flow in a T-Channel,” *Exp. Fluids*, **49**, 1231-1245, 2010.

[137] S. Thomas, T. Ameel, and J. Guilkey, “Mixing Kinematics of Moderate Reynolds Number Flows in a T-Channel,” *Phys. Fluids*, **22**, 13601-13610, 2010.

[138] J. Melin et al, “A fast passive and planar liquid sample micromixer,” *Lab. Chip,* **4**, 214–219, 2004.

---

[139] D. J. Kim et al, “An easily integrative and efficient micromixer and its application to the spectroscopic detection of glucose-catalyst reactions,” *The Analyst*, **130**, 293–298, 2005.

[140] H. Y. Wu, and C. H. Liu, “A novel electrokinetic micromixer,” Sens Actuators A, **118**, 107–115, 2005.

[141] C. Bisson, J et al, “A microanalytical device for the assessment of coagulation parameters in whole blood,” In Proc. *Solid-State Sensor and ActuatorWorkshop,* (Hilton Head, SC, 1998, 1–6).

[142] R. C Anderson et al, “Miniaturized genetic analysis systems: improvements and methods,” In Proc. *Solid-State Sensor and Actuator Workshop,* (Hilton Head, SC, 1998, 7–10).

[143] A. Soleymani, E. Kolehmainen and I. Turunen, “Numerical and experimental investigations of liquid mixing in T-type micromixers *Chem. Eng. J.*, **135S,** 219–28, 2008.

[144] E. L. Cussler, “Diffusion Mass Transfer in Fluid System,” Cambridge University Press, 1997, 67–68.

[145] J. P. Van Doormaal, G. D. Raithby, “Enhancements of the simple method for predicting incompressible fluid flows,” *Numer. Heat Transfer,* **7**, 147-163, 1984.

[146] B. Cohen, D. Huppert and N. Agmon, “Non-exponential Smoluchowski dynamics in fast acid–base reaction,” *J. Am. Chem. Soc.*, **122**, 9838-9839, 2000.

Publications and Presentations

1. C. Galletti, M. Roudgar, E. Brunazzi and R. Mauri, “ *Effect of inlet conditions on the engulfment pattern in a T-shaped micro-mixer”* Chem. Eng. J, 185, 300-313, 2012.

2. M. Roudgar, E. Brunazzi, C. Galletti, and R. Mauri, “*Numerical Study of Split T-micromixer,”* Chemical Engineering and Technology (accepted).

3. M. Roudgar, E. Brunazzi, C. Galletti, and R. Mauri, “*The Effect of Fluid Viscosity in T-shaped Micromixer*s,” SIMULTECH 2011 (1st International Conference on Simulation and Modeling Methodologies, Applications and Tools), Noordwijkerhout, The Netherlands, July 2011, pages 343-347.

4. M. Roudgar, E. Brunazzi, C. Galletti, and R. Mauri, “*Numerical Study of Two-way Split Micromixers,”* Ansys Multi-Phase Flows Simulation, Experiment and Application, Germany, Dresden, May 2011(Oral presentation).